

AN EULERIAN NUMERICAL METHOD
FOR MULTISPECIE, TURBULENT,
SUPERSONIC JET MIXING

by

PAUL T. BAUER

Bachelor of Science
Parks College of St. Louis University
East St. Louis, Illinois
1963

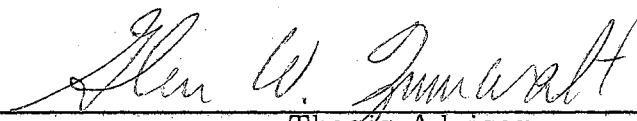
Master of Science
Oklahoma State University
Stillwater, Oklahoma
1965

Submitted to the Faculty of the
Graduate College of the
Oklahoma State University
in partial fulfillment of
the requirements for
the Degree of
DOCTOR OF PHILOSOPHY
July, 1968

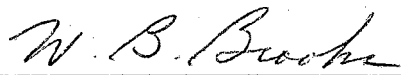
JAN 28 1969


AN EULERIAN NUMERICAL METHOD
FOR MULTISPECIE, TURBULENT,
SUPERSONIC JET MIXING

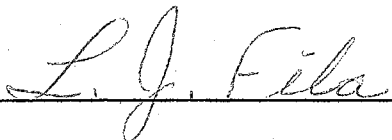
Thesis Approved:



Thesis Adviser









Dean of the Graduate College

696075

PREFACE

In this thesis, a numerical method was applied to a system of derived differential equations in an attempt to develop a way by which multispecie turbulent flow of perfect nonreacting gas could be described. The overall scheme was applied to a constant pressure, two-specie (CO_2 and air), coaxial mixing problem.

Although comparison of the results of this work was made with experimental data, analysis of the experimental data indicated a large inconsistency with the conservation of mass principle. Consequently, a currently available analytic solution for single specie was extended to the two-specie case for the purpose of comparison.

In attempting this work, the ultimate goal was the establishment of a method whereby extremely complex nonreactive flow fields, such as occur in advanced propulsion devices, may be analyzed. Major advances in techniques for such analysis have already been made by previous investigators at Oklahoma State University. Specifically, the suitability of a numerical method for the analysis of complex shock wave patterns in an inviscid flow field has been demonstrated by Drs. W. N. Jackomis, L. D. Tyler, and R. R. Eaton. In addition, Dr. W. F. Walker analyzed the interaction of a blast wave and a turbulent mixing region. Therefore, it appeared

appropriate to now consider multispecie mixing. Furthermore, while only a relatively simple isobaric jet mixing case was considered, the technique was so conceived as not to be restricted to only this type of flow. Conceivable, analysis of more complex flow fields with multispecie mixing will only require specification of appropriate boundary and initial conditions. This specification, of course, is normally the most difficult aspect of any analysis.

However, throughout this investigation it was realized that:

1.) the technique is a numerical method and therefore is capable only of approximate solutions, and 2.) the exact description of turbulent flow has stymied the scientific community for over a century and therefore it was not intended that this work would terminate the problem of turbulent analysis. Indeed, the selection of an eddy viscosity automatically biases the description of turbulent flow. However, the urgency for analysis of currently intractable flow fields warrants, at this juncture, even approximate analysis.

Time would not permit nor space allow the acknowledgement of all who have aided in the completion of this work. Nonetheless, I wish to express my deep gratitude to those who have been instrumental.

My sincerest thanks are extended to: Dr. G. W. Zumwalt for serving as my thesis adviser and graduate committee chairman and for his assistance in both the technical and mechanical aspects of this thesis; Professor L. J. Fila, whose patient ear and insight were of

considerable aid; Dr. W. B. Brooks for the short notice sacrifice of his time and the thorough consideration that he gave to this thesis; and Dr. H. S. Mendenhall for the time spent in serving on my graduate committee.

The generous assistance of Dr. D. D. Grosvenor and his computer science staff could not go unmentioned. Indeed, this work would have been impossible without their very efficient operation. Moreover, in a special way, I would like to express my thanks to Mr. F. Hajek for the many midnight shifts during which he ran my programs on the computer.

Special mention is due my colleagues at the University of Dayton. The understanding of Mr. D. H. Whitford and Professor H. E. Smith made the task of writing much lighter and the innumerable discussions with Dr. W. J. Bornhorst, Dr. L. I. Boehman, and Professor J. E. Minardi considerably aided my insight.

For the unsurpassed patience and endurance of Miss Ester Holp in the typing and monitoring of the reproduction of this thesis, I am sincerely appreciative. Thanks also are due Mr. J. Olinger and Mr. H. DeMarey for their help.

Most important of all, I wish to thank, in this meager way, my parents. Without their sacrifice, patience, and discipline, I would have never experienced the circumstances which led to the consideration of this work.

TABLE OF CONTENTS

Chapter	Page
I.	INTRODUCTION 1
	Literature Survey 3
	Method of Analysis 12
II.	DIFFERENTIAL EQUATIONS, TRANSPORT COEFFICIENTS, AND BOUNDARY AND INITIAL CONDITIONS 18
	Basic Equations 18
	Perturbation Scheme 20
	Turbulent Transport Expressions 25
	Transport Coefficients 29
	Boundary and Initial Conditions 45
	Nondimensionalization Scheme 49
III.	THE NUMERICAL METHOD 51
	The Rusanov Numerical Method 51
	Stability Requirements 61
	Centerline Equations 67
	Top Boundary Conditions 77
	Downstream Boundary Numerical Equations 78
	Computational Scheme 80
IV.	THE RESULTS OF THE NUMERICAL METHOD AND COMPARISONS WITH EXPERIMENTAL DATA 82
	The Experimental Data 83
	Basic Considerations 92
	Numerical Results and Comparisons 99
	Additional Points for Consideration 138
	Conclusions 145

Chapter	Page
V. APPROXIMATE ANALYTIC SOLUTION AND RESULTS	147
Analytic Solution for Constant Pressure	
Jet Mixing	147
Comparisons of Numeric and Analytic Results	156
VI. CONCLUSIONS AND RECOMMENDATIONS	162
Conclusions	162
Recommendations	165
BIBLIOGRAPHY	167
APPENDIX A. DERIVATION OF INSTANTANEOUS TURBULENT PARTIAL DIFFERENTIAL FLOW EQUATIONS	174
APPENDIX B. PERTURBATION AND TIME-AVERAGING SCHEME	179
Continuity Equation	180
Radial Momentum Equation	181
Axial Momentum Equation	183
Energy Equation	183
Specie Equation	185
APPENDIX C. NUMERICAL EXPANSION OF CENTER- LINE TRANSPORT EXPRESSIONS	187
APPENDIX D. DIVERGENT FLOW UPSTREAM BOUNDARY CONDITION	190
Boundary Layer Corrections	194
APPENDIX E. COMPUTER LOGIC DIAGRAM	197

LIST OF FIGURES

Figure		Page
1.	The "Supersonic Combustion Ram Jet" and the "Air-Augmented Rocket"	2
2.	Constant Pressure, Two-Specie, Coaxial Jet Mixing Configuration	16
3.	The Flow Field and Solution Boundaries.	46
4.	Node Point Nomenclature	55
5.	Assumed Positive Velocity Directions for Centerline Control Volume.	68
6.	Assumed Shear Stress and Pressure System for Centerline Control Volume	70
7.	Assumed Shear Stress and Heat Flux System for a Centerline Control Volume.	73
8.	Assumed Specie Flux Directions for a Centerline Control Volume	76
9.	Axial Location of Experimental Data Radial Profiles	85
10.	Experimental Radial Profiles of Stagnation Pressure	86
11.	Experimental Radial Profiles of Carbon Dioxide . . . Concentration	88
12.	Node Field Arrangement	93
13.	Comparison of Radial Pressure Profiles for $n = 611$ and $n = 1181$	96
14.	Boundary Layer Velocity Distribution for Run I . . .	102

Figure	Page
15. Comparison of Stagnation Pressure Radial Profiles for Run I and Run II	103
16. Radial Profile of Pressure in Unstable Region for Run I	106
17. Boundary Layer Velocity Distribution for Run II	108
18. Stagnation Pressure Comparisons of Experimental Data and Run II (n = 1068) Results	112
19. Radial Profile of Pressure in Unstable Region for Run II	113
20. Stagnation Pressure Comparisons of Run III (n = 1181) and Run II (n = 1068)	117
21. Divergent Flow Upstream Boundary Condition for Run IV	120
22. Stagnation Pressure Comparisons of Run III (611) and Run IV (n = 583)	121
23. Sketch of Wave System Indicated by the Results of Run IV	123
24. Boundary Layer Velocity Distribution for Run V in Comparison to the 1/7 Power Profile	126
25. Results of Run V for Several Time Steps in Comparison with Experimental Data	127
26. Stagnation Pressure Comparisons of Run VI (n = 350) with Experimental Data	130
27. Time-History of the Pressure at Node m = 17, $l = 3$ for Run VI	132
28. Time-History of the Density at Node m = 1, $l = 10$ for Run VI	133
29. Time-History of the Axial Velocity at Node m = 30, $l = 10$ for Run VI	134

Figure	Page
30. Time-History of the Density at Node $m = 16$, $l = 20$ for Run VI	135
31. Time-History of the Density at Node $m = 30$, $l = 30$ for Run VI	136
32. Time-History of the Pressure at Node $m = 3$, $l = 39$ for Run VI	137
33. Carbon Dioxide Concentration Comparison for Different Numerical Calculations	139
34. Carbon Dioxide Concentration Comparisons of Experimental Data and Run VI ($n = 350$).	140
35. Density Radial Profiles for Run VI ($n = 350$)	143
36. Axial Velocity Radial Profiles for Run VI ($n = 350$).	144
37. Nomenclature and Geometry for Analytic Solution	149
38. Analytic Solution Stagnation Pressure Profiles with $\sigma = 50$	157
39. Stagnation Pressure Comparison for Run VI ($n = 350$) and the Analytic Solution	159
40. Comparisons of Carbon Dioxide Concentration Profiles for Run VI ($n = 350$) and the Analytic Solution	160
41. Divergent Flow Field Nomenclature	191

NOMENCLATURE

A	= stability coefficient Eq. (3-3)
B	= stability coefficient Eq. (3-3)
b	= mixing region width
c	= local speed of sound
C	= Crocco number
c_1	= a constant Eq. (2-26)
f	= time dependent matrix variable Eq. (3-2)
F^r	= radially dependent matrix variable Eq. (3-2)
F^z	= axially dependent matrix variable Eq. (3-2)
h	= static enthalpy
h_o	= stagnation enthalpy
K_r	= $\Delta t / \Delta r$
K_z	= $\Delta t / \Delta z$
K	= $[K_r^2 + K_z^2]^{1/2}$
N	= number of species
p	= pressure
Pr_t	= turbulent Prandtl number
R_i	= gas constants

r	= radial coordinate measured from the centerline
$Sc_{t,i}$	= turbulent Schmidt number for i^{th} specie
u	= axial velocity component
V	= $[u^2 + v^2]^{1/2}$
v	= radial velocity component
X	= axial coordinate with origin at point of separation
x	= axial coordinate with origin at point of separation
Y	= transverse coordinate with origin at point of separation
y	= transverse coordinate measured from x axis
z	= axial coordinate measured along centerline
α	= See Eq. (3-5)
β	= See Eq. (3-5)
$\bar{\gamma}$	= average specific heat ratio
γ_i	= specific heat ratio of i^{th} specie
δ	= boundary layer thickness
Δr	= distance between two node points in radial direction
Δz	= distance between two node points in axial direction
Δt	= time step
ϵ_m	= eddy viscosity
ζ	= y/δ_a
η_u	= See Eq. (5-11)
η_p	= See Eq. (5-11)
Λ	= h_o/h_{o_a}

- ξ_u = See Eq. (5-7)
 ρ = density
 σ = spreading rate parameter
 $\bar{\sigma}_o$ = $(\bar{\sigma}_{m, l}^n)_{\max}$
 $\bar{\sigma}_{m, l}^n$ = See Eq. (3-15)
 ϕ = u/u_a
 χ = $\text{Arctan}(\Delta r/\Delta y)$
 ψ = matrix variable Eq. (3-2)
 ψ = x/δ_a
 w_i = concentration of i^{th} specie
 w = damping parameter

Superscript

- $-$ = time average
 $'$ = fluctuating components
 n = denotes quantities measured in n^{th} time

Subscript

- a = a mixing stream, in this case, the air stream
 b = a mixing stream, in this case, the CO_2 stream
 e = denotes variables associated with an energy profile
 i = denotes i^{th} specie
 l = an axial point number
 m = a radial point number

max = the maximum value

t = denotes variables common to turbulent flow

t, i = denotes variables common to turbulent flow for ith specie

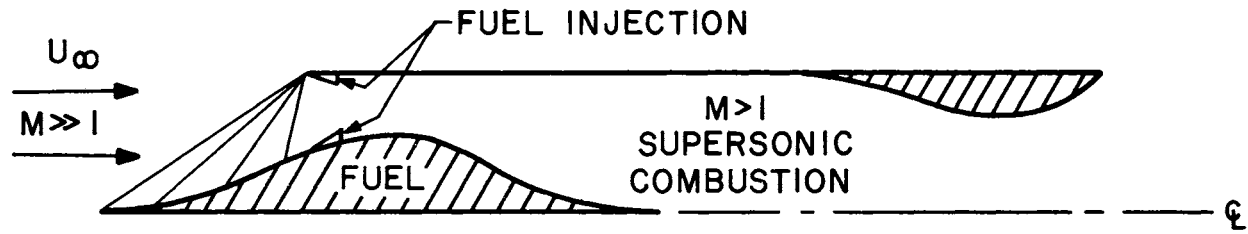
u = denotes variables associated with a velocity profile

CHAPTER I

INTRODUCTION

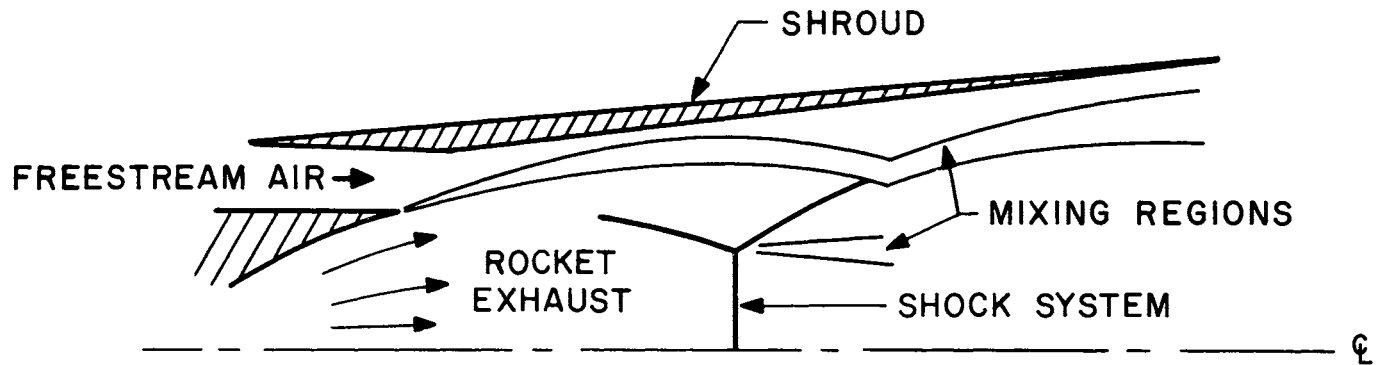
Because of the enormous cost of present day launch vehicles and some promising prognostications based on very simple analyses which have appeared in the literature (References 1 and 2), interest has been spurred in the areas of supersonic burning ramjets (SCRAM jets) and air-augmented rockets (see Figure 1). However, before practical designs are possible, the detailed flow fields of these devices must be analyzed. Moreover, a cursory inspection of the sketches contained in Figure 1 indicates the obvious complexity of the associated flow fields. That is, not only are the inviscid variations of pressure, temperature, density, and velocity very complex, but the added complications of multiple species and turbulent mixing compound the problem to an almost insurmountable level. (See Reference 3 for a brief delineation of the difficulties encountered in the analysis of heterogeneous mixing.)

The solution of these types of problems, therefore, requires a method that can describe the mass, momentum, and energy distributions of a turbulent flow field that has shock waves and other discontinuities such as occur in two-stream mixing. This means that



SUPERSONIC COMBUSTION RAM JET

(a)



AIR - AUGMENTED ROCKET

(b)

Figure 1. The "Supersonic Combustion Ram Jet" and the "Air-Augmented Rocket"

both transverse and longitudinal gradients of all the flow quantities must be permitted. In addition, consideration must be given to mixing of light and heavy gases, including the possible existence of solid particles in the flow. These conditions will not allow the assumption of a Prandtl and Lewis number equal to unity. Moreover, combustion may also take place if the gases are of a combustible nature and at a proper temperature.

Thus far, as the literature survey will indicate, the utility of currently available analytic methods is restricted in application to much simpler flow fields than of topical importance. Furthermore, the possibility of extending available analytic methods to complex flow fields appears to be remote. Consequently, this work applied a numerical method to a system of partial differential equations that were assumed to describe multispecie turbulent flow.

Literature Survey

Because of the nature of the appropriate differential equations, most investigators have been led to attack only the problem of constant pressure (or, at best, prescribed pressure gradient) turbulent jet mixing. This is not to say that the amount of investigation devoted to this topic is wanting. On the contrary, there appears to be a plethora of more or less related investigations (for example, Reference 4 contains 585 references related to ejectors and mixing streams). However, since the expressed purpose of this thesis is

the development of a technique sufficiently general to permit further extension and application to problems of the variety experienced in SCRAM jet and air-augmentation applications, a discussion of the currently available analytical tools for jet mixing analysis is here apropos. In the text of the following chapters, where information concerning experimentally determined parameters is necessary, an appropriate and brief literature survey is incorporated.

The analytic analysis of turbulent jet mixing generally breaks down into two approaches to the problem. One technique is that of the integral momentum method similar to that used by von Karman in boundary layer analysis (5). The other consists of solving the partial differential equations of motion and looking for particular solutions to match the boundary conditions.

Perhaps the best documented solution for two-dimensional jet mixing is that of Korst (6). This solution was arrived at by integration of the linearized streamwise momentum equation. Since this solution is discussed in Chapter V of this thesis, details will not be delineated here. However, it should be noted that this solution is, essentially, for constant pressure turbulent mixing, although prescribed pressure gradients have been incorporated, as, for example, was done by Zumwalt (7). The wide variety of problems to which this solution has been applied is discussed in Reference 8.

By transforming the flow equations into the von Mises coordinates with a subsequent linearization, Kleinstein (9) developed a

solution for laminar jet mixing. Because transport properties are only significant in the inverse transform, the solution in the von Mises coordinates is the same for both laminar and turbulent flow (if it is assumed that the flow equations for turbulent flow are the same as those for laminar flow with the laminar transport properties replaced by their phenomenological counterparts). This enabled Libby (10) to perform a turbulent flow analysis via the solution developed by Kleinstein but with additional assumptions which describe the turbulent transport properties. Reference 11 gives a discussion of both the laminar and turbulent solutions with this transformation technique and Reference 12 shows an application of this method to the description of both the near jet and far jet regions of a constant pressure, coaxial, chemically reacting free jet. As with the Korst solution, application of this solution is restricted to constant pressure mixing. However, because of the role the transport properties play in the inverse transformations, this method does aid in the analysis of the turbulent transport properties.

Some other attempts at handling the mixing problem that show limited application are presented in References 13, 14, and 15. Donaldson and Gray (13) assumed $Pr_t = Le_t = 1$ and considered constant pressure mixing using Crocco's integrals and a form of Prandtl's free turbulence eddy viscosity term. The constant in the eddy viscosity term was found to be a function of exit geometry which was to be expected, as Abramovich (16) indicated.

Seubold (14) transforms the partial differential equations, using a similarity variable, into an ordinary differential equation with the Lewis number assumed unity but with the Prandtl number as a parameter. An attempt was made to retain the pressure gradient term but it was found more convenient to introduce a pressure gradient through a velocity term. Consequently, the pressure gradient was considered a known quantity and not dependent on the flow situation.

In somewhat a similar manner, Cassaccio (15) transformed the equations of motion to get an ordinary differential equation assuming $Pr_t = Le_t = 1$ with Prandtl's hypothesis for turbulent mixing. Consideration was confined to a potential core and a pressure gradient parameter was defined. No experimental verification was given.

As an alternate method to the differential approach, as was noted above, investigators recognized the ability of the integral approach in describing the spreading rate of constant pressure jet mixing regions. Abramovich (16) gives extensive consideration to this approach for a multitude of primary and secondary stream conditions. With the assumption of similar velocity and stagnation profiles which display acceptable comparison with experimental data, he developed jet spreading rate expressions which require evaluation of complicated integrals imbedded in very involved equations.

In an attempt to describe the turbulent jet spreading rate more simply, Abramovich suggested another expression in Reference 17. While this expression does not determine the details of the mixing region flow field, it was found to be a useful relationship by Peters, et al. (18) in a simplified analysis of bounded coaxial turbulent mixing with chemical reactions.

Other attempts at the description of the rate of spreading of a turbulent mixing region have centered investigation on the variation of a "spreading rate parameter," σ , which is consequential to the assumption of similarity. However, the appropriate value of σ for a particular situation is dependent, to some extent, on the assumed velocity function.

To determine the value of σ for higher Mach numbers, Maydew and Reed (19) experimented in the Mach number range of 0.70 to 1.96. Several analytic curves were compared to the experimental data and it was found that Crane's or Goertler's incompressible curve fit the data best and corresponding values of σ , as a function of Mach number, were determined. The data were for the isoenergetic case.

In another attempt of similarity, Reference 20 suggested a transformation procedure that maps variable density velocity profiles onto a single constant density velocity profile. Here again, a similarity parameter, that is a function of Mach number, is introduced.

The method predicts the expected trends that have been observed previously by many others: that the rate of spreading is dependent on the density and the velocity of the jet.

Channapragada (21), with the use of Howarth's transformation and the assumption of the invariance of the shear stress under transformation, related the compressible value of σ to its incompressible value. He noted that, as the Crocco number approached unity, the ratio of the compressible spreading parameter to the incompressible value approached four; and, for a given Crocco number, the hotter the jet the lower the value of the spreading parameter ratio, hence the greater the spread. This formulation was for a jet exhausting into a quiescent medium.

In an extension of this approach to the case of two-stream mixing, Channapragada and Woolley (22) determined a relation for the spreading rate parameter as a function of the two-stream velocity ratio, the primary stream Crocco number, and the two-stream stagnation temperature ratio. For this analysis it was assumed that $Pr_t = Le_t = 1$ and the pressure was constant.

Peters (23) suggested that, for two-stream mixing, there are two predominant scales of turbulence: one of large scale that is represented by Prandtl's free turbulence eddy viscosity term, and the other of a smaller scale that can be represented by an eddy viscosity that is proportional to the local velocity. With the use of Forstall and Shapiro's cosine velocity distribution, Peters suggests yet another

similarity parameter for the integral approach. This σ compares to that presented by Abramovich (16) which is known to have given acceptable results.

Forde (24) considered similarity in the constant pressure isoenergetic mixing of two supersonic streams, one of which was CO_2 . The emphasis was on the potential region. Several methods of analysis were considered and for each method best values of σ were determined by comparison with experiment.

Bauer (25) also approached the constant pressure isoenergetic mixing problem from the similarity viewpoint. Considering a control volume over a portion of the mixing region and using the momentum integral idea, an expression for σ was developed. This σ was based on the error function velocity profile, and, as with Peters (23), was compared with Abramovich's work. The two formulations were in relative agreement.

The effect of ionization was pointed out in (26). By mixing high temperature argon with cool helium with both streams subsonic, it was noticed that spreading decreased with ionization and stayed constant for a degree of ionization greater than 10%. The technique for calculation used an integral-differential approach which simplified to a system of algebraic equations once an assumption for the jet boundary spreading was made. This report also indicated the effect of temperature and two-stream velocity ratio on the spreading rate. Again the pressure was constant.

Despite the amassing of the information and techniques delineated above, direct application of any one method to the problems of the type associated with the SCRAM jet and air-augmented rocket is, generally speaking, impossible. Consequently, a synthesis of analytical tools was the next obvious step.

For the air-augmented rocket, Chow, et al. (27) (28) combined a method-of-characteristics solution with the Korst mixing theory (6) by superimposing a mixing region on the inviscid interface between the primary and secondary streams. This method was useful in defining limiting regimes of operation. However, the method of characteristics is an isentropic solution of the flow equations for supersonic flow and in the interior (neglecting the jet mixing on the edges) of an underexpanded jet there are typically not only non-isentropic processes in evidence, such as shock waves and viscous mixing, but also parts of the flow are subsonic (see Reference 29).

In a similar attempt to solve the air-augmentation mixing problem, a technique was presented in Reference 30 that requires an inviscid calculation via the method of characteristics. On top of the inviscid jet boundary, thus calculated, was superimposed the mixing effects which were determined by a numerical calculation of linearized differential equations which had been transformed into the von Mises plane. The technique allowed for constant values of Pr_t and Le_t but could not handle the situation where shock waves appear in the flow.

Another method developed for rocket exhausts was presented in Reference 31. In this paper, Emmons transformed the linearized equations of flow into the von Mises coordinates and used Prandtl's formulation for the eddy viscosity. Suggested values were given for the turbulent Prandtl and Lewis numbers for gases and for solid particles, and results of some calculations were compared to the data given in Reference 32; the comparison seemed to be acceptable.

While the approach of Emmons could not describe flow fields which contain shock waves, it did employ a numerical solution of the partial differential equations. This approach to a solution of a system of partial differential equations has, no doubt, been inspired by the recent accessibility of large core-storage high-speed computers. Moreover, extensive effort has been expended recently in the development of numerical techniques of applying more general forms of the flow equations.

Fromm (33) employed von Neumann and Richtmyer's pseudo-viscosity concept for numerical stability (see Reference 34) and performed a Lagrangian coordinate analysis of transient normal shock waves. However, the Lagrangian coordinate system is practical only for one dimensional problems.

In the Eulerian coordinate system, Fromm (35) developed a method for computing nonsteady incompressible, viscous fluid flows. The comparison of his results with experiment is amazing. Another

numerical analysis which used Prandtl's boundary layer equations was presented for non-equilibrium laminar and turbulent boundary layer flows by Galowin (36).

Among the numerical methods which are commonly used for the analysis of inviscid transient supersonic flows, the schemes of Lax (37), Lax and Wendroff (38), Richtmyer's variation of the Lax-Wendroff method (39), and Rusanov (40) are the most popular.

In the past several years, the Rusanov method has been the subject of intensive development at Oklahoma State University: Jackomis (41) studied the passage of a blast wave over a stationary cone, Tyler (42) analyzed the propagation of a shock wave into both a still and supersonic crossflow, Walker (43) investigated the interaction of a moving shock wave and a turbulent mixing region, Eaton (44) considered a cone-cylinder in supersonic flow as it entered into and exited from a large-radius spherical blast, and Rao (45) described the transient shock wave patterns, resulting from supersonic aircraft, around ground level structures.

Method of Analysis

As the literature survey indicates, attempts to date to synthesize analytic solutions for the calculation of complex flow fields have suggested basically two conceptual difficulties. In addition to the inability of currently available analytic methods in describing some of the phenomena encountered in complex flow fields, such as

the entire shock wave system in underexpanded jets, the synthesis route requires the investigator to be as much of an artist as a scientist.

On the other hand, the application of a numerical method may proceed in a straightforward manner. The satisfaction of boundary conditions may be accomplished in direct analogy with their analytic description -- once the boundary conditions have, in fact, been defined. Furthermore, the adoption of numerical analysis does not conceptually require a restriction on the degree of generality that may be accomplished. However, it must be recognized that the numerical approach yields only an approximate solution for regions of discontinuities, such as shock waves and concentration discontinuities, smeared over several mesh spacings. Yet, one is not inclined to quibble when faced with the option of either getting a complete, but approximate, solution of a complex flow field or none at all.

Since the Rusanov numerical method (40) has been developed to a high degree (References 41 through 45), this work was an attempt to extend the method still further so that steady state flow fields which contain multispecies turbulent jet mixing could be calculated. That is, the two important extensions that were the goals of this work were the incorporation of multispecies turbulent mixing and the demonstration of the achievement of an asymptotically approached steady state solution (the Rusanov numerical method is a time-dependent

scheme and the previously cited references were devoted, almost wholly, to transient phenomena).

To accomplish these ends, a general set of flow equations, applicable to turbulent flow, were derived and are presented in Chapter II. In the derivation of these equations, no sweeping assumptions were made which would restrict their application to any particular flow situation other than the restriction that the flow must be turbulent everywhere (laminar transport mechanisms were deleted from consideration). Moreover, since consideration was restricted to turbulent flow, it was necessary to remain within the state-of-the-art in the description of the turbulent transport mechanism. On this point, it is necessary to note that the terms in the turbulent analogue of the laminar shear stress representations were investigated separately. While this may appear as a linearization, the nebulous nature of the turbulent shear stresses justified this approach. This is also discussed in Chapter II and its consequences are discussed in Chapter IV.

Chapter III presents the details of the Rusanov numerical method for axisymmetric flow. In addition, the approximate schemes for the satisfaction of the boundary conditions applicable to the flow situation which was investigated as part of this work are also presented.

In order to verify the utility of any developed program, it is necessary to compare the results of calculation with experimental

data. However, adequate experimental data for flow fields which contain shock waves with multispecie turbulent mixing is, at present, nonexistent. Consequently, because of the previous extensive investigation, an axisymmetric, constant pressure, two-specie, nonreacting, perfect gas, turbulent jet mixing case was considered (see Figure 2). However, despite the extensive consideration that has been given to this type of flow, experimental data of sufficient detail and accuracy, necessary for the application of this numerical analysis, is also nonexistent. Nonetheless, the data of Reference 24 was used for comparison in this work since reasonable assumptions could be made for the information not presented in this reference. This is discussed in Chapter IV.

Moreover, because assumptions had to be made in order to permit comparison, the effect of the differing assumptions was investigated and the results of this investigation, together with comparisons with experimental data, are also presented in Chapter IV.

Since analysis of the experimental data of Reference 24 indicated an appreciable error, an analytic analysis was performed with the use of the Korst jet mixing theory (Reference 6). However, since the Korst theory, in its most current state of development, did not include multispecie mixing, an extension of this theory was made to incorporate this phenomenon. Further, since the boundary conditions for integration differed for the momentum, energy, and specie equations, Crocco's integral, which was originally used in the Korst

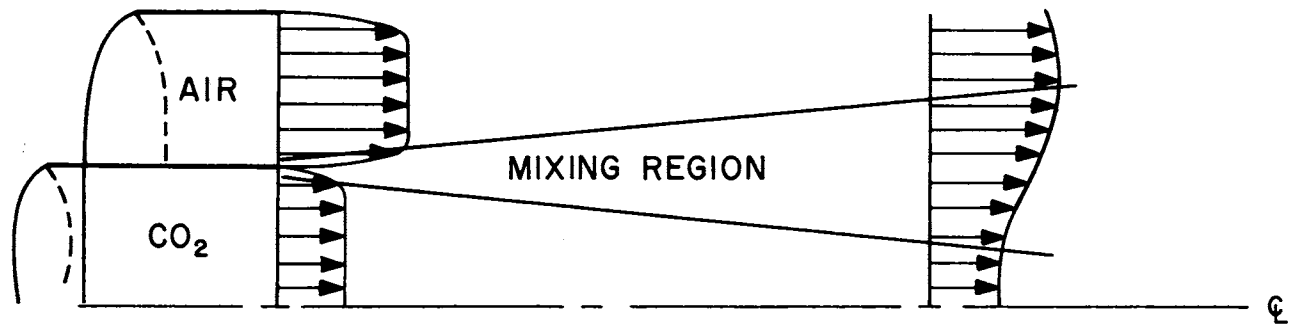


Figure 2. Constant Pressure, Two-Specie, Coaxial Jet Mixing Configuration

theory, could not be used. Consequently, slight modifications were made to account for this. These extensions and modifications are presented in Chapter V and also in Chapter V, there is contained a comparison of the numerical method results with those of the analytical theory.

Finally, it is important to note that, in this work, because of the type of flow field considered, only non-reacting perfect gases were considered. Further, while shock waves were absent from this investigation, the ability of this numerical method to describe flow fields containing such phenomena is suggested by the success contained in the above cited references.

CHAPTER II

DIFFERENTIAL EQUATIONS, TRANSPORT COEFFICIENTS, AND BOUNDARY AND INITIAL CONDITIONS

The determination of the detailed description of a fluid flow field requires application of partial differential equations to appropriate boundary conditions. The first task in any analysis, then, is to develop differential equations which describe local, or pointwise, phenomenological behavior of the variations of the dependent variables. In addition, initial and boundary conditions, which accurately model a particular situation, must be specified. In this chapter, therefore, attention is directed toward these topics.

Basic Equations

Since it was the attempt of the work herein described to determine a steady-state solution as an asymptotic result of a transient calculation for a turbulent flow condition, the appropriate fluid flow differential equations must exhibit a transient nature and permit implementation of expressions presumed to describe the turbulence phenomenon. By first assuming that all dependent variables are time dependent and, further, that the flow, assumed to be purely

turbulent, is of such a nature that laminar momentum and specie transport, and viscous flow work are of negligible importance, the axisymmetric differential equations for the conservation of mass, momentum, energy, and specie may be written (see Appendix A for the derivation and further discussion):

Conservation of mass:

$$\frac{\partial \rho}{\partial t} + \frac{\partial \rho v}{\partial r} + \frac{\partial \rho u}{\partial z} + \frac{\rho v}{r} = 0 \quad (2-1)$$

Radial conservation of momentum:

$$\frac{\partial \rho v}{\partial t} + \frac{\partial}{\partial r} (\rho v^2 + p) + \frac{\partial}{\partial z} (\rho v u) + \frac{\rho v^2}{r} = 0 \quad (2-2)$$

Axial conservation of momentum:

$$\frac{\partial \rho u}{\partial t} + \frac{\partial}{\partial r} (\rho u v) + \frac{\partial}{\partial z} (\rho u^2 + p) + \frac{\rho u v}{r} = 0 \quad (2-3)$$

Conservation of energy:

$$\frac{\partial}{\partial t} (\rho h_o - p) + \frac{\partial}{\partial r} (\rho v h_o) + \frac{\partial}{\partial z} (\rho u h_o) + \frac{\rho v h_o}{r} = 0 \quad (2-4)$$

Conservation of specie:

$$\frac{\partial \rho \omega_i}{\partial t} + \frac{\partial}{\partial r} (\rho v \omega_i) + \frac{\partial}{\partial z} (\rho u \omega_i) + \frac{\rho v \omega_i}{r} = 0 \quad (2-5)$$

$$i = 1, 2, \dots, N-1$$

and:

$$\omega_N = 1 - \sum_{i=1}^{N-1} \omega_i \quad (2-6)$$

where:

$$h_o = h + \frac{1}{2} V^2 \quad (2-7)$$

In addition to the principle assumptions delineated above, it was also assumed that there existed no body forces of sufficient significance for application in the momentum equation, that energy fluxes due to concentration gradients, pressure gradients, and body forces (Dufour effect) were unimportant, and that specie diffusion due to pressure gradients and temperature gradients (Soret effect) were also unimportant. Moreover, since application is intended solely for completely turbulent flow, all laminar, or molecular, contributions to transport of momentum, energy, and specie were considered inconsequential.

Perturbation Scheme

While equations (2-1) to (2-7) are presumed to describe the local variations of the dependent variables in (r, z, t) space, they are not practically useful within the framework of the present "state-of-the-art" turbulent flow analysis. In order to transform these equations into a more useful form, a widely adopted postulate, by and large corroborated by experiment (Reference 5) and believed to be an acceptable description of the turbulence for the case here considered, was employed. The substance of the postulate supposes that each dependent variable may be decomposed into an average value (later denoted by a bar) and a fluctuation value (later denoted by a prime) measured about the mean value. The significance of this postulate is embodied in the time-averaging of the differential equations which

result after substitution into equations (2-1) through (2-7) of the decomposing expressions for the dependent variables.

Because straightforward decomposition and substitution of each dependent variable results in a labyrinth of algebra (not to mention the evolution of terms for which there is currently no phenomenological understanding), simplifications were made in the spirit of the suggestion of Van Driest (46). Consequently, the dependent variable decomposition scheme, which was found useful in this work, is:

$$\begin{aligned}
 \rho u &= \overline{\rho u} + (\rho u)' & h &= \overline{h} + h' \\
 \rho v &= \overline{\rho v} + (\rho v)' & \rho &= \overline{\rho} + \rho' \\
 u &= \overline{u} + u' & \omega_i &= \overline{\omega}_i + \omega_i' \\
 v &= \overline{v} + v' & p &= \overline{p} + p'
 \end{aligned} \tag{2-8}$$

By employing equations (2-8) in two different ways, two sets of perturbed, time-averaged differential equations were derived. However, because of the enormous amount of computer time required to study both sets of equations, and because one set of equations seemed to be more in line with physical reasoning, only one of the two sets of perturbed, time-averaged differential equations was used and is here presented.

Conservation of mass:

$$\frac{\partial \overline{\rho}}{\partial t} + \frac{\partial \overline{\rho v}}{\partial r} + \frac{\partial \overline{\rho u}}{\partial z} + \frac{\overline{\rho v}}{r} = 0 \tag{2-9}$$

Radial conservation of momentum:

$$\begin{aligned} \frac{\partial \overline{\rho v}}{\partial t} + \frac{\partial}{\partial r} [\overline{\rho v v} + \overline{(\rho v)'v'} + \overline{p}] + \frac{\partial}{\partial z} [\overline{\rho v u} + \overline{(\rho v)'u'}] \\ + \frac{\overline{\rho v v} + \overline{(\rho v)'v'}}{r} = 0 \end{aligned} \quad (2-10)$$

Axial conservation of momentum:

$$\begin{aligned} \frac{\partial \overline{\rho u}}{\partial t} + \frac{\partial}{\partial r} [\overline{\rho u v} + \overline{(\rho u)'v'}] + \frac{\partial}{\partial z} [\overline{\rho u u} + \overline{(\rho u)'u'} + \overline{p}] \\ + \frac{\overline{\rho u v} + \overline{(\rho u)'v'}}{r} = 0 \end{aligned} \quad (2-11)$$

Conservation of energy:

$$\begin{aligned} \frac{\partial}{\partial t} [\overline{\rho h} + \frac{1}{2} \overline{\rho V^2} - \overline{p}] + \frac{\partial}{\partial r} [\overline{\rho v h} + \overline{(\rho v)'h'} + \frac{1}{2} \overline{\rho v V^2} + \overline{u(\rho v)'u'} \\ + \overline{v(\rho v)'v'}] + \frac{\partial}{\partial z} [\overline{\rho u h} + \overline{(\rho u)'h'} + \frac{1}{2} \overline{\rho u V^2} + \overline{u(\rho u)'u'} \\ + \overline{v(\rho u)'v'}] + \frac{\overline{\rho v h} + \overline{(\rho v)'h'} + 1/2 \overline{\rho v V^2} + \overline{u(\rho v)'u'} + \overline{v(\rho v)'v'}}{r} = 0 \end{aligned} \quad (2-12)$$

Conservation of specie:

$$\begin{aligned} \frac{\partial}{\partial t} \overline{\rho \omega_i} + \frac{\partial}{\partial r} [\overline{\rho v \omega_i} + \overline{(\rho v)'\omega_i'}] + \frac{\partial}{\partial z} [\overline{\rho u \omega_i} + \overline{(\rho u)'\omega_i'}] \\ + \frac{\overline{\rho v \omega_i} + \overline{(\rho v)'\omega_i'}}{r} = 0 \end{aligned} \quad (2-13)$$

where:

$$\overline{V^2} = \overline{u^2} + \overline{v^2} \quad (2-14)$$

See Appendix B for a detailed description of the perturbation scheme and a listing of both sets of time-average, perturbed differential equations.

In order for time averaged assumptions, presented below, to have meaning, brief consideration must be given to the time-averaging process, especially since the dependent variables (both the mean and fluctuation parts) are assumed to be a function of time. In the development of a mathematical description of turbulence, analysis is not applied to a particular time-history of the dependent variables that might result from a particular experiment. Rather, before time averaging a dependent variable, an average of many time-histories for repeated experiments must be performed. Indeed, because of the nature of turbulent flow and the lack of knowledge of the random processes involved in turbulent flows, consideration must be given to an ensemble of turbulent flows for the case under consideration (Reference 47). Therefore, the ignorance of turbulence is reflected by viewing all dependent variables as ensemble averages and consistency of the mathematics is maintained. Moreover, with the adoption of this concept, the conventional time averaging process (Reference 6) led to no mathematical difficulties. Specifically, if g is taken to represent any ensemble averaged dependent variable (mean, fluctuation, or product of fluctuation variables), the time-average value of the ensemble average g , denoted by \bar{g} , is determined by:

$$\bar{g} = \frac{1}{\Delta t} \int_t^{t + \Delta t} g(r, z, t) dt \quad (2-15)$$

where Δt is permitted to approach zero. Time-averaging of a differential equation, then, is accomplished by applying the concept indicated in equation (2-15) termwise to each differential equation.

After substitution of equations (2-8) into equations (2-1) through (2-8) and subsequent time-averaging, the following additional assumptions were made:

- 1.) $\overline{(u')^2} \ll \bar{u}^2$ and $\overline{(v')^2} \ll \bar{v}^2$
- 2.) $\bar{u} \overline{\rho' u'} \ll 1/2 \bar{\rho} \bar{u}^2$ and $\bar{v} \overline{\rho' v'} \ll 1/2 \bar{\rho} \bar{v}^2$
- 3.) $\overline{\rho' h'} \ll \bar{\rho} \bar{h}$

Assumption 3 above is one of several alternatives. It is possible to perturb ρh as one entity instead of the individual constituents; alternatively, it might be assumed in lieu of assumption 3, that ρ' and h' are uncorrelated. Obviously, a myriad of possibilities exist in the development of any system of differential equations which find application in turbulent flow analysis. The above arguments and assumptions represent one system of equations by which an attempt has been made to retain as much generality as current experimental knowledge of turbulent flow would permit.

Finally, special attention is directed to the enthalpy expression in equations (2-8). While perturbation of enthalpy in a single specie turbulent mixing process amounts to perturbation of temperature, the same perturbation assumption in multispecie studies for constant property nonreactive gases, incorporates, in addition to a temperature fluctuation, a concentration fluctuation since enthalpy

for a multispecie gas is a function of both the temperature and the concentrations of the cases involved.

Turbulent Transport Expressions

In order to utilize equations (2-9) through (2-13), it is necessary to specify phenomenological expressions for terms such as $\overline{(\rho v)'h'}$. Recourse was made to an analogue of laminar flow first suggested by Boussinesq and related by Schlichting (6):

$$-\overline{(\rho u)'v'} = \tau_{rz}^{(t)} = A_m \frac{\partial \bar{u}}{\partial r} \quad (2-16)$$

The essence of equation (2-16) relates assumed correlated, time-averaged perturbations such as $\overline{(\rho u)'v'}$, called "Reynolds stresses," to the product of some phenomenological coefficient, A_m , variously called an "apparent," "eddy," or "virtual" viscosity, and a partial derivative of a mean velocity. Since this hypothesis is an "a posteriori" development, the relationship of these turbulent transport expressions to physical reality is somewhat nebulous although pragmatic. Consequently, the specification of the exact expressions which are to relate assumed correlated, time-averaged, products of perturbed variables verges on arbitrariness.

However, by adopting Prandtl's physical concept of turbulent exchange of an agglomerate of fluid (Reference 6), two sets of expressions, assumed to represent turbulent transport phenomenon, were developed. Prandtl assumed that a lump of mass, for which an

average momentum, enthalpy, etc. could be assigned, moved some lateral distance, called the "mixing length" distance, while retaining its average properties. Once arriving at this new location, the lump of fluid mixes with the surrounding fluid, thereby producing a fluctuation in local properties. While the above discussion is somewhat a generalization of Prandtl's concept, as reported by Schlichting (6), it typifies the current understanding of turbulent flow.

Employment of this reasoning led to the theorization that the transport of axial momentum per unit volume, ρu , which results in an axial momentum fluctuation, $(\rho u)'$, is accompanied by a radial velocity fluctuation, v' . Furthermore, this process is precipitated by a radial gradient of axial velocity. Consequently, the terms $\overline{(\rho u)'v'}$ and $\overline{(\rho v)'u'}$ were expressed:

$$-\overline{(\rho u)'v'} = \rho \epsilon_m \frac{\partial \bar{u}}{\partial r} \quad \text{and} \quad -\overline{(\rho v)'u'} = \rho \epsilon_m \frac{\partial \bar{v}}{\partial z} \quad (2-17)$$

where the apparent eddy viscosity, A_m , has been rewritten using a kinematic eddy viscosity ϵ_m . However, since there existed no "a priori" criterion or philosophy on which to base the form of the gradient, an alternate form for $\overline{(\rho u)'v'}$ and $\overline{(\rho v)'u'}$ exists. By theorizing that the fluctuation of axial momentum per unit volume is caused by a variation of the radial velocity in the axial direction, it was possible to write:

$$-\overline{(\rho u)'v'} = \rho \epsilon_m \frac{\partial \bar{v}}{\partial z} \quad \text{and} \quad -\overline{(\rho v)'u'} = \rho \epsilon_m \frac{\partial \bar{u}}{\partial r} \quad (2-18)$$

The apparent preference exhibited in the literature for only equations (2-17) appears to be due to use of the linearized boundary layer equations whereas the sweeping assumptions associated with these equations have not been employed here. Moreover, the achievement of the above stated goals of this work forbade the use of those classical assumptions.

Application of either of the above philosophies for specification of $\overline{(\rho u)'v'}$ and $\overline{(\rho v)'u'}$, resulted in:

$$-\overline{(\rho u)'u'} = \rho \epsilon_m \frac{\partial \bar{u}}{\partial z} \quad -\overline{(\rho v)'v'} = \rho \epsilon_m \frac{\partial \bar{v}}{\partial r} \quad (2-19)$$

and the assumption that, for example, an enthalpy fluctuation due to a fluctuation in ρu is associated with a gradient of enthalpy in the axial direction resulted in:

$$\begin{aligned} -\overline{(\rho v)'h'} &= \frac{\rho \epsilon_m}{Pr_t} \frac{\partial \bar{h}}{\partial r} & -\overline{(\rho v)'\omega_i'} &= \frac{\rho \epsilon_m}{Sc_{t,i}} \frac{\partial \bar{\omega}_i}{\partial r} \\ -\overline{(\rho u)'h'} &= \frac{\rho \epsilon_m}{Pr_t} \frac{\partial \bar{h}}{\partial z} & -\overline{(\rho u)'\omega_i'} &= \frac{\rho \epsilon_m}{Sc_{t,i}} \frac{\partial \bar{\omega}_i}{\partial z} \end{aligned} \quad (2-20)$$

where, in analogy with laminar flow,

$$Pr_t = \frac{\epsilon_m}{\epsilon_h} \quad Sc_{t,i} = \frac{\epsilon_m}{\epsilon_{ci}} \quad (2-21)$$

To complete the set of equations necessary for the description of multispecie turbulent flow it was assumed that the perfect gas equations applied. Therefore, a state equation could be written as:

$$p = \rho \bar{R} T \quad (2-22)$$

where \bar{R} is the appropriate gas constant evaluated by:

$$\bar{R} = \frac{N}{\sum_{i=1}^N R_i \omega_i} \quad (2-23)$$

Furthermore, the enthalpy was evaluated by:

$$h = \frac{\sum_{i=1}^N \frac{\gamma_i R_i \omega_i}{\gamma_i - 1}}{N} \frac{P}{\rho} \quad (2-24)$$

The set of equations used in this analysis, then, consisted of the time-averaged, perturbed differential equations (2-9) through (2-14) with a combination of the expressions (2-17) through (2-20) and the auxiliary expressions (2-22) through (2-24). In cases presented in this work, equations (2-19) and (2-20) were generally used. However, in one application, to study the effect of differing assumptions for $\overline{(\rho u)'v'}$ and $\overline{(\rho v)'u'}$, equations (2-17) and equations (2-19) and (2-20) were employed in the differential equations for a set of boundary conditions, and then, equations (2-18) and equations (2-19) and (2-20) were used for the same boundary conditions and the results compared. Use of the former set will be referred to as "Case I" while application employing the latter set will be referred to as "Case II." Consideration was not given to both sets used together.

Transport Coefficients

The above discussion has presumed knowledge of the turbulent transport coefficients, Pr_t and $Sc_{t,i}$, and the eddy viscosity. However, because of the nature of turbulent flow, it is precisely the acquisition of this data that has retarded the analysis of turbulent flow problems. In fact, whereas the analogous transport coefficients for laminar flow are well known properties, the turbulent transport counterparts have thus far eluded definition in terms of functional relationships involving fluid properties and mean flow variables. Nonetheless, a cursory review of the literature reveals nearly as many proposed formulations, developed on a myriad of foundations, as investigators.

Fundamental to the precipitation of this condition is the realization that, to date, an understanding of the exact and detailed mechanism of turbulence has yet to be developed. Certainly, it is recognized that such quantities as free stream turbulence due to upstream influences, wall protuberances, pressure gradients, and high shear gradients effect both transition and turbulent flow development; but, it was, and is, the lack of knowledge of the exact interrelationship of such variables that has led, and currently does force, many investigators to postulate mathematical models which are based on limited information, and which require at least one experimentally determined constant. Furthermore, a very detailed experimental

investigation, which would determine exact occurrence for a particular situation, could not be used as a sole basis for a description of turbulence since each turbulent flow is itself unique; thus, any general description of turbulence must be viewed as a representation of an ensemble, in the statistical sense, of all possible turbulent flows.

With the recognition of the difficulties in a detailed analysis of a turbulent flow field, investigators have generally attacked the problem from one of two approaches -- both presently requiring empirical information. On the one hand, the phenomenon of turbulence is considered in a manner analogous to the kinetic theory of gases. Alternatively, a gross over-all phenomenological consideration has arisen. By the very way in which the above differential equations have been derived, the phenomenological approach has been implicitly assumed. However, since the statistical view point represents a possible avenue for turbulent flow analysis, brief consideration will be given to it at this juncture.

Basically, the statistical approach to turbulence assumes that the continuity equation and the momentum (Navier-Stokes) equations describe the instantaneous condition in a fluid flow field. Upon perturbation and time-averaging, in a manner similar to that presented above, a set of equations, similar in form to equations (2-9) through (2-11), result. In order to apply these equations, statistical assumptions, based on experimental data, are made for the correlated,

perturbed, time-averaged terms. Donaldson (48), for example, in an attempt to study transition in an incompressible flow over a flat plate, makes some assumptions relating second and third order correlations.

Because the development of the statistical approach is still somewhat in the embryonic stage, consideration has been restricted almost entirely to incompressible turbulent boundary layers on a flat plate. Consequently, a thermodynamic energy equation is not necessary for a complete set of equations. However, common to many investigators is the employment of an equation which represents a balance among the production, dissipation, and diffusion of the turbulent kinetic energy (49). This equation is often termed the "energy" equation, and it contains, as in the case of the continuity and momentum equations, perturbed, time-averaged, correlated terms. Bradshaw et al (50) includes this energy equation in the appropriate system of equations and assumes that the turbulent intensity is directly proportional to the local shear stress, that the dissipation rate is determined by the local shear stress and a length scale, and that the energy diffusion is directly proportional to the local shear stress with a factor depending on the maximum value of this shear stress. With the solution of the differential equations by use of the method of characteristics, apparently excellent agreement with experiment was achieved.

Although the technique presented in Reference 50 displays great promise in the analysis of turbulent flows, its state of development is not nearly sufficiently advanced for the analysis of the more complex problems of current interest. However, it is significant to note that one of the principal points that Bradshaw, et al. strives so hard to make is that the turbulent shear stress is not simply related to the velocity gradient as suggested in equations (2-17) through (2-19). Moreover, the acceptance of this suggestion implies that the relationships (2-20) are likely not to represent adequately the turbulence phenomenon. While contemplating these thought it should also be borne in mind that the statistical approach has thus far been limited to incompressible uniform type of flow. Consequently, only momentum transport in the vicinity of a wall has been considered. G. I. Taylor (51) points out that wall turbulence effects differ from free jet turbulence effects. On the other hand, the phenomenological approach, while making rather sweeping assumptions regarding turbulent transport processes, has demonstrated moderate success in a wide variety of turbulent flow problems (see Reference 6). Consequently, until turbulence is more fully understood and the statistical method refined, the phenomenological method offers the best immediate gains in the solution of many current turbulent flow situations.

The phenomenological approach is primarily based on the assumption that turbulent transport terms which appear in the perturbed, time-averaged differential equations, equations (2-10)

through (2-13), may be simply expressed in terms of mean flow values by an analogy with laminar transport expressions. Therefore, equations (2-17) through (2-21) result -- the phenomenological viewpoint was adopted for this work. This assumption is predicated on the supposition that it is possible to determine expressions for the eddy viscosity, the turbulent Prandtl number, Pr_t , and the turbulent Schmidt number, $Sc_{t,i}$ (or turbulent Lewis number $Le_{t,i}$).

At this juncture a brief presentation of suggested eddy viscosities ensues, followed by a discussion of the turbulent Prandtl and Schmidt numbers. Notice that these quantities only have relevance within the framework of the phenomenological viewpoint. Furthermore, it might be noted in passing that this viewpoint appears to be the most popular within the realm of turbulent flow. This is due, no doubt, to the lack of involved mathematics which seems to pervade the statistical approach. As a consequence of this popularity, a myriad of formulations for the eddy viscosity have been developed.

One of the first and most prolific analysts in the eddy viscosity field was Prandtl (see Reference 6). He idealized turbulent motion by considering agglomerations of fluid which travel some length, l , called the "mixing length." This length is analogous to the kinetic theory mean-free-path for molecules and, in traversing the mixing length distance, the agglomerations, or lumps, of fluid retain the properties they initially had before this submotion on the mean motion occurred. Upon arriving at the new location the lump of fluid

mixes with the surrounding fluid which produces a fluctuation in the fluid properties (such as velocity, density, etc.) at the new location. This line of reasoning led to the "mixing-length" eddy viscosity:

$$\epsilon_m = \ell^2 \left| \frac{\partial \bar{u}}{\partial y} \right| \quad (2-25)$$

While it may appear that this formulation does not represent an improvement since ℓ is not a fluid property, as Schlichting (6) points out, under some circumstances it is easier to make plausible assumptions regarding the form of ℓ than it is to assume expressions for ϵ_m . Nikuradse (52) (reported by Schlichting (6)) found that a plot of the ratio of ℓ to R , a pipe radius, versus the radial coordinate, normalized by R , was independent of the Reynolds number for a smooth pipe. Also, it was observed that a linear variation of ℓ in the vicinity of the wall was a good approximation. In considering several free jets, Tollmien (53) achieved only fair agreement with experiment with the assumption that ℓ is a linear function of the axial coordinate of a free jet.

G. I. Taylor (51) argued that vorticity was transferred rather than momentum as Prandtl suggested. His derivation resulted in a similar formulation for ϵ_m except that his mixing length differed by a factor of $\sqrt{2}$ from Prandtl's mixing length. The significance of Taylor's result is that the region of temperature variations due to, say, turbulent mixing of two streams of differing temperatures should be larger than the region of velocity variations. Prandtl's

formulation would not predict such a difference. As is well known, this difference does exist. However, in contrast to Prandtl's expression, Taylor's formulation has not found wide application.

With a philosophy somewhat similar to that of Taylor's, others, for example Black (54), have attempted to describe a turbulent flow field by a system of vortex patterns. Black supposes that a vortical system dictates the velocity and shear stress distributions and a "tempo-spatial" sublayer instability generates and maintains the characteristic vortex structures. However, this approach is still in the embryonic stages, as is the statistical approach.

From an analysis of free jet data collected by H. Reichardt, Prandtl derived another expression for the eddy viscosity (see Reference 6). In his derivation, Prandtl assumed that the dimensions of the lumps of fluid which move in a transverse direction during turbulent mixing are of the same order of magnitude as the width of the mixing zone. The formulation which results was termed the "constant exchange" eddy viscosity:

$$\epsilon = c_1 b (u_{\max} - u_{\min}) \quad (2-26)$$

Although the experimental data was for a jet which mixes with a quiescent surrounding, Prandtl generalized his idea to arrive at expression (2-26). Goertler (see Reference 6) applied Prandtl's "constant exchange" expression in an analysis of Reichardt's data and found excellent agreement. Moreover, Goertler's analysis was

for the more general case of two stream jet mixing. More will be said about this later.

However, Prandtl's original expression leads to the obvious realization that, at $u_{\max} = u_{\min}$, $\epsilon_m = 0$. This implication has been demonstrated to be incorrect by the results of the experiments of Forstall and Shapiro (55) and, more recently by Alpinieri (56). Recognizing this disparity between equation (2-26) and experiment, investigators suggested new expressions which generally amount to some alteration of Prandtl's expression (equation (2-26)). Perhaps foremost among the many are those suggested by Ferri, et al (57), Alpinieri (56), and Boehman (58). The expression suggested by Ferri eliminates the objection to Prandtl's expression; but it results in a similar singularity for $\rho_e v_e = \rho_j u_j$. Consequently, it shows little value for general application. Alpinieri's formulation resulted from experiments conducted in the flow regimes where Prandtl's and Ferri's correlations indicated zero eddy viscosity. While this new correlation shows great promise and is free from objections, it has not been employed for cases outside of the range for which it has been developed. This criticism of Alpinieri's equation is generally true for every expression for eddy viscosity due to a lack of complete and accurate data with which several versions might be investigated.

In addition to the objections raised to Prandtl's and Ferri's eddy viscosities, recent investigators have considered the effects of

compressibility and radial variations of ϵ_m and $\rho\epsilon_m$. These effects have been, in some respects, segregated and, in other respects, integrated into one overall consideration. Where the effect of compressibility on a spreading rate parameter, σ , is considered, the effect of radial variations is generally ignored. However, others considered density variations, as a consequence of compressibility, to have the same effect as variations due to a difference in gas properties across the mixing region (as, for example, might occur when two streams of widely different molecular weights mix). In addition, these latter investigators considered the radial variations of ϵ_m due to the nature of turbulent mixing itself. The former group will be considered later.

Foremost in the latter group is, perhaps, Boehman (58) and Zakkay, et al (59) (60). Boehman assumes several similar velocity functions known to represent experimental data for two-stream incompressible turbulent jet mixing. Employing independently the conservation principles and experimental data, he shows that ϵ_m , as expected, does vary in the radial direction. In addition, in contrast to the results of Zakkay and Krause (60), Boehman's eddy viscosities display physically realizable variations with the radial coordinate.

Zakkay and Krause's reported radial variations of ϵ_m and $\rho\epsilon_m$ are incorrect because the authors specify a similar radial concentration profile, a centerline concentration decay, and a half radius

variation. Of these three functions, the last two were determined from data in Reference 59. As noted by Boehman, the conservation principles do not permit these to be independently specified.

Reference 60 also presents radial variations of ϵ_m and $\rho\epsilon_m$ which result from using a transform suggested by Ting and Libby in Reference 61. The essence of this transformation is a conversion of an incompressible eddy viscosity to one applicable to compressible flow. This conversion requires knowledge of the radial density profile. However, the results of this transformation, using the data of Reference 59, are in accord with the conclusions reached by Boehman. Therefore, this transformation admits possible practical application.

Inhibiting implementation of this transform, however, is the added complexity it implies. In addition, Reference 60 indicates that $\rho\epsilon_m$ is not a strong function of the radial coordinates, thus permitting it to be considered a constant. The problem still remains to determine which, ϵ_m or $\rho\epsilon_m$, should be used as either an average or a correct incompressible form for the Ting and Libby transformation.

Looking at the problem from another viewpoint, Maydew and Reed (19) presented thoroughly documented experimental results for a compressible jet mixing study. They concluded that the resulting similar velocity profiles were the same as those for incompressible mixing. Since similar velocity profiles for incompressible flow have been analytically derived using incompressible eddy viscosities

(generally Prandtl's) and have been shown to compare very favorably with experiment, one is led to conjecture the use of incompressible eddy viscosities which are constant in the radial direction (especially in the light of the conclusions drawn from the results of the Ting and Libby transformation reported by Zakkay and Krause (60)). Before pursuing this thought further, however, several facets of Reference 19 must be noted.

For the similar profiles considered by Maydew and Reed, a jet spreading rate parameter, σ , was used with Prandtl's eddy viscosity. For incompressible flow it has been found that σ is a constant. However, for compressible flow experiment, specifically Maydew and Reed's, it has been found that σ is a function of the jet exit Mach number (assuming a free jet). In essence, then, the effect of compressibility is contained in the parameter σ , while ϵ_m is assumed to be a function of the axial coordinate only. Furthermore, since compressible velocity profiles have been found to be essentially the same as those for incompressible flow, the use of an incompressible eddy viscosity should be adequate.

There is, however, one drawback. The experiments of Maydew and Reed were for an isoenergetic free jet of air mixing with air. While the variation of σ with compressibility (Mach number) has been considered, investigation of variations of σ for cases of two gases of widely different densities has yet to be conducted. Since the

results presented in this paper are for mixing of CO_2 with air, this drawback was not considered significant.

Rather than use Prandtl's eddy viscosity in its original form, further consideration was given to the form of ϵ_m . In the derivation presented by Goertler (see Reference 6), for the case of two-stream incompressible jet mixing, if one makes a simple substitution for the constants in equation (2-26) and uses the results of Goertler, it will be discovered that ϵ_m takes the form

$$\epsilon_m = \frac{z}{4\sigma^2} (u_{\max} + u_{\min}) \quad (2-27)$$

This form of the eddy viscosity has been used by Korst (6) in his analytical theory. Notice that this form does not display the objections previously raised. In fact, the case of $u_e = u_j$ may be viewed as a problem of determining the appropriate σ (experimentally by use of a tracer gas). In this light, equation (2-27) may be viewed as a definition of σ much the same as the convective heat transfer equation defines h , the convective heat transfer coefficient. Furthermore, the variation of σ with large density gradient across the mixing region may be well worth considering in future experiments.

It needs yet to be mentioned that the incorporation of an eddy viscosity in an iterative computer program requires that the expression be as simple as possible for feasible run times. Furthermore, since numerical method techniques have the tendency to "smear" any

regions containing gradients, only a reasonable approximation of ϵ_m is required.

Thus far, the discussion has centered on the eddy viscosity (momentum transport coefficient). The energy and specie transport coefficients are related to the eddy viscosity by the turbulent Prandtl and Schmidt numbers respectively. Implicit, of course, are the assumptions that, first, such quantities as the turbulent Prandtl and Schmidt numbers can be meaningfully expressed in terms of the mean flow variables and, second, that such quantities are more easily expressed than the respective transport coefficients themselves.

While, certainly, definitive proofs of the above assertions are lacking (and are most likely to remain so), it appears that good approximations can be made. In fact, experimental data, as the following discussion will show, indicate that, at worst, the turbulent Prandtl and Schmidt numbers are a function of the axial coordinate only (free jet mixing), and, generally, it is sufficient to assume these quantities constant. The precise value of these quantities varies from investigator to investigator and naturally the values quoted are associated with a particular theory under consideration. This is due to a lack of a concise definition which would precisely explain what these turbulent quantities are.

In their classical experiment, Forstall and Shapiro (55) used experimental data, together with Squire and Trouncer's (62) mixing length coefficient and integral method, to determine a turbulent

Prandtl and Schmidt number equal to 0.7 (and therefore a turbulent Lewis number of unity).

Both Kleinstein (11) and Alpinieri (56) investigated experimental data for constant pressure coaxial jet mixing using an analytical method presented by Libby (10). The analytical method transforms the boundary layer turbulent flow differential equations into the von Mises coordinates. The solution in the transformed plane is that of the heat conduction equation. The eddy viscosity and turbulent Prandtl and Schmidt numbers act as coordinate stretchers. While the solution in the transformed plane does not require knowledge of the turbulent transport coefficients, transformation back to the physical plane does require knowledge of these quantities. With the use of this feature of the analytical solution, Kleinstein determined the turbulent Schmidt number to be 0.708 and the turbulent Prandtl number to be 0.715. He considered an air jet exhausting into a quiescent air receiver for the determination of the Prandtl number and helium-air injection data from the experiments of Kergy and Weller (63) for the determination of the Schmidt number. These experiments and the subsequent results are for the "main" region of mixing (i. e. the region downstream of where the mixing has affected the centerline -- upstream of this location is termed the "potential core" region).

Alpinieri (56) found that the turbulent Schmidt number varied between 0.5 and 0.7 in the main region of mixing of a hydrogen jet exhausting into an air stream with the same velocity. Moreover, in

his analysis of the experimental data he showed that, in the main region of mixing, turbulent Schmidt numbers of 0.6 and 1.0 produced identical results.

Zakkay, et al (59) investigated analytically and experimentally hydrogen, helium, and argon jets individually exhausting into a coaxial moving air stream. They also investigated the main region of mixing and determined the turbulent Schmidt number to vary between 0.3 and 2.3 and the turbulent Lewis number to vary between 0.4 and 1.0. The wide variation of these variables can possibly be explained by considering the technique employed for their evaluation. The laminar conservation differential equations are assumed to describe turbulent flow where the laminar transport coefficients are supposed then to be the turbulent analogues. These equations were solved for these turbulent transport coefficients (here under consideration) and evaluation was considered at the centerline. In order to carry out this evaluation, first and second derivatives on the centerline were necessary. These derivatives were determined by casting six radial experimental data points, at several axial locations, into similar profile expressions for the axial velocity and concentration.

Morganthaler (64) discussed this work and points out: (1) six widely spaced data points are insufficient for the determination of first and second derivatives on the centerline, (2) Hinze (49) shows that true similarity does not exist for the general case considered in Reference 59, and (3) in the reduction of the raw data, a constant

stagnation temperature is assumed which, from consideration of the assumed energy equation, requires that the turbulent Prandtl and Lewis numbers be equal to unity.

Emmons (31) considered the rate at which liquid droplets diffused in a gas stream. By injecting liquid diesel fluid into a turbulent airstream and comparing concentration measurements at various axial locations to similar data obtained with naphtha gas as the injected fuel, he found that the gas to liquid Lewis numbers varied approximately from 1.2 to 2.0.

Finally, Forde (24) compared the mixing region width for concentration to that for velocity in the potential core region. With the use of this scheme for the determination of the turbulent Schmidt number Forde determined $Sc_t = 0.92$. Forde's experiments were for CO_2 co-axially mixing with an airstream. The data from this reference was used for comparison.

As the above discussion has indicated, there are a large number of eddy viscosities available for use in a turbulent flow analysis. One then must select a particular form for ϵ_m that best suits his needs. Since most of the formulations discussed above are functions of a "half-radius" (that radius where the velocity has a value equal to the average of the adjacent free stream velocities), a quantity that is not readily determinable with the scheme suggested in this work, and since an iterative procedure, such as employed here,

demands as simple an expression as possible for feasible computer run times, equation (2-27) was selected for application in this work.

Further, as the above discussion also indicated, the turbulent Prandtl and Schmidt numbers tend to be constant. The question is: "What are their values?" Because comparison was to be made with the experimental data of Reference 24, the Schmidt number that was reported in that reference was used for all cases. Since the above discussed experiment data indicated that the turbulent Lewis number tended to be approximately one, the turbulent Prandtl number was assumed to be equal to the turbulent Schmidt number.

Boundary and Initial Conditions

Now that the equations which describe turbulent flow have been developed, specification of the boundary and initial conditions is necessary. That is, the conditions which define a flow problem must be described mathematically. In this section the conditions necessary for the description of the multispecies, coaxial, compressible, turbulent jet mixing geometry depicted in Figure 3 will be delineated. Chapter IV contains a detailed discussion of the reasons for the selection of this problem.

Because an asymptotic steady state solution was desired it was necessary to define initial conditions for the entire flow field and boundary conditions for all time under consideration. Two different initial conditions were considered in this analysis. One initial

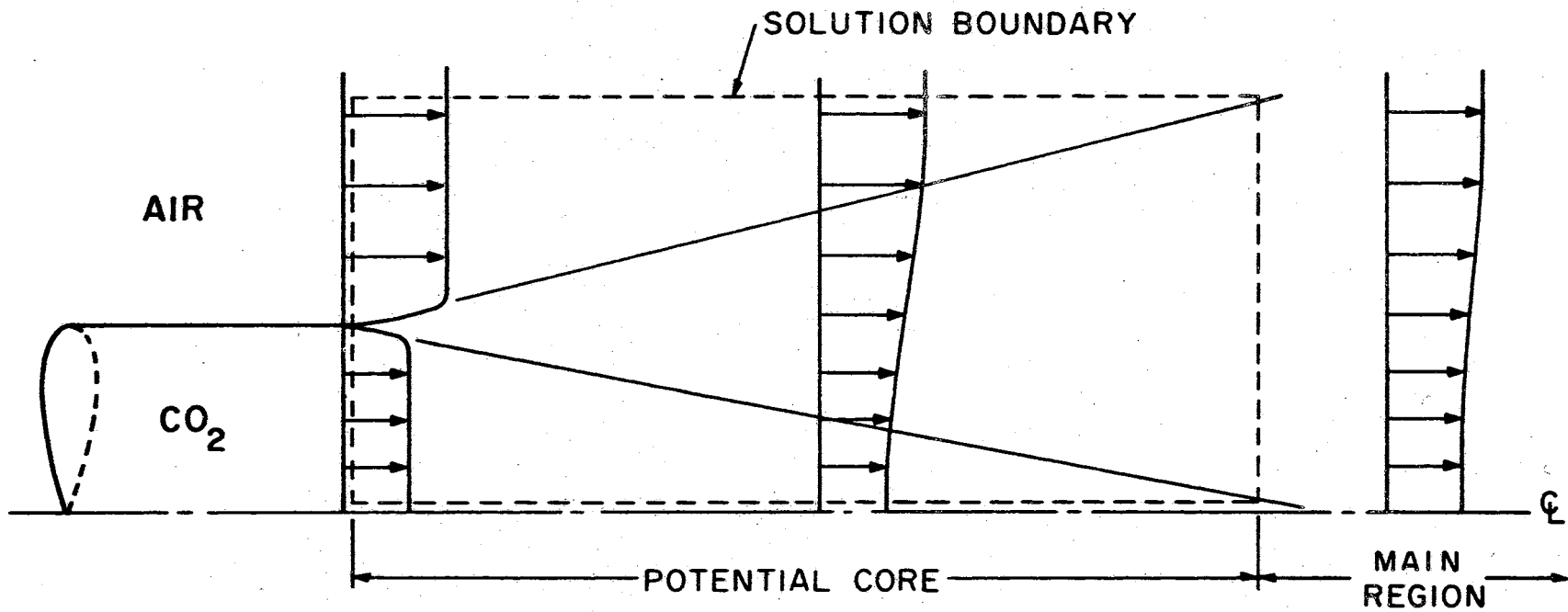


Figure 3. The Flow Field and Solution Boundaries

condition assumed that the entire flow field was exactly the same as the upstream boundary conditions. That is, radial profile of all dependent variables assumed at the upstream boundary was exactly the same at all downstream locations. In essence, then, physically, at successive times, the solution represented what would result if the initial conditions were as just described. The adoption of this viewpoint is predicated on the assumption that, if the calculation is made for sufficiently long times, initial condition discrepancies will be immaterial (assuming, of course, that the boundary conditions are constant with time).

The other initial condition that was assumed employed the results for the analytic solution developed in Chapter V. This analytic solution is for a steady state case and, consequently, it should be close to the correct solution which results from the numerical analysis thus reducing the time for computer computation.

The specification of the boundary conditions required some practical considerations of the technique for developing a solution. While it is hypothetically possible to consider exact integration of the equations developed in this chapter and, therefore, integrate to easily definable boundaries such as walls, in practice, since the solution was to be developed with the use of a numerical method on a digital computer which practically limits the storage available, a less convenient boundary had to be chosen. This boundary, and the region which it encloses, is shown in Figure 3. The exact length and width

of this region varied somewhat from computer run to computer run.

Because the exact upstream boundary which corresponds to the experimental results with which comparison was to be made was unknown, several different profiles for the dependent variables were assumed. However, each set of the assumed upstream profiles for the dependent variables were held constant with time for each computer run.

The top boundary was described by demanding that the radial gradients of all the dependent variables were zero. That is:

$$\frac{\partial f}{\partial r} = 0 \quad (2-28)$$

where f is a vector whose elements are:

$$f = (\rho, u, v, p, \omega_1, \omega_2). \quad (2-29)$$

The adoption of this assumption assumed that all significant gradients would be contained within the assumed boundaries and, consequently, a uniform flow (or zero radial derivative) could certainly be considered a legitimate boundary condition.

Moreover, this assumption was justified by Reference 24. In this reference, Forde indicates that the effect of mixing on the outer edge of the secondary stream did not influence the potential core region. No proof was given for this, however.

At the downstream boundary, both the values of the dependent variables and their gradients were permitted to be whatever the calculations required.

In a similar manner, the centerline dependent variables were determined by computation. However, the centerline was recognized to be a line of symmetry (the above differential equations have this condition incorporated in them) and, consequently, the radial velocity component was required to be zero.

Nondimensionalization Scheme

Rather than be encumbered by the units of the dependent variables, the nondimensional technique used by Walker (43) was employed. Briefly, the scheme consists of nondimensionalizing the thermodynamic properties of pressure and density by some appropriate reference values. In this work the reference pressure and density were taken to be those which exist at the center of the inner jet at the exit.

To nondimensionalize the velocity, it was required that the Mach number that is determined from dimensional quantities be equal to the Mach number that is determined from nondimensional quantities. If a prime (') denotes dimensional quantities and the lack of a prime denotes nondimensional quantities, the nondimensionalizing relationship for velocity has the form:

$$u = \sqrt{\frac{u'}{p' / \rho'}} \quad (2-30)$$

Lengths are nondimensionalized with respect to the inner jet exit radius and, from the use of any one of differential equations

presented above, time was nondimensionalized by

$$t = \frac{t'}{r_j} \sqrt{\rho_r' / \rho_r'} \quad (2-31)$$

With the use of this scheme the differential equations that were presented above have exactly the same form for both the nondimensionalized and the dimensionalized variables.

CHAPTER III

THE NUMERICAL METHOD

In order to solve the system of equations that were presented in Chapter II, recourse was made to implementation of a numerical method. Such an approach has certainly found its impetus with the advent of the digital computer. Moreover, as was pointed out in the introduction, the primary purpose of this work is to extend the capability of the Rusanov numerical method, which has shown remarkable success in solving a wide variety of problems thus far, to the problem of multispecies turbulent jet mixing. Consequently, this chapter is devoted to the description of the numerical method for this type of problem and, in addition, necessary supplementary numerical equations are presented.

The Rusanov Numerical Method

This method is based upon a technique presented by Von Neumann and Richtmyer (34) who suggested a scheme for the numerical solution of the one-dimensional gasdynamic equations in Lagrangian coordinates. The principle of Von Neumann and Richtmyer centered on the description of a moving shock wave. However, as

Rusanov (40) noted, Lagrangian coordinates are only convenient in one-dimensional problems. In multi-dimensional problems the Lagrangian coordinate system is so complex that there is seldom any doubt of the superiority of the Eulerian approach. Furthermore, Rusanov pointed out that, not only are the Lagrangian coordinates useless, but their use predicts unnecessarily distorted flow fields when applied to a numerical method.

In order to apply Von Neumann's scheme of artificial viscosity (which will be discussed below), the Rusanov method considers the differential conservation equations to be expressed as one matrix differential equation of the form:

$$\frac{\partial f}{\partial t} + \frac{\partial F^r}{\partial r} + \frac{\partial F^z}{\partial z} + \frac{\Psi}{r} = 0 \quad (3-1)$$

where, for the equations developed above, the dependent matrix variables have the form:

$$f = \begin{bmatrix} \rho \\ \rho u \\ \rho v \\ \rho h_o - p \\ \rho \omega_i \end{bmatrix} \quad F^r = \begin{bmatrix} \rho v \\ \rho uv + \overline{(\rho u)'v'} \\ \rho v^2 + p + \overline{(\rho v)'v'} \\ \rho v h_o + \overline{(\rho v)'h'} + u \overline{(\rho v)'u'} + v \overline{(\rho v)'v'} \\ \rho v \omega_i + \overline{(\rho v)'\omega'_i} \end{bmatrix}$$

$$F^z = \begin{bmatrix} \rho u \\ \rho u^2 + p + \overline{(\rho u)'u'} \\ \rho v u + \overline{(\rho v)'u'} \\ \rho u h_o + \overline{(\rho u)'h'} + u \overline{(\rho u)'u'} + v \overline{(\rho u)'v'} \\ \rho u \omega_i + \overline{(\rho u)'\omega'_i} \end{bmatrix} \quad (3-2)$$

$$\psi = \frac{\rho v}{\rho v^2} + \frac{(\overline{\rho u})'v'}{(\overline{\rho v})'v'} + \frac{\rho u h_0 + (\overline{\rho u})'h'}{\rho u \omega_i + (\overline{\rho v})'\omega_i'} + u(\overline{\rho u})'u' + v(\overline{\rho u})'v'$$

In the above equations, in addition to the assumptions made in Chapter II, second order correlations of the form $\overline{\rho' u'}$ and third order correlations of the form $\overline{\rho' u' v'}$ have been neglected. This permitted $\overline{\rho u} \overline{v}$ to be evaluated as $\overline{\rho} \overline{u} \overline{v}$ and transformed terms of the form $(\overline{\rho u})'v'$ (called "Reynolds stresses" above) into the more usual form $\overline{\rho} \overline{u'v'}$ thus maintaining consistency in the use of ρ_{sm} . It should also be recalled from the discussion of Chapter II, that the terms in equations (3-2) which represent turbulent transport of enthalpy and specie (which appear in the last two elements of each matrix with the exception of the f matrix) are expressed in terms of mean flow quantities always by equations (2-30). The terms in equation (3-3) which represent turbulent shear stresses are alternately expressed by equations (2-17), (2-19) and (2-20) (Case I) or by equations (2-18), (2-19) and (2-20) (Case II). The eddy viscosity was listed as equation (2-27).

While a rigorous demonstration that all finite-difference forms of equations (3-1) are unstable has not been presented, previous finite-difference attempts have not been successful. Consequently, addition terms have been added to equation (3-1) such that the stability of the resulting finite-difference equation might be enforced. The form of these additional terms, and the associated conditions imposed upon them, is precisely the significance of Von Neumann and Richtmyer's work. The Eulerian counterpart of this

modification, presented by Rusanov, assumes the form, in axisymmetric coordinates:

$$\frac{\partial f}{\partial r} + \frac{\partial F^r}{\partial r} + \frac{\partial F^z}{\partial r} + \frac{\psi}{r} = \frac{1}{r} \frac{\partial}{\partial r} \left[rA \frac{\partial f}{\partial r} \right] + \frac{\partial}{\partial z} \left[B \frac{\partial f}{\partial z} \right] \quad (3-3)$$

The coefficients A and B are determined from stability considerations. Specifically, A and B must be of such a nature that (see Reference 34 and 43):

1. the modified conservation equations result in solutions without discontinuities,
2. the thickness of discontinuities must be of the order of the spatial distances between node points,
3. the effect of the terms containing A and B must be negligible outside of regions of sharp discontinuities, and
4. the Rankine-Hugoniot equations must hold across shock layers, should shock waves exist in the flow field.

In this work a discontinuity of specie concentration, such as exists at the exit of the concentric nozzles (see Figure 3), was considered analogous to the property discontinuities which result across a shock wave.

With the supposition of the modified conservation differential equations (equation (3-3)), application is implemented by a finite-differencing of equation (3-3). To accomplish this finite-differencing,

a forward difference is used for the time derivative and centered differences are employed for all space derivatives (see References 43 and 44 for an illustration of this differencing).

Before presenting the result of this differencing scheme, some qualifying and clarifying remarks are in order. The very fact that a finite-difference approximation is made connotes the idea that a flow field will be described by a discrete number of points, or nodes, rather than a determination of the values of the flow variables at any arbitrary point. Each point will be identified by a pair of numbers (m, ℓ) such that the radial location is determined by $r = (m-1)\Delta r$ and the axial location by $z = (\ell-1)\Delta z$ where Δr and Δz are the radial and axial distances between node points respectively (see Figure 4). Notice that the centerline is described by $m = 1$ and the upstream boundary by $\ell = 1$. The number of steps in time is given by the superscript n .

The above description of the finite differencing scheme refers to a field point, that is, a point interior to the boundaries. Furthermore, the stability requirements presented below were determined from an analysis of the field point finite difference scheme. The last point of note concerns some of the elements of F^r , F^z , and Ψ matrices. If substitution is made for turbulent transport quantities in accordance with equations (2-17) through (2-20), it will be observed that derivatives which themselves must be finite differences, are contained in these matrices. The scheme for this finite differencing does

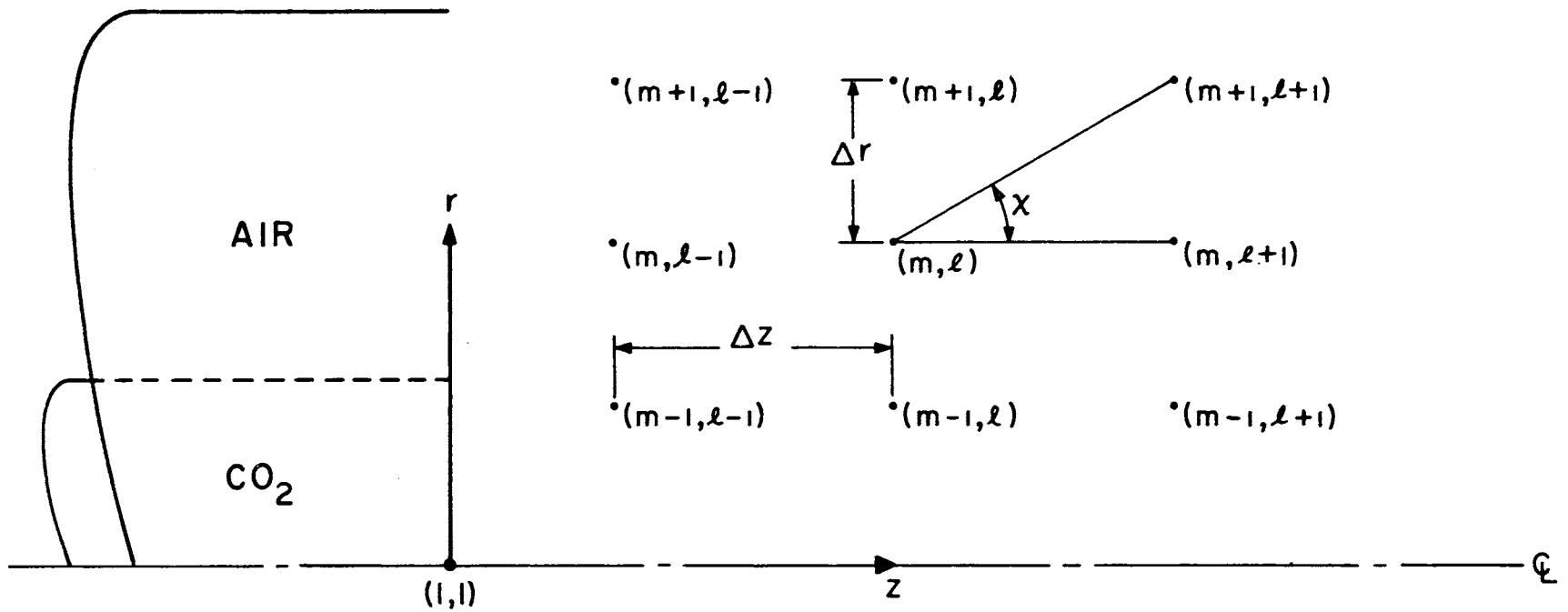


Figure 4. Node Point Nomenclature

not follow the rule outlined above.

If, then, a field point is considered and the differencing scheme that was outlined above is employed, the finite difference approximation of equation (3-3), which represents all the conservation principles, is:

$$\begin{aligned}
 f_{m, \ell}^{n+1} = & f_{m, \ell}^n - \frac{K_r}{2} [F_{m+1, \ell}^r - F_{m-1, \ell}^r] - \frac{K_z}{2} [F_{m, \ell+1}^z \\
 & - F_{m, \ell-1}^z] - \frac{K_r}{(m-1)} \Psi^n + \frac{1}{2(m-1)} [(m-1/2)\alpha_{m+1/2, \ell}^n \\
 & (f_{m+1, \ell}^n - f_{m, \ell}^n) - (m-3/2)\alpha_{m-1/2, \ell}^n (f_{m, \ell}^n - f_{m-1, \ell}^n)] \\
 & + \frac{1}{2} [\beta_{m, \ell+1/2}^n (f_{m, \ell+1}^n - f_{m, \ell}^n) - \beta_{m, \ell-1/2}^n (f_{m, \ell}^n - f_{m, \ell-1}^n)] ,
 \end{aligned} \tag{3-4}$$

where:

$$\begin{aligned}
 K_r = \frac{\Delta t}{\Delta r} & & K_z = \frac{\Delta t}{\Delta z} \\
 \alpha = \frac{2A\Delta t}{(\Delta r)^2} & & \beta = \frac{2B\Delta t}{(\Delta z)^2}
 \end{aligned} \tag{3-5}$$

In the application of equation (3-4), as well as all following equations, information was only known at node points. Consequently, information at the "half-spaces" could only be gotten from adjacent nodes. In the above equation, α and β were determined at the half-spaces by averaging their respective values at adjacent node points.

Because F^r , F^z , and Ψ themselves contain derivatives, consideration must be given to the technique that was employed for the differencing of these derivatives. In general, the differencing

scheme was so devised that only the eight points surrounding the point (m, ℓ) (see Figure 4) were used for field points. This overall plan was implemented by recognizing that four types of second derivatives may appear:

$$\frac{\partial}{\partial r} \left[s \frac{\partial t}{\partial r} \right], \quad \frac{\partial}{\partial z} \left[s \frac{\partial t}{\partial z} \right], \quad \frac{\partial}{\partial r} \left[s \frac{\partial t}{\partial z} \right], \quad \frac{\partial}{\partial z} \left[s \frac{\partial t}{\partial r} \right] \quad (3-6)$$

where s and t are generalized variables. The variable s may possibly represent: $\rho \epsilon_m$, $\rho \epsilon_m / Pr_t$, $\rho \epsilon_m / Sc_{t,i}$; and the variable t may possibly represent: u , v , h , w_1 .

It should be recognized that those terms which appear in (3-6) and whose outside derivative is $\frac{\partial}{\partial r}$ are associated with F^r only, and those terms, whose outside derivative is $\frac{\partial}{\partial z}$, are associated with F^z only; the Ψ matrix contains only first derivatives. Each term may be differenced in the following manner:

$$\begin{aligned} \frac{\partial}{\partial r} \left[s \frac{\partial t}{\partial r} \right] &\rightarrow \frac{1}{\Delta r} \left[\left(s \frac{\partial t}{\partial r} \right)_{m+1/2, \ell} - \left(s \frac{\partial t}{\partial r} \right)_{m-1/2, \ell} \right] \\ &\quad \frac{1}{2(\Delta r)} \left[\underbrace{2s_{m+1/2, \ell} (t_{m+1, \ell} - t_{m, \ell}) / \Delta r}_{\text{contained in } F_{m+1, \ell}^r} \right. \\ &\quad \left. - 2s_{m-1/2, \ell} (t_{m, \ell} - t_{m-1, \ell}) / \Delta r \right] \\ &\quad \underbrace{\hspace{10em}}_{\text{contained in } F_{m-1, \ell}^r} \end{aligned} \quad (3-7)$$

$$\begin{aligned}
\frac{\partial}{\partial z} \left[s \frac{\partial t}{\partial z} \right] &\rightarrow \frac{1}{\Delta z} \left[\left(s \frac{\partial t}{\partial z} \right)_{m, \ell+1/2} - \left(s \frac{\partial t}{\partial z} \right)_{m, \ell-1/2} \right] \\
&\quad \frac{1}{2(\Delta z)} \left[\underbrace{2s_{m, \ell+1/2} (t_{m, \ell+1} - t_{m, \ell-1}) / \Delta z}_{\text{contained in } F_{m, \ell+1}^z} \right. \\
&\quad \left. - 2s_{m, \ell-1/2} (t_{m, \ell} - t_{m, \ell-1}) / \Delta z \right] \\
&\quad \underbrace{\hspace{10em}}_{\text{contained in } F_{m, \ell-1}^z}
\end{aligned} \tag{3-8}$$

$$\begin{aligned}
\frac{\partial}{\partial r} \left[s \frac{\partial t}{\partial z} \right] &\rightarrow \frac{1}{2\Delta r} \left[\left(s \frac{\partial t}{\partial z} \right)_{m+1, \ell} - \left(s \frac{\partial t}{\partial z} \right)_{m-1, \ell} \right] \\
&\quad \frac{1}{2\Delta r} \left[\underbrace{s_{m+1, \ell} (t_{m+1, \ell+1} - t_{m+1, \ell-1}) / 2\Delta z}_{\text{contained in } F_{m+1, \ell}^r} \right. \\
&\quad \left. - s_{m-1, \ell} (t_{m-1, \ell+1} - t_{m-1, \ell-1}) / 2\Delta z \right] \\
&\quad \underbrace{\hspace{10em}}_{\text{contained in } F_{m-1, \ell}^r}
\end{aligned} \tag{3-9}$$

$$\begin{aligned}
\frac{\partial}{\partial z} \left[s \frac{\partial t}{\partial r} \right] &\rightarrow \frac{1}{2\Delta z} \left[\left(s \frac{\partial t}{\partial r} \right)_{m, \ell+1} - \left(s \frac{\partial t}{\partial r} \right)_{m, \ell-1} \right] \\
&\quad \frac{1}{2\Delta z} \left[\underbrace{s_{m, \ell+1} (t_{m+1, \ell+1} - t_{m-1, \ell+1}) / 2\Delta r}_{\text{contained in } F_{m, \ell+1}^z} \right. \\
&\quad \left. - s_{m, \ell-1} (t_{m+1, \ell-1} - t_{m-1, \ell-1}) / 2\Delta r \right] \\
&\quad \underbrace{\hspace{10em}}_{\text{contained in } f_{m, \ell-1}^z}
\end{aligned} \tag{3-10}$$

The 2's that have been inserted in equations (3-7) and (3-8) are for the purpose of maintaining consistency with the derivation of equation (3-4).

In the development of above system of equations, an attempt has been made to avoid the necessity of determining information at the half-spaces. This was done for computer programming convenience. Moreover, it was desired in this work to use only the eight surrounding nodes for the evaluation of a property at a central node (the downstream and centerline boundaries are exceptions). Further, where half-space information was required, all involved properties were first determined at the half-spaces by a linear interpretation and then the required combination of these was evaluated.

The procedures presented above were followed consistently for both the Case I and the Case II studies.

Stability Requirements

In the finite difference approximation (equation (3-4)) to the modified gasdynamic conservation equations (equation (3-3)), the variables $\alpha_{m, \ell}^n$ and $\beta_{m, \ell}^n$ were used in place of the coefficients A and B which were introduced in equation (3-3). Further, it should be noted that, in equation (3-4), it is implied by the subscript notation that both α and β are a function of location. This should certainly be expected by the very nature of the restrictions applied to A and B, and consequently, to α and β respectively. Moreover, since application utilizes equation (3-4), rather than develop stability relationships for A and B directly, expressions for α and β have been developed. In this section only a brief outline of the stability analysis technique and the results of the stability analysis will be presented. See References 43 and 44 for the detailed discussion and development of the expressions presented below.

One of the most common techniques employed in stability analysis of finite difference approximations to differential equations is a method which is attributed to Von Neumann and discussed in Reference 65. The stability scheme consists of assuming that, at some time step, the numerical value of a dependent variable that is calculated by use of the finite difference equation is different from the exact value which applies to the finite difference equations. This error is due to the practical limitations in evaluating any algebraic

equation. Instability results when, because of the nature of the finite difference scheme, these errors are permitted to grow with successive calculations. Von Neumann's stability analysis describes the production of an error as a perturbation of the mean value. The perturbation is then expanded in to a Fourier series. For stability, it is subsequently required that each term, at least, remain bounded but preferably, diminish with successive calculations.

Quite obviously, the mechanics of this analysis are dependent, ultimately, on the form of the approximated differential equation. Casual inspection indicates that the gasdynamic equations are nonlinear, and, as Richtmyer (39) has mentioned, there exists no rigorous analysis of stability for this first order nonlinear system of equations. The Von Neumann scheme which was outlined above, attacks a nonlinear system by applying the method to small regions so that the coefficients may be approximated by constants.

Rusanov (40) applied the Von Neumann stability analysis to the finite difference scheme presented in equations (3-4). The elements of f , F^x , F^z , and Ψ where those that apply to a two-dimensional inviscid flow, Walker (43) performed a stability analysis to a system of equations that were assumed to represent turbulent flow. He found that the incorporation of viscosity, albeit eddy viscosity, tended to relax the stability requirements so that a closer approximation (than is permitted by the inviscid stability requirements) to the correct

flow equations (equation (3-1)) by the modified flow equations (equations (3-3)) could be achieved.

At this juncture mention of a peculiarity of equation (3-3) is in order. If, for the moment, one considers the matrices in equation (3-1) to have only the elements that would produce the inviscid gasdynamic equations, then equation (3-3) has a form similar to the viscous gasdynamic equations (especially when consideration is limited to only the momentum equations). The addition of the terms on the right hand side of equation (3-3) has, therefore, the mathematical effect of adding an additional viscosity (an "artificial" or "pseudo" viscosity) to the gasdynamic equations. Consequently, it is not surprising that the incorporation of real viscosity (of the turbulent or laminar variety) relaxes the stability requirements defining the artificial viscosity. Of course, since turbulent shear stresses are much greater than laminar shear stresses, it should be anticipated that the relaxation of stability requirements will be greater in an analysis of turbulent flows than in an analysis of laminar flows.

Although Walker (43) performed a stability analysis which included turbulent viscosity, because of the immense complexity of the mathematics involved, he did not arrive at a definitive expression for the stability requirements for the turbulent conservation equations. In the analysis considered here, the stability requirements which are applicable to the inviscid gasdynamic equations (derived by Rusanov (40) and also by Walker (43)) were employed.

It was, however, recognized that the stability requirements for the inviscid gasdynamic equations could be relaxed and still achieve a stable solution. In fact, under this condition, a closer approximation of reality should be achieved, as will be observed below.

With the application of the Von Neumann linear stability analysis for the inviscid gasdynamic equations, Rusanov (40), and eventually Walker (43), developed expressions for $\alpha_{m, \ell}^n$ and $\beta_{m, \ell}^n$ of the form:

$$\alpha_{m, \ell}^n = \omega K(V+c)_{m, \ell}^n \sin^2 \chi \quad (3-11)$$

$$\beta_{m, \ell}^n = \omega K(V+c)_{m, \ell}^n \cos^2 \chi$$

where

$$K = [K_r^2 + K_z^2]^{1/2} \quad (3-12)$$

$$V = [u^2 + v^2]^{1/2} \quad (3-13)$$

and χ is the angle defined in Figure 4. The parameter ω has been termed the "damping parameter" and it is also obtained from stability considerations. Specifically, if the "Courant" number is defined by:

$$\bar{\sigma}_{m, \ell}^n = K(V+c)_{m, \ell}^n \quad (3-14)$$

stability requires that:

$$\left| \bar{\sigma}_{m, \ell}^n \right|^2 \leq \omega \bar{\sigma}_{m, \ell}^n \leq 1. \quad (3-15)$$

Further, with the notation that $\bar{\sigma}_0$ represents the maximum

allowable Courant number, the damping parameter, ω , must satisfy the inequality:

$$\bar{\sigma}_o \leq \omega \leq \frac{1}{\bar{\sigma}_o}. \quad (3-16)$$

The definition of $\bar{\sigma}_o$ also permits the determination of K , which, in essence, determines the time step Δt :

$$K = \frac{\bar{\sigma}_o}{(V+c)_{\max}} \quad (3-17)$$

That K determines the time step may be seen by consideration of its definition:

$$K = [K_r^2 + K_z^2]^{1/2} = \frac{[(\Delta r)^2 + (\Delta z)^2]^{1/2}}{(\Delta r) (\Delta z)} \Delta t \quad (3-18)$$

Normally, the mesh spacing, which defines Δr and Δz , may be considered known. Moreover, once K , and consequently the time step Δt , has been determined, K_r and K_z are also defined. With the consideration of χ defined in Figure 4 and equation (3-18), K_r and K_z may be evaluated by:

$$\begin{aligned} K_r &= K \sin \chi \\ K_z &= K \cos \chi \end{aligned} \quad (3-19)$$

The calculation procedure, then, consists of choosing a value of $\bar{\sigma}_o$ and ω in correspondence with equation (3-16). The parameter $\bar{\sigma}_o$ can be chosen rather arbitrarily (except that it must be less than 1. However, because the $\bar{\sigma}_o$ selection determines the time step,

consideration must be given to the number of time steps (and, consequently, computer run time) necessary for any fixed time interval under investigation. Certainly, the mesh is bound up in these considerations. Although a coarser grid spacing will permit a larger time step, in accordance with stability requirements, the solution that results will be less accurate than that which would result from a smaller grid spacing.

Once $\bar{\sigma}_0$ is selected, an ω that satisfies the inequality (3-16) is selected; at least, this is the requirement for an inviscid fluid calculation. Since, in general, as ω is permitted to approach zero, equation (3-3) better approximates equation (3-1) and a numerical solution better approximates reality, the smallest possible ω is desirable. Consequently, in this work, ω was selected considerably lower than the inequality (3-16) would permit.

With the selection of $\bar{\sigma}_0$ and ω , the stability requirements for each time step are satisfied by evaluating K in accordance with equation (3-17) where $(V+c)_{\max}$ is the maximum value of $(V+c)$ in the most recent time plane. The parameters K_r and K_z are evaluated in accordance with equations (3-19), and since the entire flow field is initially defined at the start of any calculation, the first time step offers no difficulty.

Centerline Equations

To develop the equations necessary for the determination of the centerline values of the dependent variables, a "control volume" was imagined to surround an arbitrary centerline node. The integral conservation equations were then applied to this node (much the same way the differential equations are normally derived). Since the centerline was considered an axis of symmetry, the radial conservation equation was not considered.

In general, the properties at the node in the control volume were assumed to represent the average of the control volume and fluxes across the boundaries of the control volume were evaluated by taking the averaged value of the two adjacent points on either side of the control volume surface. Further, the convention that all gradients are positive was adopted for evaluation of all turbulent transport terms in the derivations presented below.

Continuity Equation

Figure 5 depicts the assumed control volume and indicates the assumed positive directions for the velocities. These assumptions will be maintained in this and subsequent derivations in this chapter.

The integral equation which describes the conservation of mass is:

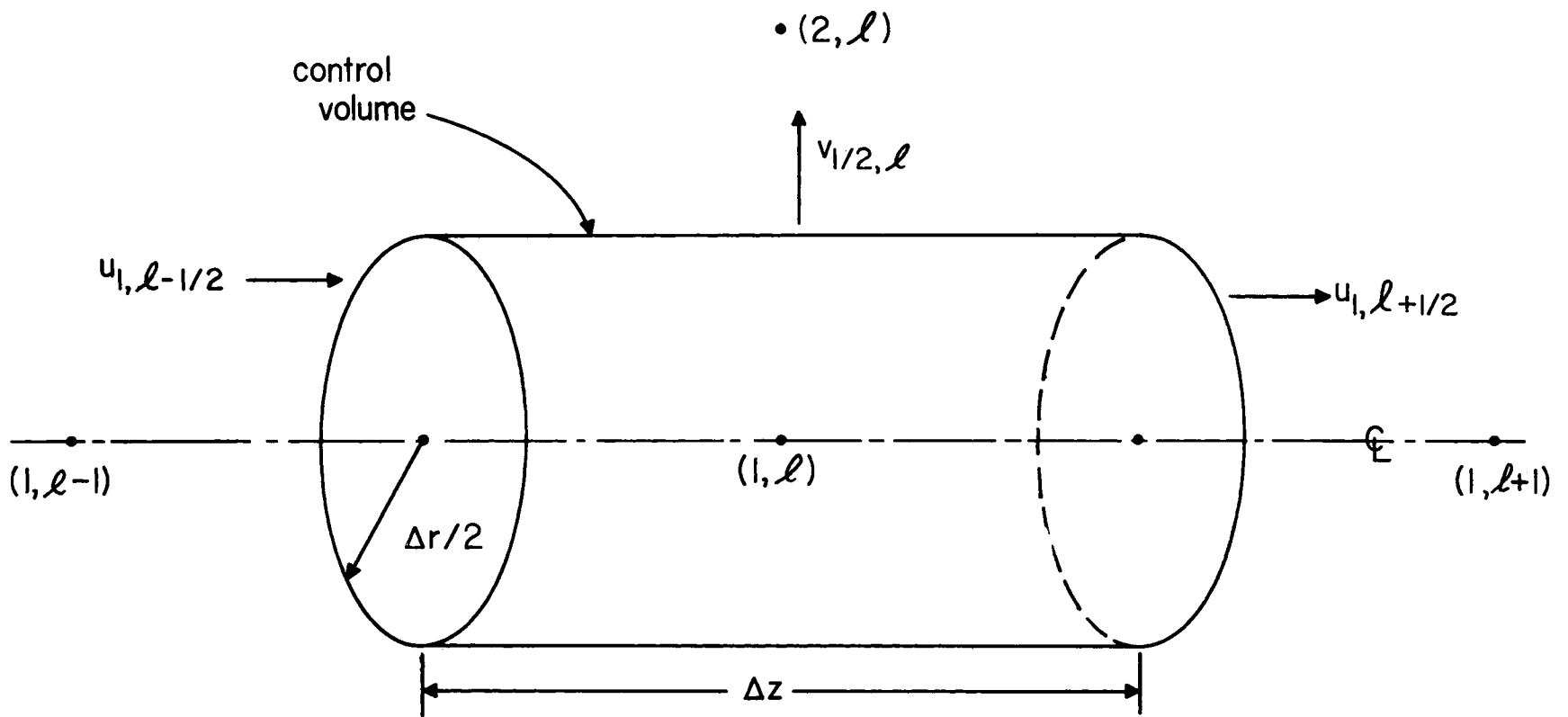


Figure 5. Assumed Positive Velocity Directions for Centerline Coaxial Volume

$$\frac{d}{dt} \int_{c.v.} \rho dV_s + \int_{c.s.} \rho V_n dA_s = 0 \quad (3-20)$$

This was approximated by:

$$\begin{aligned} \left(\pi \frac{(\Delta r)^2}{4} \Delta z \right) \left(\frac{\rho^{n+1} - \rho^n}{\Delta t} \right)_{1, \ell} + \left(\pi \frac{\Delta r^2}{4} \right) \left[\frac{(\rho u)_{1, \ell+1} + (\rho u)_{1, \ell}}{2\Delta z} \right. \\ \left. - \frac{(\rho u)_{1, \ell} + (\rho u)_{1, \ell-1}}{2\Delta z} \right]^n \quad (3-21) \\ + \left(2\pi \frac{\Delta r}{2} \Delta z \right) \left[\frac{(\rho v)_{2, \ell} + (\rho v)_{1, \ell}}{2\Delta r} \right]^n = 0 \end{aligned}$$

Rearrangement produced:

$$\rho_{1, \ell}^{n+1} = \rho_{1, \ell}^n - \frac{K_z}{2} [(\rho u)_{1, \ell+1} - (\rho u)_{1, \ell-1}]^n - 2K_r (\rho v)_{2, \ell}^n = 0 \quad (3-22)$$

Axial Momentum Equation

The conservation of axial momentum was accomplished by an approximate satisfaction of the equation:

$$\Sigma F_z = \frac{d}{dt} \int_{c.v.} \rho u dV_s + \int_{c.s.} \rho u V_n dA_s \quad (3-23)$$

where

$$\Sigma F_z = - \int_{c.s.} p \bar{n} \cdot \bar{i}_z dA_s + \int_{c.s.} \bar{\tau} \cdot \bar{i}_z dA_s \quad (3-24)$$

where \bar{n} is a unit outward pointing normal to the control surface and \bar{i}_z is a unit vector which points in the positive z-direction. The evaluation of the above force integrals was accomplished in the following manner (see Figure 6):

$$- \int_{c.s.} p \bar{n} \cdot \bar{i}_z dA_s \cong \pi \frac{\Delta r^2}{4} \left[\frac{p_{1, \ell} + p_{1, \ell-1}}{2} - \frac{p_{1, \ell+1} + p_{1, \ell}}{2} \right]^n \quad (3-25)$$

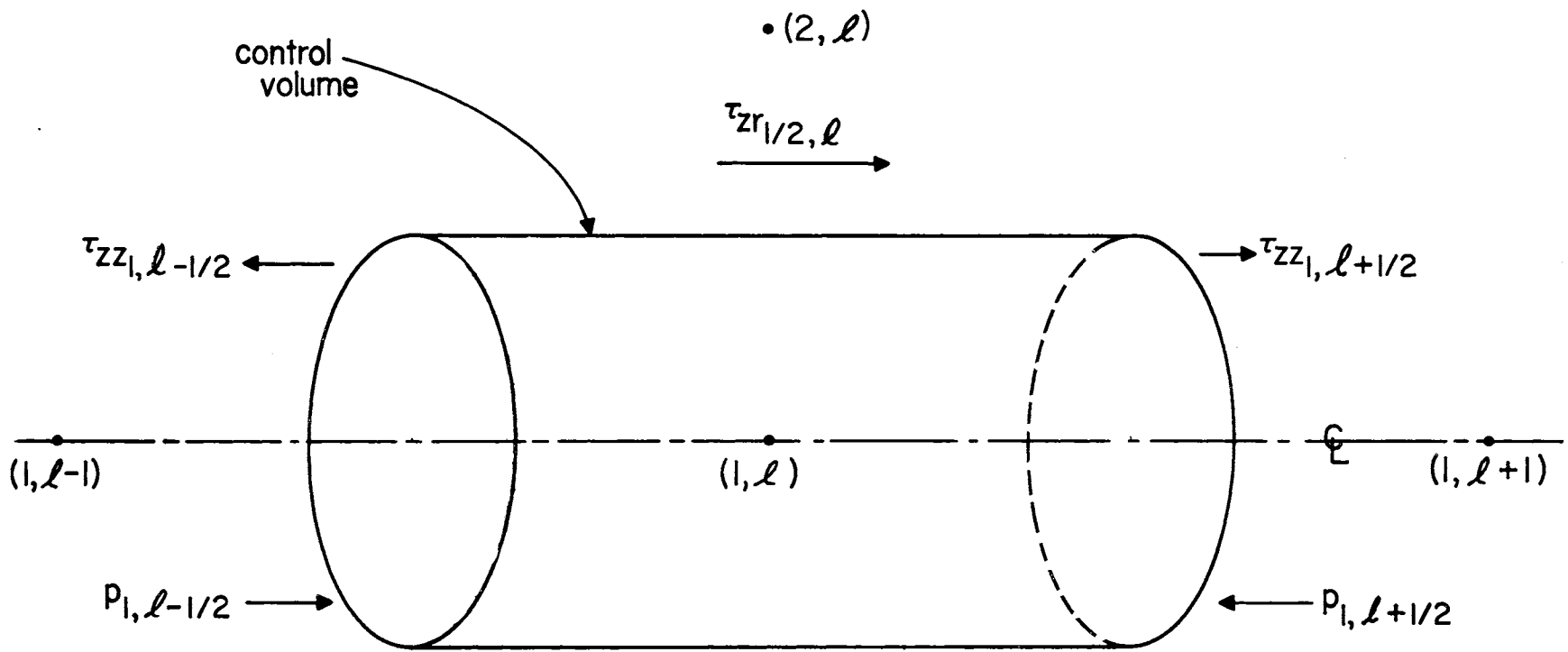


Figure 6. Assumed Shear Stress and Pressure System for Centerline Control Volume

$$\begin{aligned}
\int_{c. s.} \bar{\tau} \cdot \bar{i}_z dA_s &\cong \frac{\Delta r^2}{4} \left[\frac{(\tau_{zz})_{1, \ell+1} + (\tau_{zz})_{1, \ell}}{2} \right. \\
&\quad \left. - \frac{(\tau_{zz})_{1, \ell-1} + (\tau_{zz})_{1, \ell}}{2} \right]^n \\
&\quad + (2\pi \frac{\Delta r}{2} \Delta z) \left[\frac{(\tau_{zz})_{2, \ell} + (\tau_{zz})_{1, \ell}}{2} \right]^n
\end{aligned} \tag{3-26}$$

The flux integral and the storage integral were approximated:

$$\begin{aligned}
\frac{d}{dt} \int_{c. v.} \rho u dV_s + \int_{c. s.} \rho u V_s dA_s &\cong (\pi \frac{\Delta r^2}{4} \Delta z) \left[\frac{(\rho u)_{1, \ell}^{n+1} - (\rho u)_{1, \ell}^n}{\Delta t} \right] \\
&\quad + (\pi \frac{\Delta r^2}{4}) \left[\frac{(\rho u^2)_{1, \ell+1} + (\rho u^2)_{1, \ell}}{2} \right. \\
&\quad \left. - \frac{(\rho u^2)_{1, \ell-1} + (\rho u^2)_{1, \ell}}{2} \right]^n \\
&\quad + (2\pi \frac{\Delta r}{2} \Delta z) \left[\frac{(\rho uv)_{2, \ell} + (\rho uv)_{1, \ell}}{2} \right]^n
\end{aligned} \tag{3-27}$$

where $v_{1, \ell}$ was eventually set to equal zero.

Combination and rearrangement led to:

$$\begin{aligned}
(\rho u)_{1, \ell}^{n+1} &= (\rho u)_{1, \ell}^n - \frac{K_z}{2} [(\rho u^2)_{1, \ell+1} - (\rho u^2)_{1, \ell-1}]^n - 2K_r [(\rho uv)_{2, \ell}]^n \\
&\quad + \frac{K_z}{2} (p_{1, \ell-1} - p_{1, \ell+1})^n + \frac{K_z}{2} [(\tau_{zz})_{1, \ell+1} - (\tau_{zz})_{1, \ell-1}]^n \\
&\quad + 2K_r (\tau_{zr})_{2, \ell}^n
\end{aligned} \tag{2-28}$$

The numerical expansions of the turbulent stress terms for a general centerline node and end nodes on the centerline are presented

in Appendix C. However, suffice it to say at this point that these stresses were assumed to be of the form:

$$\begin{aligned}\tau_{zz} &= \rho \epsilon_m \frac{\partial u}{\partial z} \\ \tau_{zr} &= \rho \epsilon_m \frac{\partial u}{\partial r}\end{aligned}\tag{3-29}$$

Energy Equation

The form of the integral energy that was employed is:

$$\frac{d}{dt} \int_{c.v.} \rho \left(e + \frac{1}{2} V^2 \right) dV_s + \int_{c.s.} \rho \left(h + \frac{1}{2} V^2 \right) V_n dA_s = \int_{c.s.} q_n'' dA_s + \int w'' dA_s \tag{3-30}$$

where q'' represents the energy transported into the control surface by turbulent motion. Here q'' was evaluated via the assumption:

$$q_n'' = \frac{\rho \epsilon_m}{Pr_t} \frac{\partial h}{\partial n} \tag{3-31}$$

where n is a direction perpendicular to the surface of the control volume.

The work per unit area is denoted by w'' and it accounts for the work effect of the turbulent stresses. See Figure 7 for depiction of additional assumptions.

The evaluation of the q'' and w'' integrals was as follows:

$$\begin{aligned}\int_{c.s.} q_n'' dA_s &= \left(\pi \frac{\Delta r^2}{4} \right) \left[\frac{q_{1,l+1}'' + q_{1,l}''}{2} - \frac{q_{1,l}'' + q_{1,l-1}''}{2} \right]^n \\ &+ \left(2\pi \frac{\Delta r}{2} \Delta z \right) \left[q_{2,l}'' + q_{1,l}'' \right]^n\end{aligned}\tag{3-32}$$

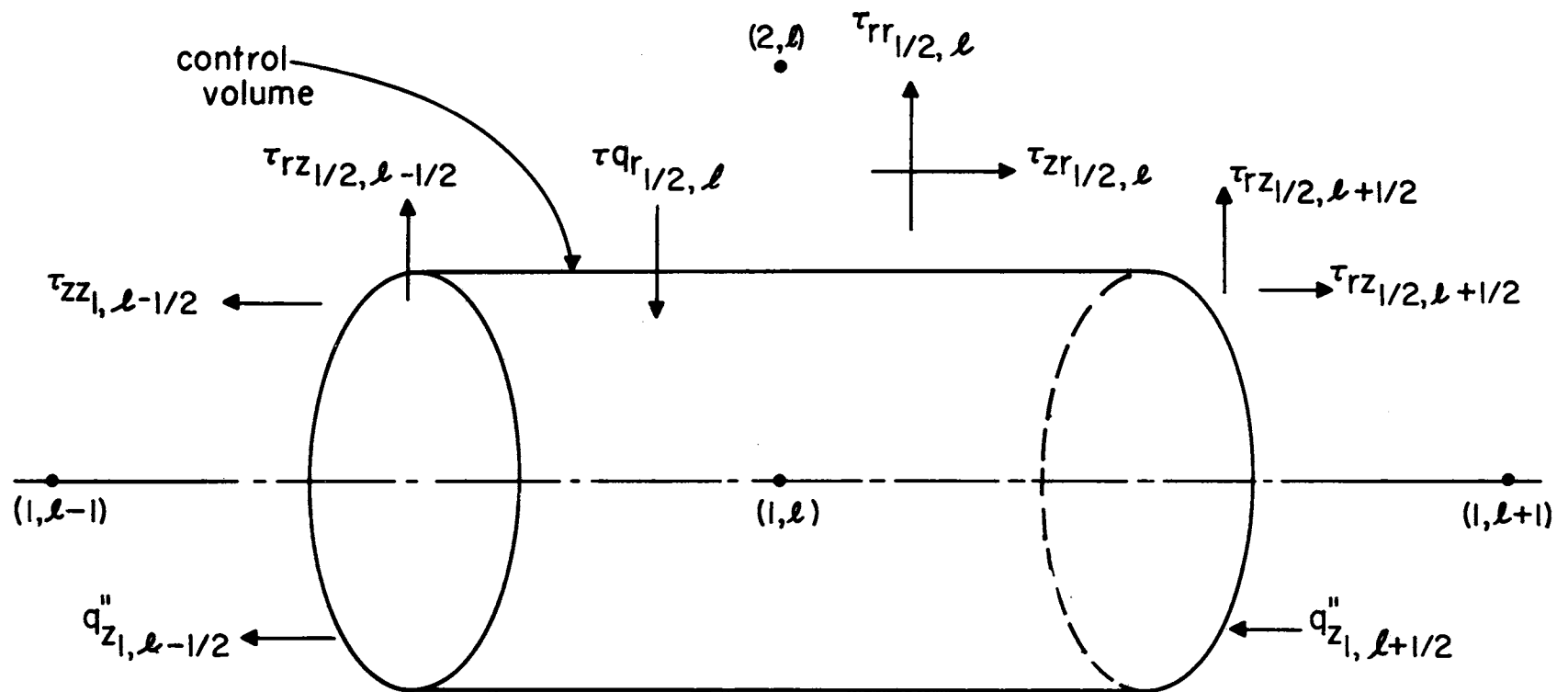


Figure 7. Assumed Shear Stress and Heat Flux System for a Centerline Control Volume

$$\begin{aligned}
\int_{c. s.} w'' dA_s &= (\pi \frac{\Delta r^2}{4}) \left[\frac{(\tau_{zz} u)_{1, l} + (\tau_{zz} u)_{1, l-1}}{2} - \frac{(\tau_{zz} u)_{1, l} + (\tau_{zz} u)_{1, l+1}}{2} \right]^n \\
&+ (2\pi \frac{\Delta r}{2} \Delta z) \left[\frac{(\tau_{zr} u)_{1, l} + (\tau_{zr} u)_{2, l}}{2} \right]^n \\
&+ (\pi \frac{\Delta r^2}{4}) \left[\frac{1}{4} \frac{(\tau_{rz} v)_{2, l-1} + (\tau_{rz} v)_{2, l}}{2} \right. \\
&\quad \left. - \frac{1}{4} \frac{(\tau_{rz} v)_{2, l+1} + (\tau_{rz} v)_{2, l}}{2} \right]^n \\
&+ (2\pi \frac{\Delta r}{2} \Delta z) \left[\frac{(\tau_{rr} v)_{1, l} + (\tau_{rr} v)_{2, l}}{2} \right]^n
\end{aligned} \tag{3-33}$$

In equations (3-34) and (3-35) it has been assumed that radial derivatives evaluated at the axis are zero as well as is the radial velocity at the axis.

The storage and flux integrals were evaluated in a manner exactly analogous to the way that the similar flux and storage integrals in axial conservation of momentum equation and the continuity equation were evaluated. The final form of the energy equation that was employed for centerline calculations in this work is:

$$\begin{aligned}
[\rho(e + \frac{1}{2} V^2)]_{1, l}^{n+1} &= [\rho(e + \frac{1}{2} V^2)]_{1, l}^n - \frac{K_z}{2} \{ [\rho(h + \frac{1}{2} V^2) u]_{1, l+1} \\
&\quad - [\rho(h + \frac{1}{2} V^2) u]_{1, l-1} \} - 2K_r [\rho(h + \frac{1}{2} V^2) v]_{2, l}^n \\
&\quad + \frac{K_z}{2} [(q_z'')_{1, l+1} - (q_z'')_{1, l-1}]^n + 2K_r (q_r'')_{2, l}^n \\
&\quad + \frac{K_z}{2} [(\tau_{zz} u)_{1, l+1} - (\tau_{zz} u)_{1, l-1}]^n + 2K_r (\tau_{zr} u)_{2, l}^n \\
&\quad + 2K_r (\tau_{rr} v)_{2, l}^n + \frac{K_z}{4} [(\tau_{rz} v)_{2, l+1} - (\tau_{rz} v)_{2, l-1}]^n
\end{aligned} \tag{3-34}$$

In addition to the forms of the turbulent transport expressions presented in equations (3-29) and (3-31) the following additional assumptions were made:

$$\begin{aligned}\tau_{rr} &= \rho \epsilon_m \frac{\partial v}{\partial r} \\ \tau_{rz} &= \rho \epsilon_m \frac{\partial v}{\partial z}\end{aligned}\tag{3-35}$$

The numerical expansions of these expressions, as well as equation (3-31), will also be presented in Appendix C.

Specie Conservation Equation

Finally, the satisfaction of the specie conservation requirement was achieved by a numerical approximation of the integral conservation of specie equation:

$$\frac{d}{dt} \int_{c. v.} \rho \omega_i dV_s + \int_{c. s.} \rho \omega_i V_n dA_s = \int_{c. s.} D_{ni} dA_s\tag{3-36}$$

where D_{ni} represents the flux of specie i in the n -direction due to turbulent transport processes. See Figure 8 for the assumed directions of D_{ni} which correspond to the assumption that D_{ni} may be evaluated by:

$$D_{ni} = \frac{\rho \epsilon_m}{Sc_{t,i}} \frac{\partial \omega_i}{\partial n}\tag{3-37}$$

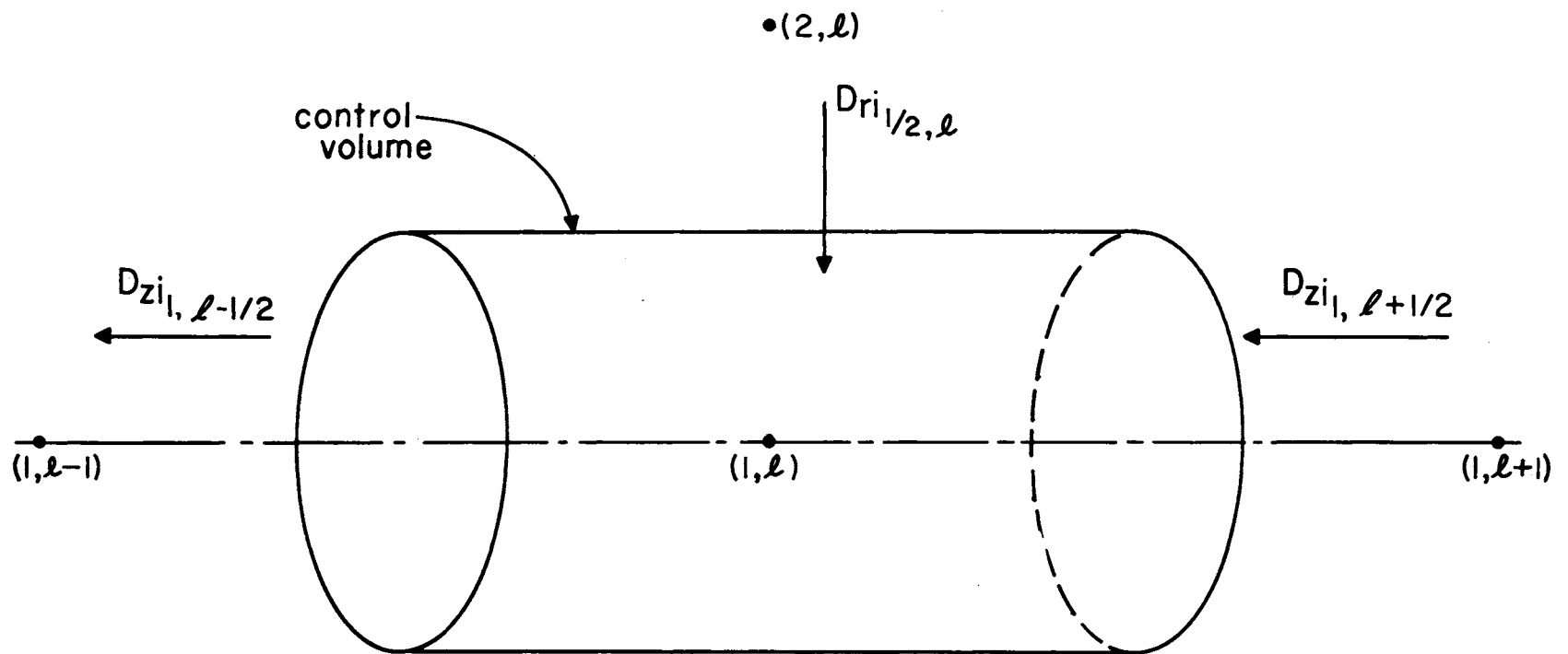


Figure 8. Assumed Specie Flux Directions for a Centerline Control Volume

The integral equation (3-36) was approximated by:

$$\begin{aligned}
 (\pi \frac{\Delta r^2}{4} \Delta z) \frac{(\rho \omega_i)_{1, \ell}^{n+1} - (\rho \omega_i)_{1, \ell}^n}{\Delta t} + [(\pi \frac{\Delta r^2}{4}) (\rho u \omega_i)_{1, \ell+1/2} - (\rho u \omega_i)_{1, \ell-1/2}]^n \\
 + (2\pi \frac{\Delta r}{2} \Delta z) [(\rho v \omega_i)_{1/2, \ell}]^n = \\
 (\pi \frac{\Delta r^2}{4}) \left[\frac{(D_{zi})_{1, \ell+1} + (D_{zi})_{1, \ell}}{2} - \frac{(D_{zi})_{1, \ell-1} + (D_{zi})_{1, \ell}}{2} \right]^n \\
 + (2\pi \frac{\Delta r}{2} \Delta z) \left[\frac{(D_{ri})_{2, \ell} + (D_{ri})_{1, \ell}}{2} \right]^n \quad (3-38)
 \end{aligned}$$

which, after rearrangement, produced:

$$\begin{aligned}
 (\rho \omega_i)_{1, \ell}^n = (\rho \omega_i)_{1, \ell}^n - \frac{K_z}{2} [(\rho u \omega_i)_{1, \ell+1} - (\rho u \omega_i)_{1, \ell-1}]^n - 2K_r (\rho v \omega_i)_{2, \ell}^n \\
 + \frac{K_z}{2} [(D_{zi})_{1, \ell+1} - (D_{zi})_{1, \ell-1}]^n + 2K_r (D_{ri})_{2, \ell}^n \quad (3-39)
 \end{aligned}$$

See Appendix C for a delineation of the numerical expansions employed for D_{zi} and D_{ri} .

Top Boundary Conditions

As was pointed out in Chapter II, it was assumed that the top boundary was sufficiently removed from the mixing region to permit the boundary defining condition that the radial gradients of all dependent variables are zero, equation (2-28). In the numerical sense, this was accomplished by assigning to the dependent variables at the top line of nodes the value that was calculated for the dependent variables at the nodes which are one line below the top. That is,

if M represents the maximum number of radial nodes, it was assumed that:

$$\begin{aligned} u_{M, l} &= u_{M-1, l} \\ v_{M, l} &= v_{M-1, l} \\ p_{M, l} &= p_{M-1, l} \\ &\text{etc.} \end{aligned} \tag{3-40}$$

Downstream Boundary Numerical Equations

At the downstream boundary no particularly restrictive assumptions were employed since the flow was supersonic. Instead, calculations were performed in a manner similar to the field point calculations. However, rather than employ a central difference scheme for the axial derivatives in equation (3-3), a backward difference technique was used. This resulted in a finite difference approximation to equation (3-3) of the form:

$$\begin{aligned} f_{m, l}^{n+1} &= f_{m, l}^n - \frac{K_r}{2} [F_{m+1, l}^r - F_{m-1, l}^r]^n - \frac{K_z}{2} [F_{m, l}^z - F_{m, l-1}^z]^n \\ &- \frac{K_r}{(m-1)} \psi_{m, l}^n + \frac{1}{2(m-1)} [(m-1/2) a_{m+1/2, l}^n (f_{m+1, l}^n - f_{m, l}^n) \\ &- (m-3/2) (f_{m, l}^n - f_{m, l-1}^n)] + \frac{1}{2} [\beta_{m, l-1/2} (f_{m, l}^n - f_{m, l-1}^n) \\ &- \beta_{m, l-3/2} (f_{m, l-1}^n - f_{m, l-2}^n)] \end{aligned} \tag{3-41}$$

where, of course, l has its maximum value; that is, this equation applies to the last column of the mesh field (see Figure 3).

Here, again, consideration had to be given to the manner in which the derivatives contained in F^r , F^z , and Ψ were to be evaluated. Any radial derivatives in F^r were finite differenced by following the scheme presented in equation (3-7). Any axial derivatives in the F^r were finite differenced by employing a backward difference. With the use of the nomenclature described above, this differencing scheme has the form:

$$\frac{\partial}{\partial r} \left[s \frac{\partial t}{\partial z} \right] \rightarrow \frac{1}{2\Delta r} \left[2s_{m+1/2, l} (t_{m+1/2, l}^t - t_{m+1/2, l-1}^{-t}) / \Delta z \right. \\ \left. - 2s_{m-1/2, l} (t_{m-1/2, l}^t - t_{m-1/2, l-1}^{-t}) \Delta z \right] \quad (3-42)$$

where, again, the 2's within the brackets have been inserted for differencing consistency.

Any radial derivatives in F^z were handled in a manner similar to equation (3-10) where centered radial differences were taken across two mesh spacing. For the downstream boundary:

$$\frac{\partial}{\partial z} \left[s \frac{\partial t}{\partial r} \right] \rightarrow \frac{1}{2\Delta z} \left[2s_{m, l} (t_{m+1, l}^t - t_{m-1, l}^{-t}) / 2\Delta r \right. \\ \left. - 2s_{m, l-1} (t_{m+1, l-1}^t - t_{m-1, l-1}^{-t}) / 2\Delta r \right] \quad (3-43)$$

and any axial derivatives in F^z were approximated by:

$$\frac{\partial}{\partial z} \left[s \frac{\partial t}{\partial z} \right] \rightarrow \frac{1}{2\Delta z} \left[2s_{m, l-1/2} (t_{m, l-1}^t - t_{m, l-1}^{-t}) / \Delta z \right. \\ \left. - 2s_{m, l-3/2} (t_{m, l-1}^t - t_{m, l-2}^{-t}) / \Delta z \right]$$

The radial derivatives in Ψ were approximated by a centered difference across two mesh spacings and any coefficients of the derivatives were evaluated at the center node of the centered difference. The axial derivatives in Ψ were differenced by a backward difference over one mesh spacing and derivative coefficients were taken as averages between the two nodes used for the differencing.

Computational Scheme

After all flow variables were defined at every node point, the maximum value of $(V+c)$ was determined by checking each node. Then, equation (3-17) was used to calculate K since $\bar{\sigma}_o$ was specified at the start of the program. Next, K_r and K_z were calculated by equations (3-19). With the use of equations (3-2), (3-4), and (3-11), together with the second derivative finite difference forms, equations (3-7) through (3-10), all flow variables for each field point (i. e., not on a boundary) were calculated. The top boundary flow variables were determined by equations of the form expressed by equations (3-40). Centerline properties were calculated by using equations (3-22), (3-28), (3-34), and (3-39) together with the finite difference expressions for the turbulent transport fluxes which are presented in Appendix C. The centerline radial velocity was defined to be zero. The downstream boundary was calculated by equations (3-2), (3-11),

and (3-41) together with the finite difference expressions for the turbulent transport fluxes -- equations (3-42) through (3-44).

Once all flow variables for all nodes had been calculated, the $n+1$ time step variables were redefined as the n time step variables and the calculation process repeated.

CHAPTER IV

THE RESULTS OF THE NUMERICAL METHOD AND COMPARISONS WITH EXPERIMENTAL DATA

Since the relative merit of any analysis may be gauged only after solutions produced via the proposed method have been compared with appropriate data, such a comparison was made a part of this work. Moreover, to test thoroughly the method, ideally it would have been desirable to consider cases which were as general in nature as the assumptions inherent in the method would permit. With regard to the analytic development in the two previous chapters, this would require consideration of axisymmetric, non-constant pressure, non-isoenergetic, nonreactive, perfect gas, multispecies, turbulent jet mixing. However, such considerations would also require comparable accurate experimental data; but, extensive review of the literature revealed no such data even approaching the generality desired. In fact, only constant pressure mixing studies have been reported with any detail (24), (32), (56), (58) for two species. Further, in the area of constant pressure jet mixing, in those cases where differing stagnation temperatures existed, no flow field temperature measurements have been reported. As a consequence

of these considerations, interest was restricted to a constant pressure, multispecie turbulent jet mixing case.

The Experimental Data

The data from one of the cases reported in Reference 24 was used for comparison purposes. This experiment consisted of a central axisymmetric jet of carbon dioxide and a circumferential jet of air, both of which flowed in the same direction (see Figure 2). Both streams had a stagnation temperature of 675 degrees Rankine (which was measured by thermocouples in the respective plenum chambers). The exit Mach numbers were 1.47 and 1.62 for the carbon dioxide and air jets respectively. A static pressure was reported to 5.5 psia; however the location and technique for the determination of this quantity is not discussed in the reference. Further, the reference made no mention of any experimental checks to determine if, indeed, the pressure was constant throughout the entire investigated flow field. Mass flow measurements of each stream were made (although this information was not incorporated in the report) and, the reference indicated that the nozzles for each stream were calibrated so that this could have been the means by which the static pressure was determined. At any rate, the discussion in Reference 24 appears to indicate that the static pressure was assumed to be constant.

The major effort in the experimental investigation was the determination of radial profiles of the stagnation pressure and CO_2 concentration in the potential core region. Three axial locations of the flow field were probed and these locations are shown in Figure 9. The stagnation pressure radial profiles were obtained by using a motorized rake so that the pitot tubes could be moved without interruption of a particular run. The data itself were obtained by using a Statham temperature-compensated strain gauge transducer; the output from the transducer was continuously recorded. By these means, as Forde notes, a continuous profile of total pressure could be obtained. Forde also points out that the total pressure measurements displayed axial symmetry so that measurements from both sides could be used to develop the total pressure radial profiles. See Figure 10 for a reproduction of the p_0/p radial profiles presented in Reference 24. Forde also indicates that temperature measurements were made by using thermocouples but the readings that were obtained were largely unusable and consequently were not reported.

Concentration measurements (obtained at the same axial locations as the total pressures) were obtained by employing a sampling rake. Each probe on the rake was connected by flexible tubing to a sampling bottle. The separation of the species in the sampling bottles was achieved by gas-solid chromatography, and only those results which were repeatable were used in the report. Since

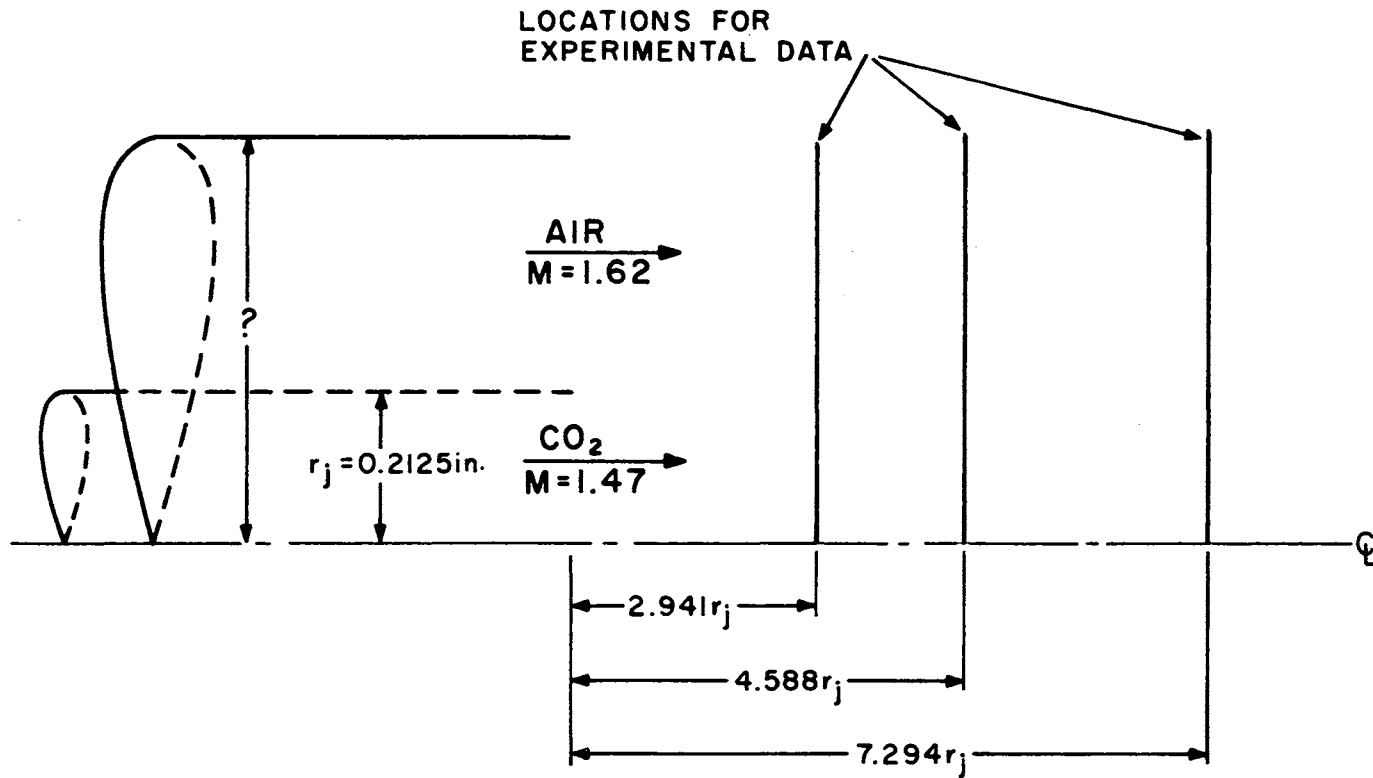


Figure 9. Axial Location of Experimental Data Radial Profiles

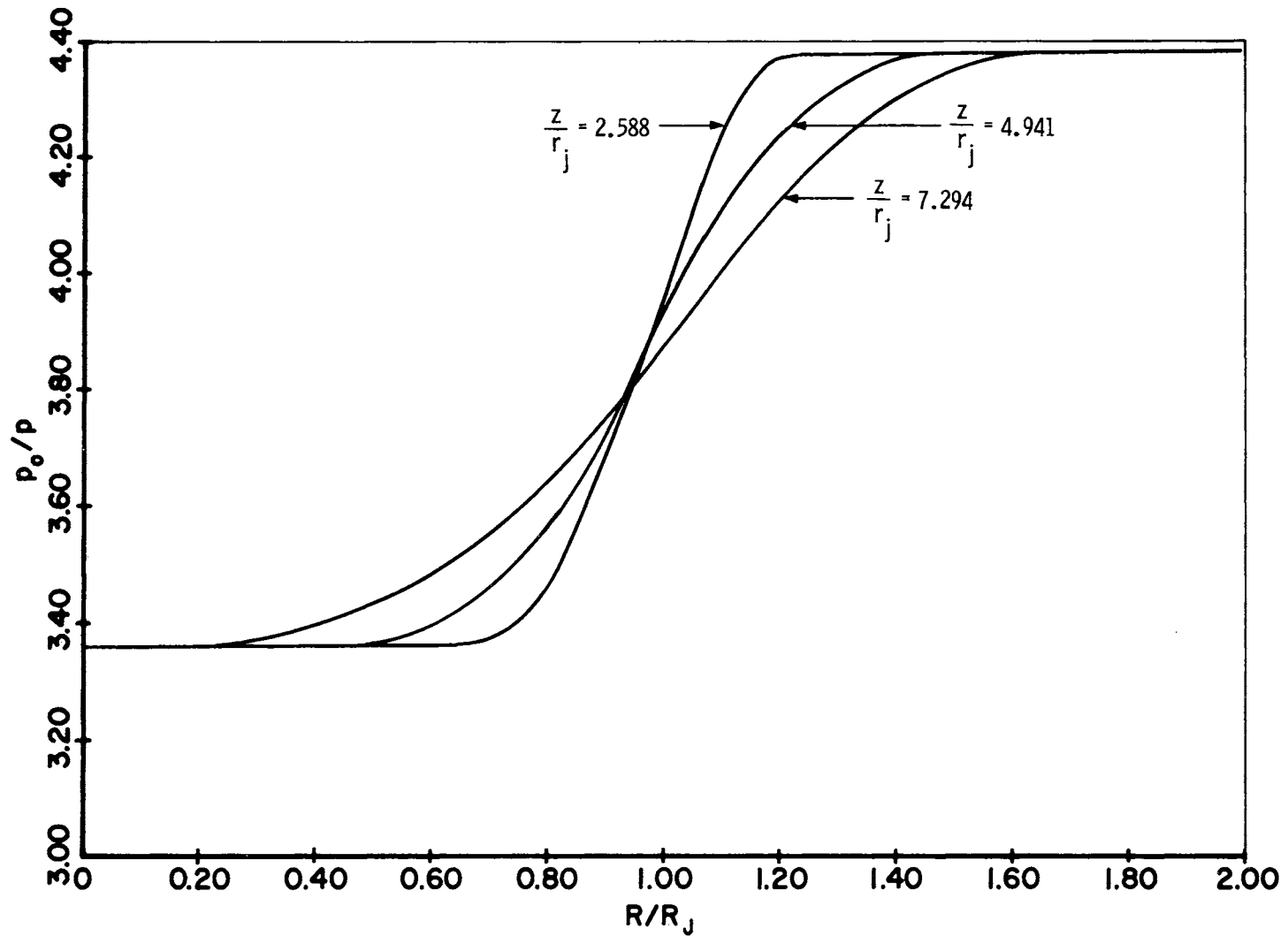


Figure 10. Experimental Radial Profiles of Stagnation Pressure

sampling rakes were used, only a discrete number of data points could be obtained and Reference 24 displays only six such measurements in the half jet. This data has been reproduced and is presented in Figure 11.

These two variables, p_o/p and ω_{CO_2} represent the information generally gleaned from experiment and they incorporate as little reduction of the raw data as is possible. This latter point is important since errors in data reduction of the raw data to reported data could lead to fallacious conclusions when compared to results of this study. Therefore, any discrepancies between the experimental data of Reference 24 and the results determined by the above theories must arise from inabilities of the above theories to describe turbulent jet mixing, incorrect modeling of the experiment to which the data apply, experimental error, or some combination of these.

Notwithstanding the questionability of the above described data, no better data appeared to be in the offing at the initiation of this investigation. Generally, that data on constant pressure, axisymmetric, turbulent jet mixing which was available in the literature fell into one of two categories depending on whether the experimentation concerned (1) the potential core, or (2) the main region of mixing (see Figure 3). With the addition of the restriction that consideration had to involve mixing of different gases, the number of reported data sets available in the literature was further diminished.

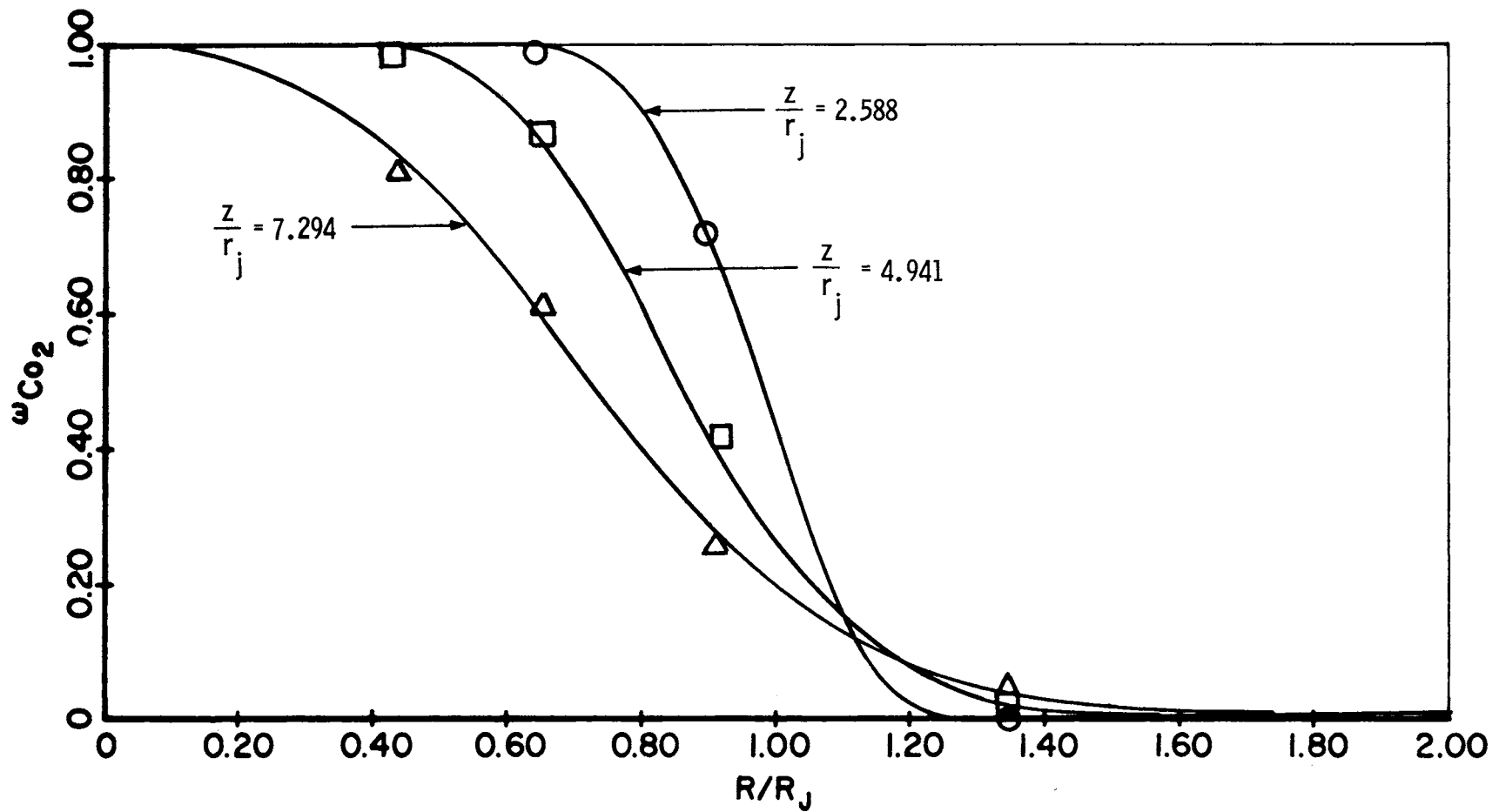


Figure 11. Experimental Radial Profiles of Carbon Dioxide Concentration

In fact, there appeared to be only two other sources of experimental data (References 56 and 59) for constant pressure, multispecies, turbulent jet mixing. Both of these references were concerned with the main region of mixing. Moreover, it was this very deficiency of experimental data for the potential core region which led both Forde (24) and Boehman (58) to perform experiments in this flow regime. (Boehman's results only became available at the conclusion of this investigation.)

In the two references that are concerned with the main region of mixing, both raw and reduced data for the radial profiles of, variously, velocity, concentration, or pressure at several axial locations are presented. To model numerically any one of the experimental cases presented in either of these two references, detailed information for the upstream boundary for a system of nodes would be necessary. While the most upstream axial location for which experimental data is presented might be considered the upstream boundary of the nodal system, the gleanings of the detailed information necessary would be extremely difficult and, at best, probably a poor approximation of reality for several reasons. Perhaps the most severe consideration concerns the number of data points for any radial profile at any axial location. In Reference 59 only five data points are used and Reference 56 used, at most, nine data points to define a radial profile (the numerical method typically employed

thirty-two radial nodal points at every axial location). Furthermore, because of the nature of the quantities that are typically measured, it is only possible to determine with any precision the axial velocity, the concentrations, and the density (if the assumptions of constant T_o and p are momentarily accepted). This, however, is not sufficient information for the numerical method since the radial velocity (albeit is small) must also be known. To obtain the radial velocity, recourse would have to be made to the continuity equation; here, again, the deficiency of experimental data points would severely hamper the determination of the radial velocity, with any accuracy, at the large number of nodal points which the numerical method employs.

This lack of data points appears to be due, in part, to the difficulty of performing large scale experiments. In Reference 59, the inner jet radius was approximately 0.3 inch and, in Reference 56, the inner jet radius was approximately 0.7 inch. In this latter reference, the outside diameter of the sampling probe was approximately ten percent of the inner jet radius.

The constancy of the static pressure and the stagnation temperature was not considered to any great extent in References 56 and 59. Of course, it must be admitted that these constant value assumptions are probably not bad in the main region of mixing. Reference 56 measured the wall static pressure and found it to be essentially constant and inferred that it was constant everywhere.

Also, since the velocity differences were not great, and the plenum chamber temperatures were reported to be equal, the assumption of constant T_o was probably adequate. Moreover, the axial velocity and concentration profiles look reasonable. However, the axial velocity profiles which result from the reduction of the data in Reference 59, with the assumption of constant p and T_o are highly distorted which makes these assumptions highly suspect for the experiments presented in this reference.

Because of the considerations delineated above in regard to the main region of mixing, it appeared easier to make plausible assumptions about the flow pattern at the nozzle exits (the upstream boundary of the potential core) than it would be to interpolate reasonably the main region experimental data for the quantities which would be necessary for the implementation of the analysis presented in this work. However, the process of estimating the nozzle exit conditions is not without its own difficulties. Since Reference 24 does not present the detailed upstream dimensions of the nozzles, it is impossible to calculate the degree of boundary layer growth and the degree of flow divergence in both the inner and outer streams. Furthermore, while the inner jet radius is given, the outer jet radius is not (see Figure 9). In addition, the thickness of the wall separating the inner jet from the outer jet is also not indicated; presumably, it is very thin. Finally, since no elaboration is made concerning the static

pressure (and the mass flow rates are not given) and no optical investigations were performed to check for shock waves or expansion fans which would indicate a disparity in exit pressure, an assumption which dictated the exit pressures was necessary.

In all fairness to the experimental efforts presented above, it should be noted that these experiments were performed to corroborate some analytic theory. While the assumptions that are necessary for the work presented here may seem sweeping in nature, the analytic methods associated with the respective experiments either had incorporated in them these assumptions already or these assumptions were of little significance. Nonetheless, the need still exists for extensive and thorough large scale experimentation in the field of multispecies turbulent mixing.

Basic Considerations

The node point arrangement for the numerical study of the potential core mixing region is shown in Figure 12. In all cases discussed below the maximum radius of the field of node points was twice the central jet radius. Since two types of node point arrangements (that is, two different sets of grid spacings) were considered, each will be discussed where appropriate.

The majority of the computations that were performed as a part of this thesis employed an IBM 7040. In addition, some of the upstream boundary conditions, as well as output plots, were

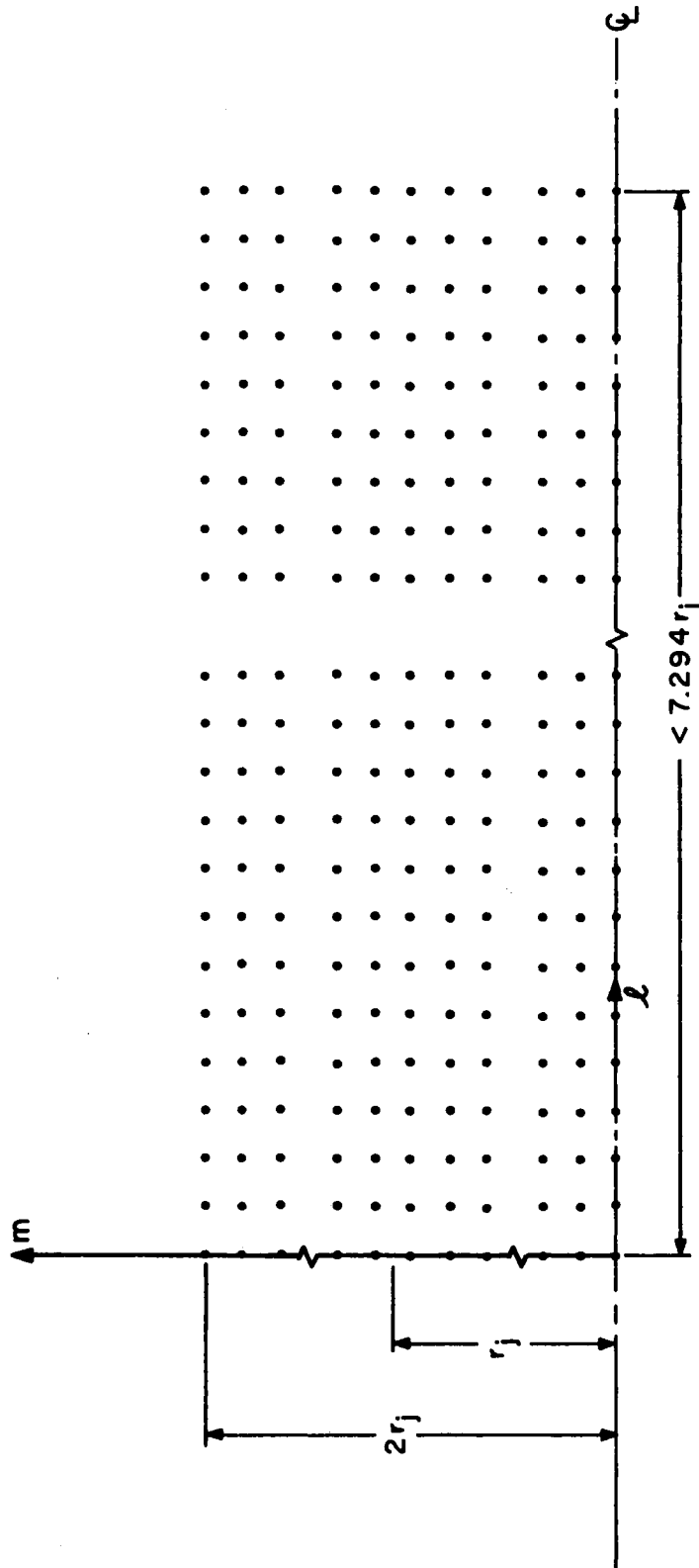


Figure 12. Node Field Arrangement

determined on an IBM 1620. Both of these machines were on the Oklahoma State University campus.

The analysis of any particular set of boundary and initial conditions by a particular combination of the above presented equations generally required three computer programs. This situation was demanded by computer storage limitations. The first program simply loaded a tape with information that was pertinent to a particular study. The second program performed the calculations. Because of time limitations it was necessary to segment the use of this second, or main program, into a series of short runs; at the beginning of each segmented run, the master tape was read. This tape contained only the most recent values of all the flow variables and other parameters necessary for further calculation. At the end of each segmented run of the second program, the current values of the quantities necessary for future calculations were written on the master tape. Each segmented run could be ended either by the depression of a sense switch on the computer console or by the program reaching a preassigned time step number, see Appendix E.

The third program read the master tape and printed on paper and punched on cards values of the calculated variables. The card data was used for plotting, using the IBM 1620.

In the course of the investigation presented here, it was discovered that the time required for the calculation of the entire flow field (that is, one time step calculation) was very sensitive to the

main program logic. Initially, the main program took approximately 3.5 minutes per time plane. However, with slight alterations of the main program logic the length of a time plane calculation was reduced to approximately 2.33 minutes. Obviously, these time rates strongly suggested a termination of any particular run at as early a time as possible. Yet a steady state condition was sought.

To determine when and if a steady state solution was reached, two alternate approaches were pursued (although not simultaneously). The first consisted of comparing plots of p_o/p (since these were the most sensitive to time stepping and also were to be compared with experimental data) at various time intervals. If the plots of p_o/p at some time in the calculation were not significantly different from those at some time much previous to the current time, then it was assumed that the steady state condition was approached. Normally, a time interval corresponding to 100 to 200 time steps was used. In this regard, attention is directed to Figure 13. In this figure p_o/p curves are presented for two different times for the axial locations for which the experimental data is available. The solid lines correspond to a time step number of 611 and the dashed lines are for a time step number of 1181 -- a difference of 570. Notice that the only significant difference appears in the p_o/p curve at a z/r_j of 7.294 (this is very near the downstream boundary of the node point field). However, this condition amounts to only about a 4 percent

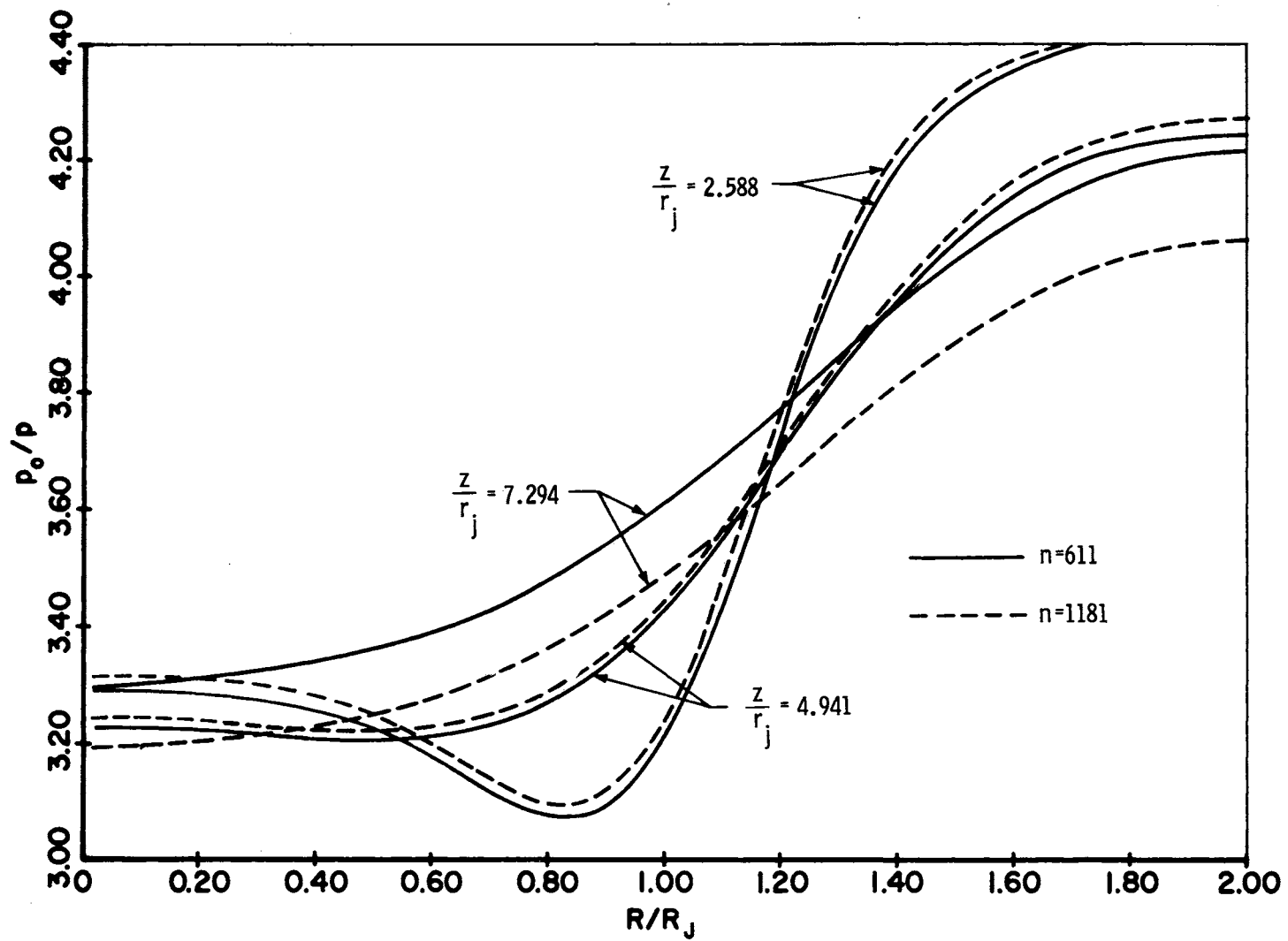


Figure 13. Comparison of Radial Pressure Profiles for $n = 611$ and $n = 1181$

change of the values at the 611 time step. Therefore, it seemed unreasonable to continue calculation for approximately thirty additional hours for only a four percent improvement in downstream data.

This point was further emphasized when calculations were made to determine how long a particle would take to travel from the upstream boundary to the downstream boundary of the node point field. Based on the slower stream velocity (the CO₂ stream) and the normal time step increment used for each time iteration, calculations indicate that 558 time steps would be required. Further, if the effect of the speed of sound is included in the calculations, only 363 iterations should be necessary for upstream influences to be signaled at the downstream boundary.

Before pursuing the discussion of the results of the numerical investigation, one final point needs to be made. This point is also emphasized in Figure 13. While the p_o/p curves for z/r_j location of 7.294 appears to be noticeably different, the difference is only of the order of 4 percent. Consequently, attention must be given to the expanded scale values for interpretation of the following figures.

As outlined in the "Experimental Data" section of this chapter, upstream boundary data were meager. This necessitated some fundamental assumptions regarding this boundary. In order to determine input conditions, it was assumed that the nozzle exit pressures of both streams were equal and had a value of 5.5 psia. Further, the

respective Mach numbers, together with the given stagnation temperatures, were used to determine the exit flow conditions. With the assumption of a semi-perfect gas (i. e., a gas that obeys the perfect gas equation but has variable specific heats), the exit conditions were determined as:

<u>Primary Stream (CO₂)</u>	<u>Secondary Stream (Air)</u>
M = 1.47	M = 1.62
T _o = 675°R	T _o = 675°R
T = 514.47°R	T = 446.99°R
p _o = 18.48 psia	p _o = 23.98 psia
p = 5.5 psia	p = 5.5 psia
γ = 1.28878	γ = 1.38874
R = 35.13 lb _f -ft/lb _m -°F	R = 53.3 lb _f -ft/lb _m -°F
u = 1272.57 fps	u = 1671.44 fps
ρ = 0.04382 lb _m /ft ³	ρ = 0.03324 lb _m /ft ³

To nondimensionalize the flow variables in the manner discussed in Chapter II, the reference pressure was taken as the exit pressure, 5.5 psia, and the reference density was taken to be the exit density of the primary stream, 0.04382 lb_m/ft³.

In addition to the assumptions mentioned above and which were employed in all cases to be discussed here, it was further assumed that the wall, which separated the inner flow from the outer, or secondary flow, was of zero thickness.

Finally, in regard to basic assumptions, for all cases presented below, the spreading rate parameter, σ, was assigned the value of 15.3. This value was found by Forde (24) to result in

similar velocity profiles which were determined by the reduction of experimental data. Also, in accordance with a suggestion from Walker (43), in all computer runs, the maximum allowable Courant number, $\bar{\sigma}_o$, was given the value of 0.5. Basically, the selection of the value of $\bar{\sigma}_o$ is a compromise between the computer run time required and the accuracy of the results of computation.

Numerical Results and Comparisons

Because of the nebulous nature of the knowledge of the exit conditions (in particular, the size of the exit plane boundary layers), a rather fruitful investigation was undertaken to ascertain the effects of slightly different flow conditions at the exit of the concentric nozzles. Generally speaking, both the size and the shape of the exit plane boundary layers was varied, and one case was considered with slightly divergent flow in both streams. Also, two different node arrangements were employed. Finally, the effects of varying both the damping parameter, ω , and the effective axial length in the eddy viscosity equation (2-27) were investigated.

For all the studies described below, with the exception of one, which will be specifically noted, the Case I type eddy viscosity was employed. Also, in the discussion that follows, attention will be directed almost entirely to the nature of p_o/p which resulted from various upstream boundary conditions. The concentration profiles

exhibited very limited dependence on the type of upstream boundary conditions assumed. This point will be elaborated upon in more detail after the different types of upstream boundary conditions have been described.

To distinguish between different various studies, each will be assigned a run number such as I, II, III, etc.

Run I

For this study, forty node points were used in the radial direction, and thirty-three were used in the axial direction. The maximum radius covered by these nodes, as mentioned previously, was equal to two carbon dioxide jet radii, and the ratio of $\Delta z/\Delta r$ was 4.5. This was approximately the maximum node spacing suggested by Walker (43) and extends over the region covered by the experimental data. The intention was to accomplish a closer spacing in the radial direction than in the axial direction since gradients in the radial direction are much steeper than those in the axial direction.

The damping parameter, ω , was assigned the value of 0.1 everywhere. This value is below the value required by the stability analysis (equation 3-16), but since turbulent flow was being investigated, it was the opinion of this author, based on the results of Walker (43), that this low value was adequate.

The free streams of the exit flows were assumed to be uniform (i. e., of constant value and parallel). The boundary layers were assumed to be distributed over four node points for the CO₂ stream and over five node points for the air stream (see Figure 14). Even in the boundary layers, no radial component of the velocity vector was assumed even though a more refined boundary layer analysis would indicate (as a consequence of the continuity equation) that these velocity components certainly do exist.

The conditions in the boundary layers were determined by assuming that the velocity profiles followed the one-seventh power rule. The velocity at each node point was thus assumed, and the density was obtained by assuming the gases were perfect, the pressure was constant across the boundary layers, and the adiabatic energy equation held across the boundary layer.

Also, it might be noticed that in Figure 14, the node points straddle the wall between the CO₂ stream and the air stream. This scheme was devised to avoid stagnation conditions which, as Eaton (44) points out, are difficult to handle. This assertion was confirmed in preparatory work performed by this author but not reported here.

The results of calculation for 658 time planes are shown by the solid lines in Figure 15. Comparison with experiment, Figure 10, is obviously poor, notably in the vicinity of $r/r_j = 1$.

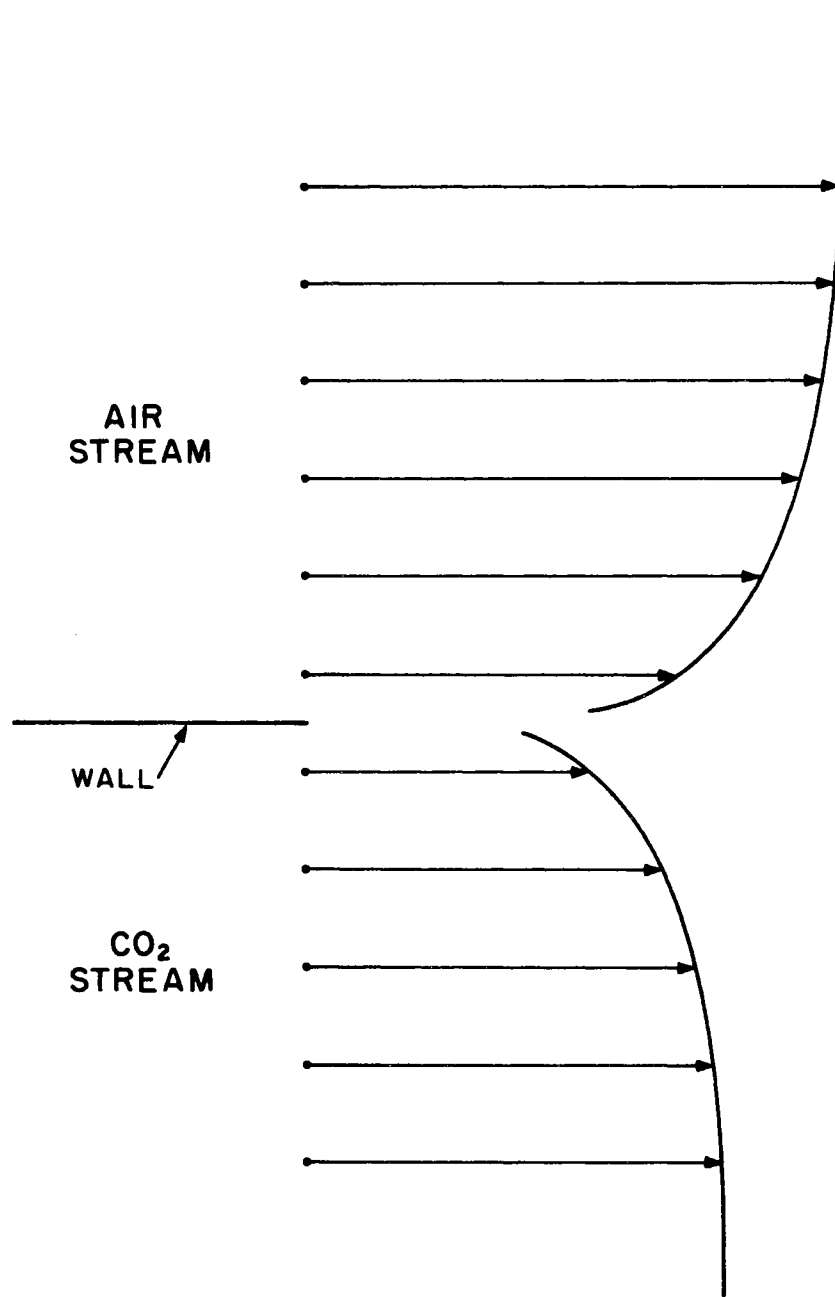


Figure 14. Boundary Layer Velocity Distribution for Run I

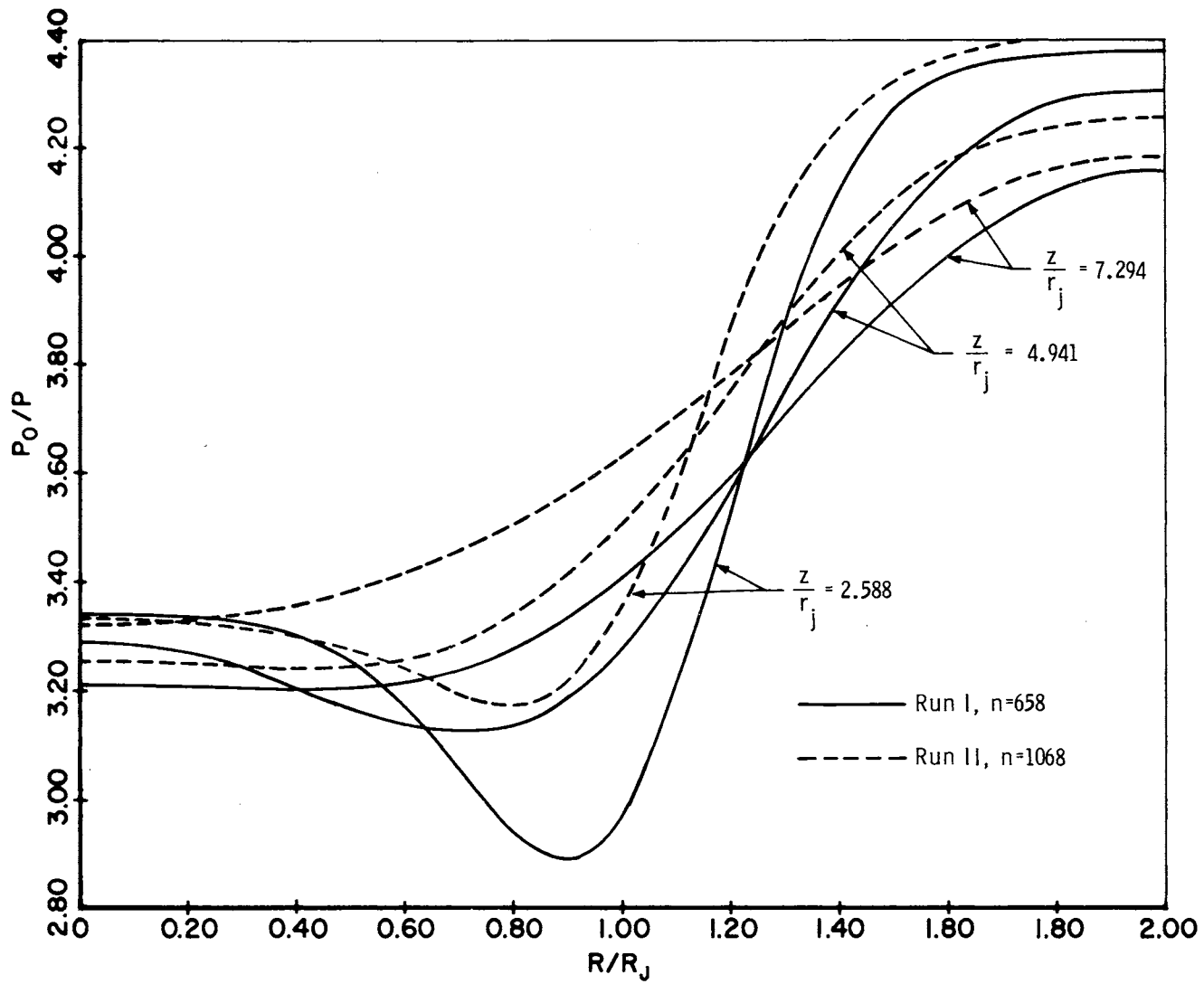


Figure 15. Comparison of Stagnation Pressure Radial Profiles for Run I and Run II

While the comparison at first glance looks poor, several aspects of these results need to be considered. First, the profile at $z/r_j = 7.294$ displays the greatest inaccuracies at both the centerline and at $r/r_j = 2.00$. Yet, at these locations the calculated values of p_o/p are of the order of only five percent different from the values indicated by experiment. Further, in the vicinity of $r/r_j = 1$, the "dips" in the curves are evidently due to boundary layer effects. However, the fact that the experimental data does not exhibit a boundary layer effect is also subject to suspicion. While the extent to which initial boundary layer influences persist in free turbulent mixing has not been, to this author's knowledge, defined, the seemingly low values at the $z/r_j = 7.294$ location may be attributed to boundary layer effects, especially in view of the results of Run II discussed below. Moreover, it should be recalled that the initial radius of central jet is small, and it is possible that the pitot tube diameter may have been so large that these dips in the p_o/p curve may have gone unnoticed. It must be admitted, however, that the results depicted in Figure 15 for the Run I study suggest that the assumed exit boundary layers were too large.

Another difficulty was indicated by the results of this case. In a region several mesh lengths downstream of the point of separation (the end of the wall separating the air from the CO_2 stream),

static pressure instabilities were indicated (see Figure 16). The cause of this instability was attributed to the low value of ω . Since the magnitude of the turbulent shear stresses is a function of z , the axial coordinate, which is measured from the exit plane, the equations in the region of this instability are essentially those of an inviscid fluid. The inviscid stability requires that an ω of 0.5 (for the $\bar{\sigma}_o = 0.5$) should be used. This difficulty was rectified in Run VI.

The initial conditions for this case were such, that at every axial location, all radial profiles were the same as at the exit plane (upstream boundary of the node system). The achievement of a steady state condition was checked by simple comparison of the p_o/p curves at various time planes as outlined above.

At time plane 658 (at which data for Figure 15 was extracted) an integral check over the boundaries of the nodal system was made for conservation of mass, axial momentum and energy. The errors indicated by these conservation checks were 0.25, 0.32, and 0.25 percent respectively for mass, axial momentum, and energy. Consequently, it may be concluded that the pseudo-viscous effects of the Rusanov method produce a negligible overall error as far as the conservation principles are concerned.

Run II

With the exception of the upstream boundary, the flow field variables for the entire nodal field are the same as those calculated

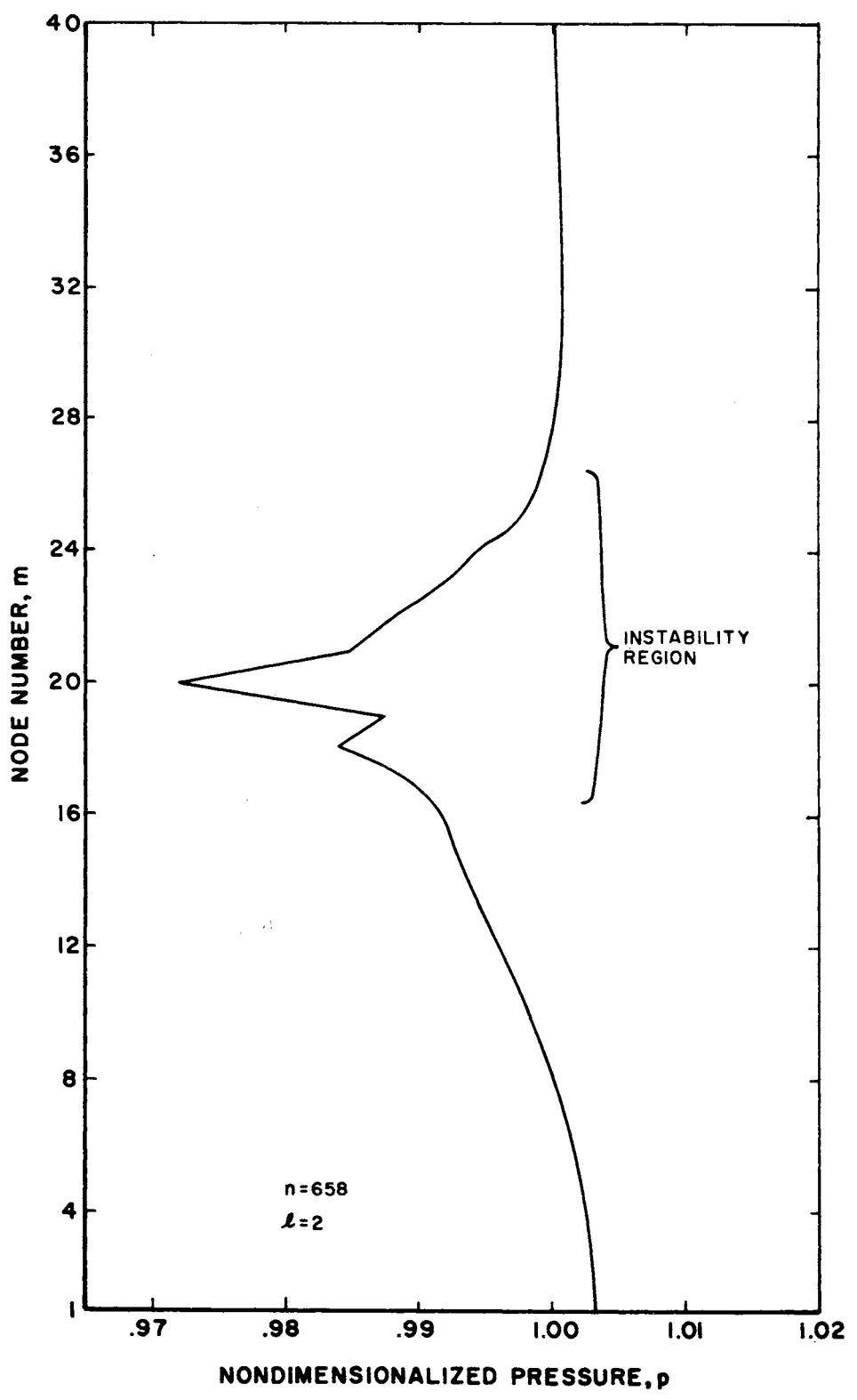


Figure 16. Radial Profile of Pressure in Unstable Region for Run I

at time plane 658 for Run I. The grid spacings for this case are necessarily also the same as those for Run I.

However, two significant changes have been made. Because it was judged that the boundary layer sizes that were assumed in Run I were too large, smaller boundary layers were assumed for this case. In order to eliminate the instabilities in the static pressure in the region downstream of the point of separation, an attempt was made to mathematically increase the level of turbulence in this region.

With respect to the boundary layers, it was assumed that one node point was located in each boundary layer. The velocity at each node point was assumed to have a magnitude equal to one-half of the respective free stream magnitude (see Figure 17). The densities at each of the node points in the respective boundary layers were calculated in the same manner as in Run I. The attempt was to simulate the physical no-slip condition at the wall by a simplified boundary layer profile. While it was admitted that this was a rather severe assumption in regard to the boundary layer profiles, the overriding purpose was to ascertain the effect of various upstream boundary conditions. A more realistic linear profile was assumed in Run VI.

Moreover, a linear velocity profile assumption may be justified on several bases. Results from many experiments indicate that the effect of initial boundary layers does not persist very far

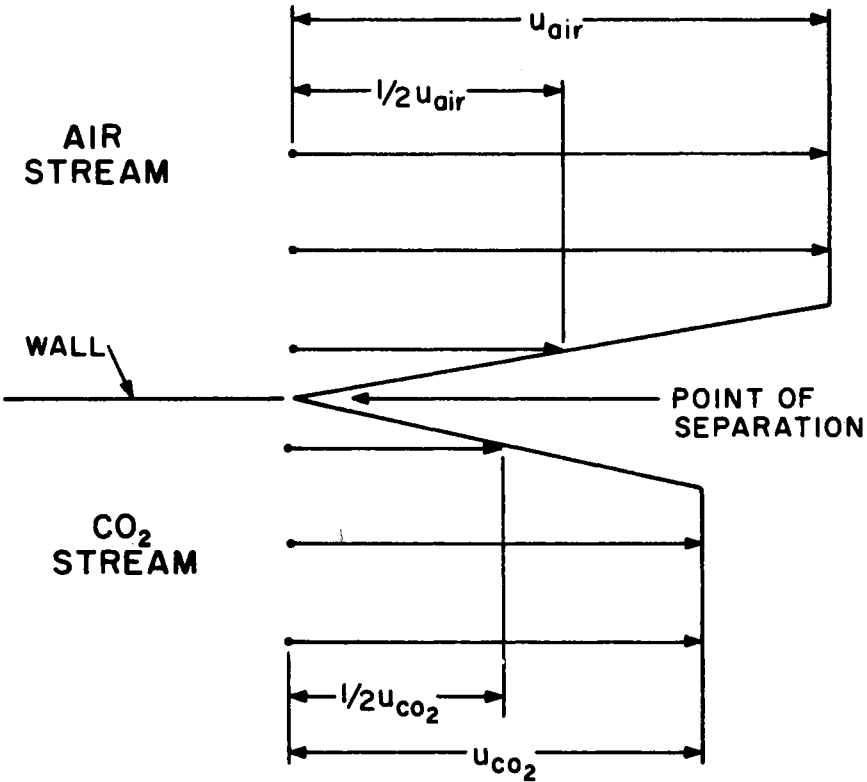


Figure 17. Boundary Layer Velocity Distribution for Run II

downstream. Therefore, any reasonable velocity profile should only effect a region several radii downstream of the point of separation. From a pragmatic viewpoint, implementation of an analytic solution presented in Chapter V requires integrations of the boundary layer velocity profiles. Use of more realistic (and, consequently, more complicated) profiles would necessitate numerical integration; whereas, insertion of linear functions permits analytic integration. Furthermore, the numerical method utilizes only spatial average values so that, regardless of the actual functional relationships assumed for the velocity profile, a linear profile may be substituted in such a way that the value at the node point is equal to the average value of the actual function -- averaged over the region the node represents.

To increase the level of turbulent stresses at the point of separation, the axial coordinate for the eddy viscosity, equation (2-27), was measured from a point upstream of the point of separation. In order to make a rough estimate of this shift, the distance, z_0 , between the point of separation and the upstream ordinate was determined by assuming that the boundary layer developed in a manner analogous to the way similar velocity profiles "spread" in the free jet mixing region as predicted by the Korst theory of mixing (see Chapter V). That is, either boundary layer was assumed to be like one-half of the velocity profile for free jet mixing. The Korst

theory of mixing indicates that error function velocity profiles are a function of one variable, η , which is a function of both the downstream coordinate and the transverse, or in this case, the radial coordinate. Specifically η is roughly of the form

$$\eta = \sigma \Delta r / z . \quad (4-1)$$

For an error function velocity profile the edge of the mixing region is reached at an η of 3.0. With the boundary layer size that was assumed for this case, the upstream coordinate shift was determined by:

$$z_o = \frac{\sigma \delta}{3} . \quad (4-2)$$

Because of the node arrangement:

$$\delta = \Delta r \quad (4-3)$$

where Δr numerical had the value of 0.05128205. With the use of these expressions, z_o was assigned the value of 0.52307691. It perhaps needs to be further emphasized that this analysis was, by no means, intended to describe the actual boundary layer phenomena near the point of separation, but merely to make a rough guess at the value of z_o .

After the upstream boundary layer alterations were made, calculations proceed from time plane 627 of Run I to time plane 1695 (a time plane span of 1068). However, the addition of the upstream shift of the z ordinate in the eddy viscosity was not added until time plane 927 -- an oversight on the author's part.

The pressure ratio curves at time plane 1068, measured from the start of Run II, are shown as dashed lines in Figure 15. It should be noted in this figure that the boundary layer effects are very much reduced in comparison to those of Run I. A comparison of these Run II pressure ratio curves with experimental data is shown in Figure 18. This comparison indicates only fair agreement of the calculated values with those of experiment. However, attention is directed to earlier remarks which concerned the percent of error indicated by curves such as those in Figure 13. At the centerline and the outer edge of the indicated flow field, the maximum error is of the order of five percent. In the region of maximum turbulent shear, where the error appears to be rather large, consideration must be given to the degree of experiment accuracy. While this information was not presented in Reference 24, it is a well-known fact (Reference 66) that pitot tubes inserted in a region where steep velocity gradients exist, tend to shift the measured total pressure toward the high pressure values.

In Figure 19 is shown the nondimensionalized pressure distribution at an axial location just downstream of the point of separation. As in Run I, instabilities are indicated. While it was expected that the assumed boundary layer velocity distributions would decrease the pressure in the region downstream of the point of separation, it was also hoped that the inclusion of z_0 would have a stabilizing effect.

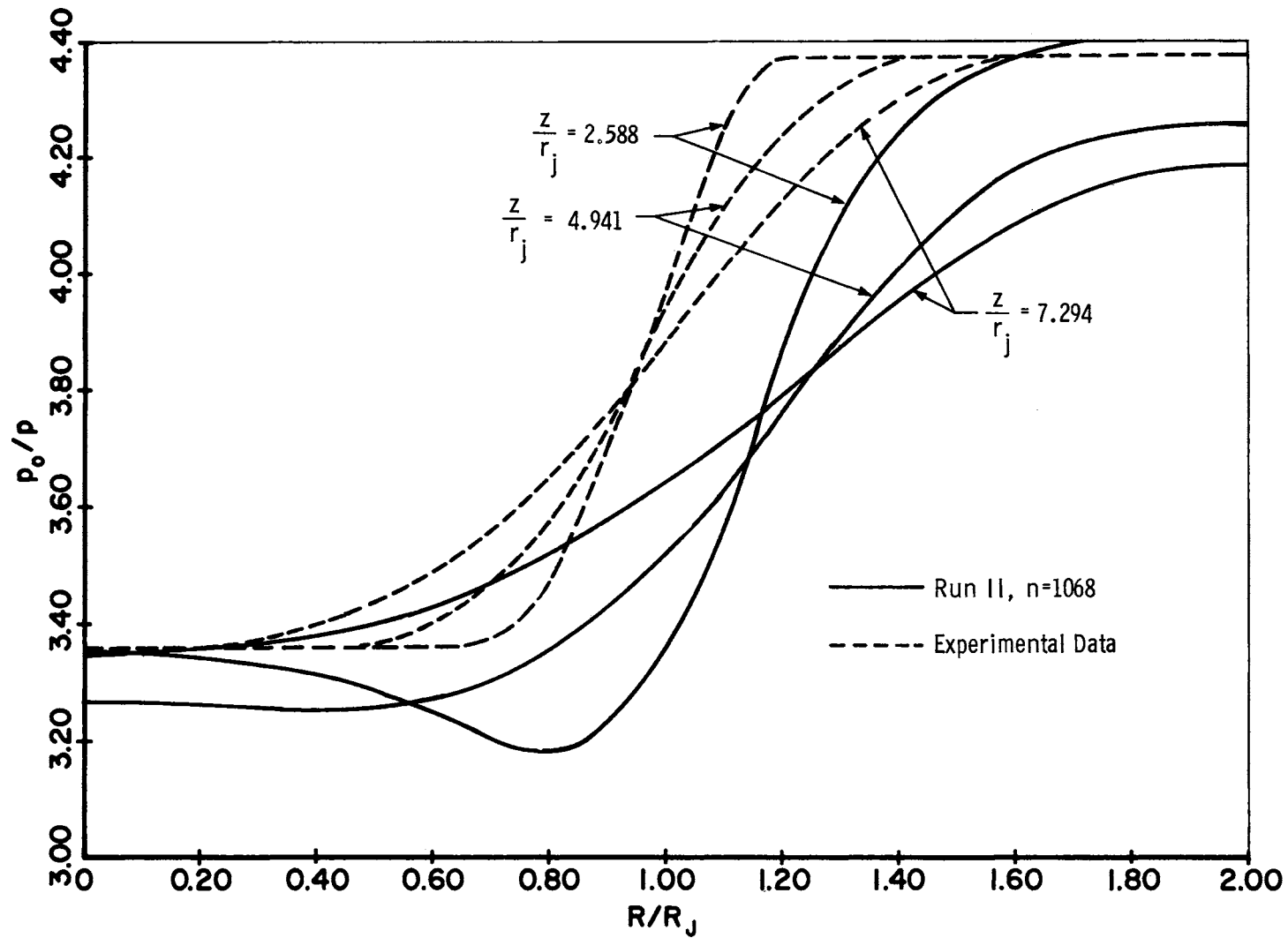


Figure 18. Stagnation Pressure Comparisons of Experimental Data and Run II (n = 1068) Results

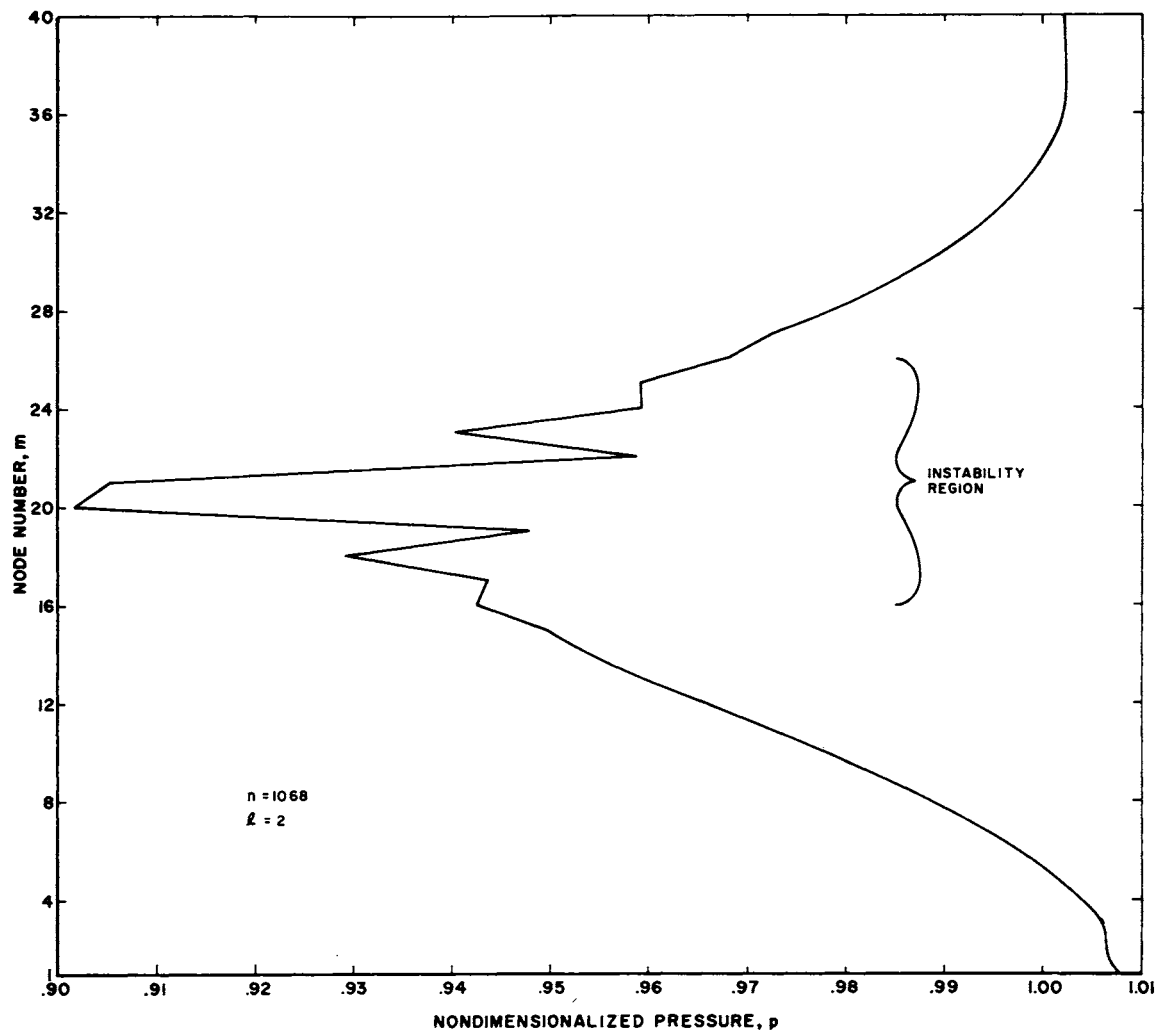


Figure 19. Radial Profile of Pressure in Unstable Region for Run II

Apparently it did not. Curiously enough, it appears that the instability is symmetric.

There is one final note to be made. Although an instability did appear to exist in a small local region just downstream of the point of separation, examination of pressure distributions in other regions of the flow field for this and all other cases reported herein did not reveal any other instabilities. Further, because the pressure ratio profiles exhibit expected trends, it was concluded that the slight upstream instabilities had little or no effect on downstream profiles.

Run III

With the observation that the previous numerical calculations indicated a greater degree of turbulent mixing than did the experimental data, attention was directed towards the effect of the grid spacing. It was the opinion of this author that, in the previous two cases, the turbulence effects could more easily propagate in the radial direction than in the axial direction due to rather large value of the ratio of $\Delta z/\Delta r$. To rectify this a smaller ratio of $\Delta z/\Delta r$ was used. This was accomplished by decreasing the number of nodes in the radial direction to thirty-two and increasing the number of nodes in the axial direction to forty-one. The ratio of $\Delta z/\Delta r$ became 2.906.

This sort of arrangement was dictated by two considerations. The first consideration pertained to available core storage in the IBM 7040 computer. Approximately 1300 nodes could be

accommodated. Node fields bigger than herein described would require very time consuming data shuffling on tape units.

The other consideration concerned the geometrical area that had to be covered by node field. Previous experience (Runs I and II) indicated that, indeed, the ratio of r_{\max}/r_j should at least have a value of two. Furthermore, the experimental data extends a distance of $z/r_j = 7.294$ downstream. The node system, therefore, had to extend several mesh spacings beyond this location in order to decrease the possible upstream influence of the downstream boundary calculation scheme.

Under these restrictions, the axial spacing, Δz , assumed the value of 0.1875 and the radial spacing, Δr , 0.06451613.

In addition to the rearrangement of the node field, a modification of the damping parameter, ω , was incorporated in this study. Because the desire was to decrease the degree of apparent downstream mixing, ω was assumed to have a value of 0.1 for the first fifteen nodes and a value of 0.05 for the remainder of the nodes. The effect of such a scheme is to decrease the mathematically effective viscosity for downstream locations.

The upstream boundary was assumed to have the same distribution as those used for Run II. However, since Δr for this study is slightly greater than that for Run II, the assumed boundary layers are also slightly larger. This slight difference was felt to have

negligible significance.

The initial conditions were developed in the same manner as was done for Run I. That is, all downstream locations were identical to the upstream boundary.

The ensuing results of calculations for the above described conditions are displayed as dashed lines in Figure 20. Also shown in this figure are the results of Run II. The results for Run II are for time plane 1068 and those for Run III are for time plane 1181 so that the comparison is at comparable time planes (after 1000 time steps only insignificant changes occur in less than one-hundred time steps).

Since the comparison is very close, these results were examined with two questions in mind. First, what, if any, is the effect of the node rearrangement, and, second, how much did the ω modification influence these results? To answer these questions, the second question was considered first. The answer was determined by performing calculations for several additional time steps for Run III and examining the order of magnitude of the terms in the finite difference equations. In both the region where $\omega = 0.1$ and the region where $\omega = 0.05$, the pseudo-viscous dissipation terms were approximately three orders of magnitude smaller than other significant terms in the finite difference equations. This led to the conclusion that, by decreasing the downstream value of ω by one-half of its upstream value, little, if any, effect was accomplished.

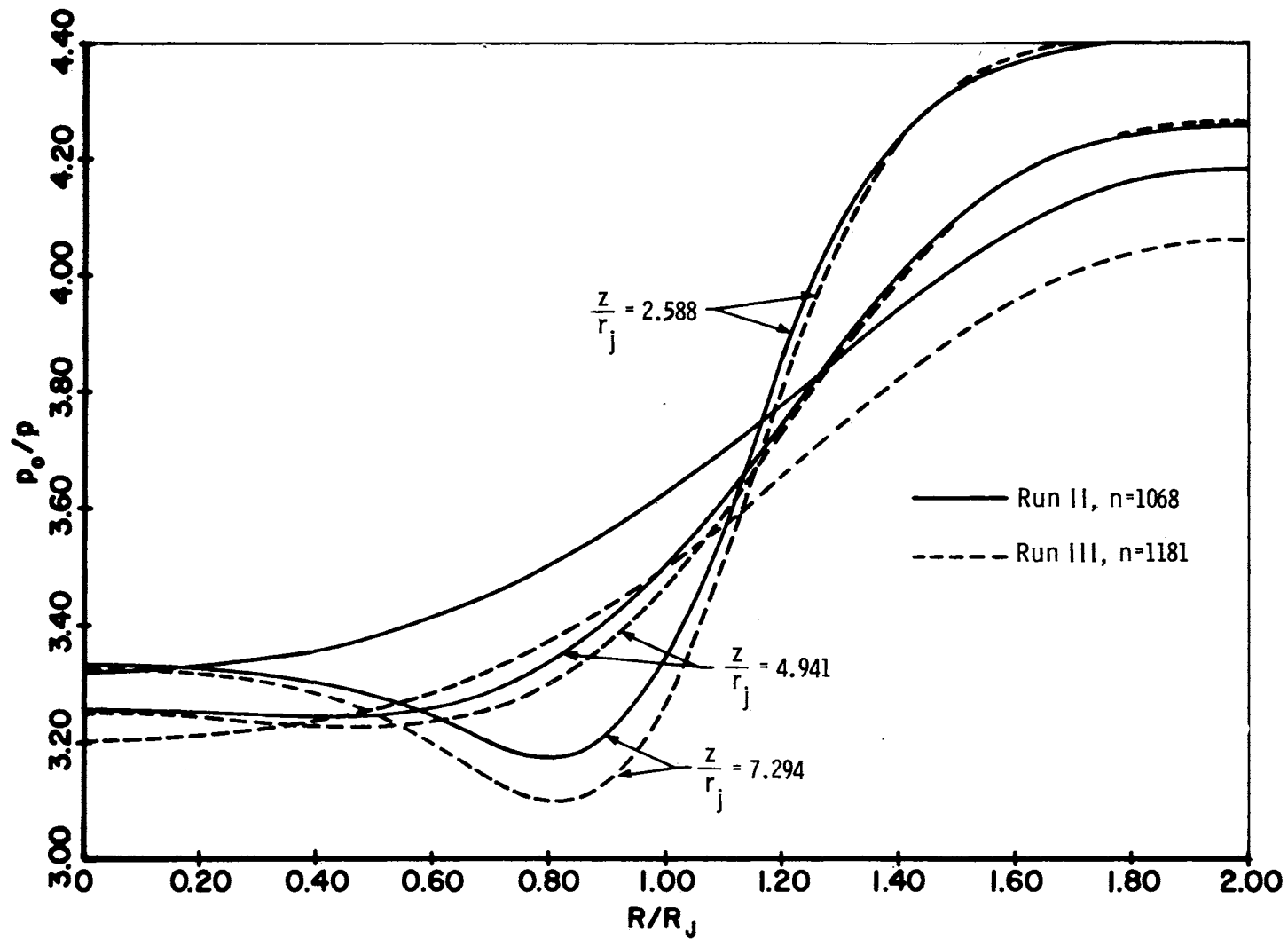


Figure 20. Stagnation Pressure Comparisons of Run III (n=1181) and Run II (n = 1068)

Further, this answer to the above posed second question also answered the first question. That is, the change in mesh spacings considered here had only a small effect. The largest difference in the $z/r_j = 7.294$ pressure ratio curve is of the order of four percent.

Finally, it should be noted that the comparison made in Figure 13 above is for this run at time plane 611 and 1181 for the solid and dashed lines respectively. As pointed out above, this is a demonstration of the degree with which the steady state condition was approached. More will be said concerning this in connection with the results of Run VI.

Run IV

In the previous three runs, it was assumed that everywhere on the upstream boundary, the flow was parallel with no radial components of the velocity vector. Since, experimentally, this condition is difficult to achieve, this study was conducted to ascertain the effect of slightly divergent flows which are more commensurate with reality. The mesh spacings for this run were the same as those for Run II and the initial conditions were established in the same manner as those for the previously discussed runs. In fact, all the computer programs associated with Run III were unchanged for this study -- only the upstream boundary conditions (and, consequently, the initial conditions) were changed.

To develop the divergent flow, it was assumed that the flow from each nozzle could be described as a "source" flow. That is, it was assumed that the flow at the exit of a divergent nozzle is such that it may be described by a flow emanating from a point with straight streamlines (see Figure 21). In the analysis for this study, it was assumed that the wall divergence angle, θ , was small and that the magnitude of the velocity vector for each nozzle was constant (excluding the boundary layers) with only a change in the direction of the vector. The divergence angle for the air stream θ_o , was approximately 2.9 degrees and that of the CO₂ stream, θ_j , was approximately 5.5 degrees.

In the boundary layers, the velocity magnitude, as with Runs II and III, was assumed to be one-half the magnitude of the free-stream velocity and consequently, the shape of the profiles were similar to those of Runs II and III. The direction of the velocities in the boundary layers was determined by, first, a satisfaction of the requirements of the "source" flow hypothesis, and, then, a correction was made which was based on a crude satisfaction of the continuity equation. See Appendix D for the details of this divergent flow analysis.

The results of the numerical analysis for these upstream boundary conditions are presented in Figure 22. In this figure, the data for this Run are for time plane 583 and are contrasted with the

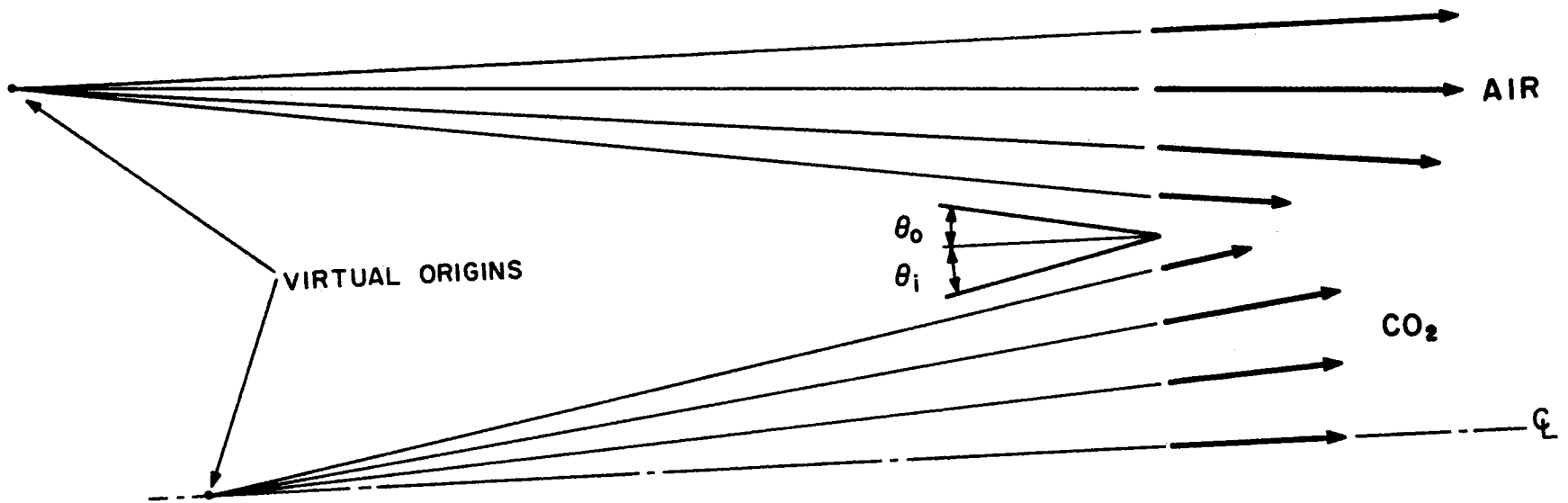


Figure 21. Divergent Flow Upstream Boundary Condition for Run IV

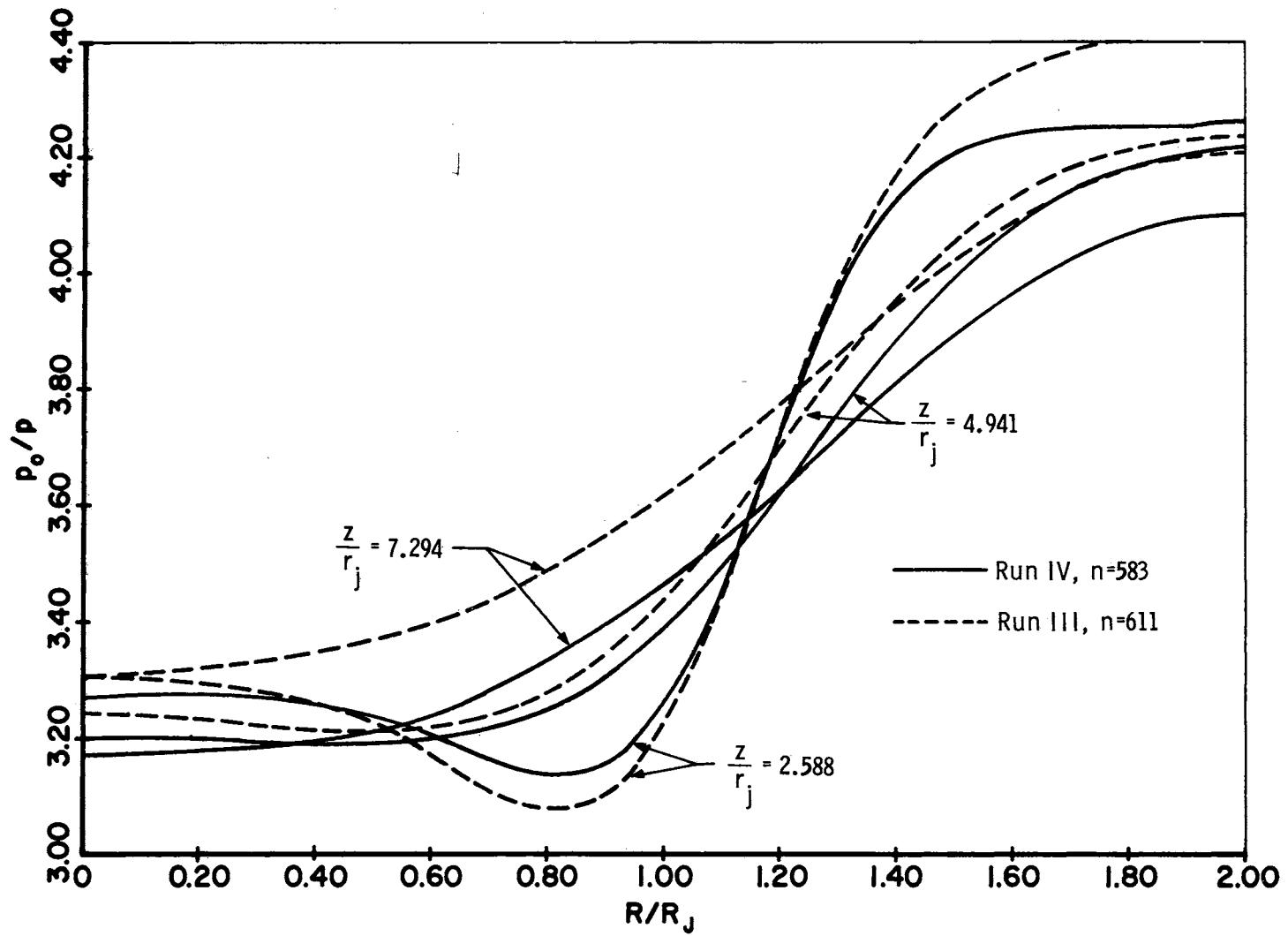


Figure 22. Stagnation Pressure Comparisons of Run III (611) and Run IV ($n = 583$)

data from Run III for time plane 611. There are only two significant differences indicated. At radii greater than approximately $r/j_j = 1.5$, the $z/r_j = 2.588$ curve is about three percent lower than that for the Run III results. Also, the $z/r_j = 7.294$ curve is, at worst, five percent lower than that for the Run III results. Nonetheless, at either end of the curves the maximum error, in comparison with experiment, is no greater than approximately six percent.

Perhaps the most significant effect of the upstream boundary conditions for this run was exhibited by the pressure in the vicinity of the point of separation. It no longer displayed the instabilities which appeared in the previous runs. Furthermore, in this region, printed "output" indicated the existence of weak compression waves which are eventually dissipated by expansion waves which emanate from the nozzles due to the assumed expanding nature of the exit flow. Figure 23 is a sketch of the effects exhibited by the nodal pressure values.

Run V

Thus far, all numerical method calculations have used the Case I type of turbulent shear stresses which were discussed in Chapter II. In this run, the effects of the Case II type turbulent shear stresses were used. It is important to note that where Case I type stresses were used, only these stresses were involved and, correspondingly, in this run only Case II stresses were considered.

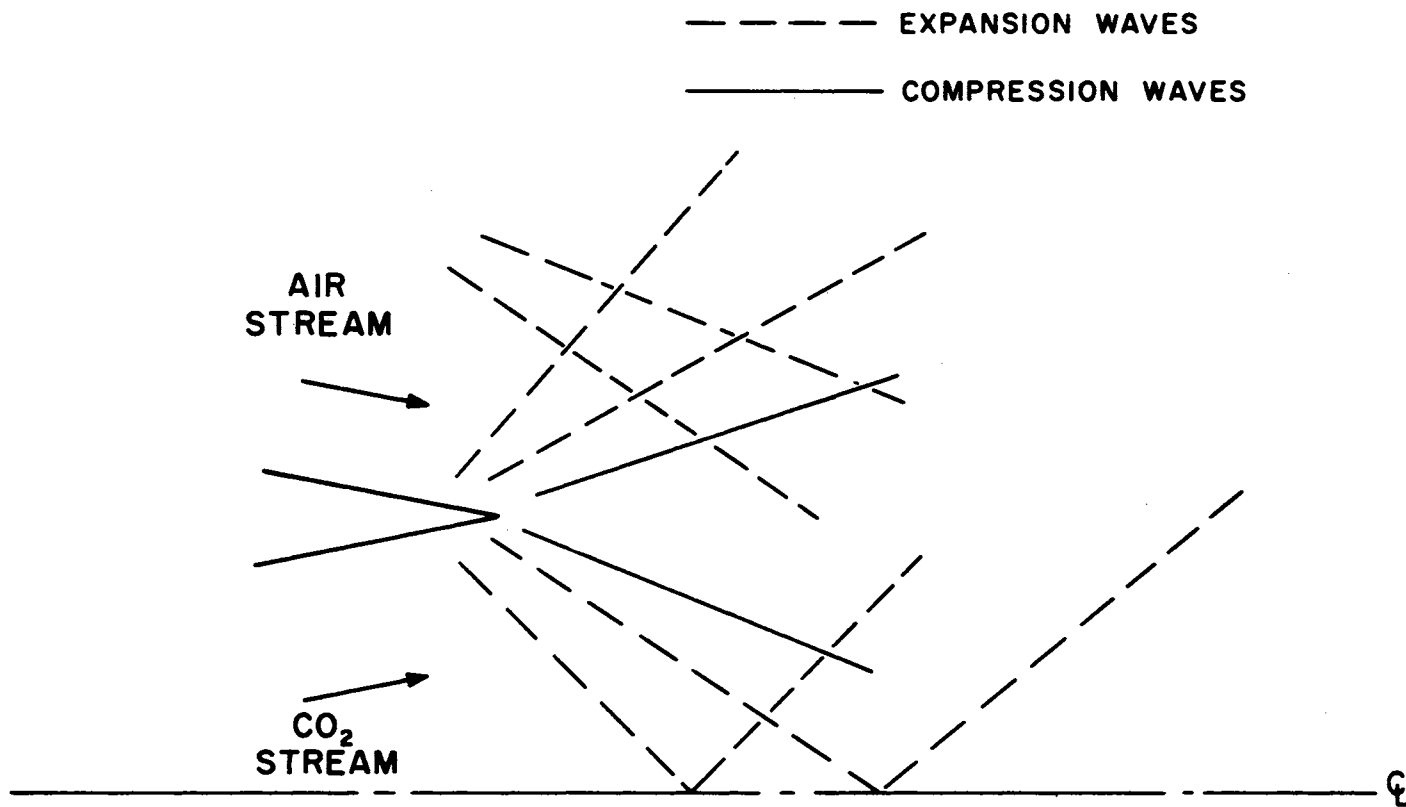


Figure 23. Sketch of Wave System Indicated by the Results of Run IV

Never were stresses of the form

$$\tau_{xy}^{(t)} = \rho \epsilon_m \left(\frac{\partial u}{\partial r} + \frac{\partial v}{\partial z} \right), \quad (4-4)$$

which involve both Case I and Case II stresses, and which are the analogue of laminar type stresses, used. This point will be emphasized later.

Further, with the advantage of insight and experience, four additional changes were made. By rearranging the logic of the main computer program, the run time was reduced from approximately three and one-half minutes per time step to approximately two minutes a time step. While this modification contributes nothing to the theoretical development and the understanding of results, future investigators will greatly profit financially by bearing this point in mind.

In a more theoretical vein, the damping parameter, ω , was modified so that in the vicinity of the point of separation, it had a value which equaled the inviscid stability value at the point of separation and decreased exponentially to a value of 0.1. The equation for ω was:

$$\omega = 0.1 + 0.4 e^{-2z} \quad (4-5)$$

where z is the axial coordinate.

This modification was made in an attempt to prevent the pressure instabilities which arose in all previous runs with the exception of Run IV. It was anticipated that these instabilities would occur

since recourse was again made to a uniform parallel flow with boundary layers at the upstream boundary for this run. However, instead of the rather severe boundary layer shapes which were previously employed, the average velocity for a turbulent boundary layer shape was determined by a straightforward integration of the one-seventh velocity profile over the area. This, of course, neglects density variations, but the inclusion of these variations would unduly complicate the analysis. Once the average velocity was determined, a linear velocity profile was assumed which would yield the same average velocity. This substitution of velocity profiles was more for the purposes of the analysis in Chapter V than for this investigation. In any event, the average velocity for each boundary layer was imposed at each respective node point in the respective boundary layers (see Figure 24).

The initial conditions were assumed to be the solution of the analytic theory presented in Chapter V. This was a further attempt to decrease the necessary run time for the asymptotic approach to a steady state solution. That is, it was predicated that the closer the initial conditions conformed to the steady state solution, the shorter the computer run time required. This point will be justified in the discussion of the results of Run VI.

For this run, pressure ratio curves for a $z/r_j = 2.588$ and at various time steps are displayed in Figure 25. If consideration is

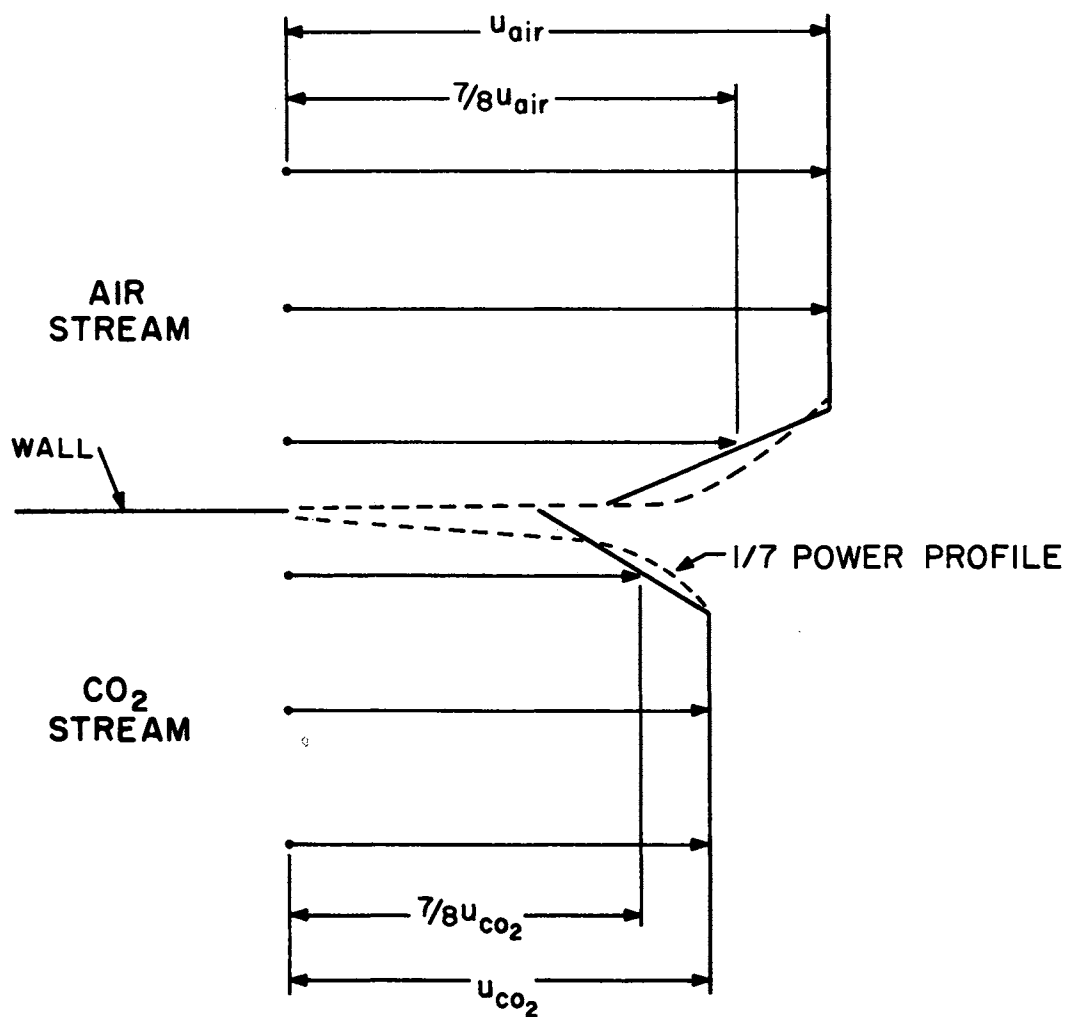


Figure 24. Boundary Layer Velocity Distribution for Run V in Comparison to the $1/7$ Power Profile

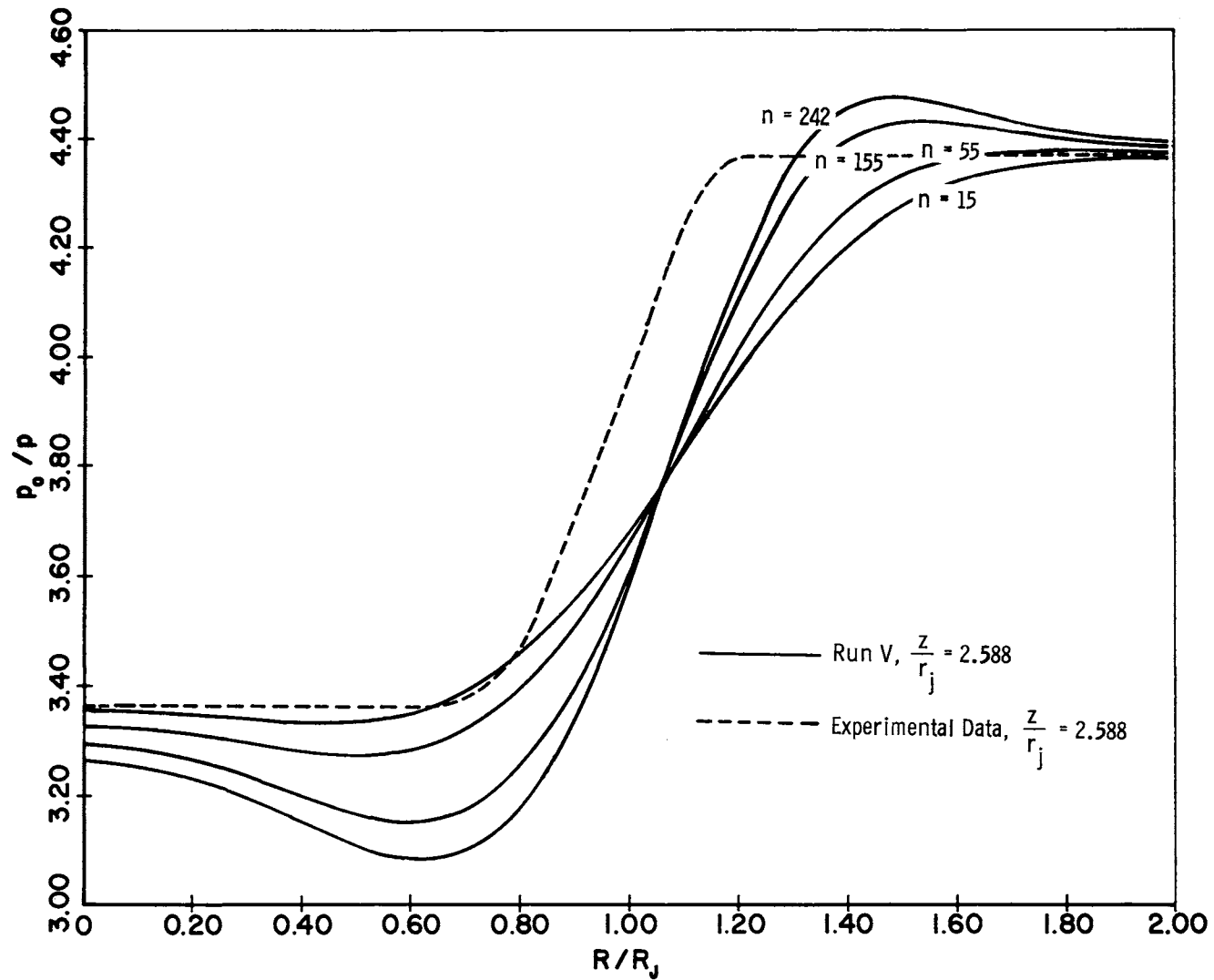


Figure 25. Results of Run V for Several Time Steps in Comparison with Experimental Data

given to the degree of change for each of the three intervals (e. g. between $n = 15$ and $n = 55$, etc.) it appears that, due to the small change between $n = 155$ and $n = 242$ as contrasted to that which occurred between $n = 55$ and $n = 155$, the calculation was approaching a solution albeit an unrealistic solution. Consequently, it was concluded that, although incorporation of Case II type turbulent shear stresses does not inhibit the approach to a steady state solution by themselves, they do not represent physical reality by themselves.

In the region downstream of the point of separation, results of calculation indicate only a slight degree of instability (the radial pressure variations are of the order of three percent or less -- generally less). Because both the boundary layers and the value of ω were altered, the contribution of each change to the stability of the pressure was not discernible. Certainly, the form of exit condition affects the stability of the calculation. This was demonstrated by Run IV. However, it must also be recognized that ω was below the minimum value for inviscid stability in a region where turbulent viscous effects were a minimum.

Run VI

In order to gauge the effect of the "simulated" turbulent boundary layer which was used in Run V without the complexity introduced by consideration of Case II type of turbulent shear stresses, the initial and boundary conditions for Run V were reconsidered with the

incorporation of only Case I type of turbulent shear stresses. Again, the damping parameter ω was taken as expressed in equation (4-5).

After 350 time steps, the pressure ratio curves were as shown in Figure 26. Also shown in Figure 26 is the experimental data-comparison, which appears to be fair. At this point attention is directed to Figure 25 which contains a comparison of some results from Run V with appropriate experimental data. Consideration of these two figures indicates that whereas incorporation of Case I turbulent shear stress terms tends to equalize the stagnation pressures across a mixing region, incorporation of Case II turbulent shear stress terms tends to maintain not only a disparity in the stagnation pressures, but increase the difference in the stagnation pressures. Consequently, these results built a strong case for the hypothesis that a linearization of the flow equations, in this case a linearization of the turbulent analogue of the laminar shear stress expressions, may produce erroneous results when incorporated in a finite difference method. Moreover, one may suppose in view of these results, that, indeed, the flow equations are of such a nature that even in their application to simple flow problems, it is preferable to maintain complete generality when using finite difference equations.

The pressure downstream of the point of separation displayed only one unexpected sudden change and this change was only of the order of four percent. Thus it appears, in the light of the results of

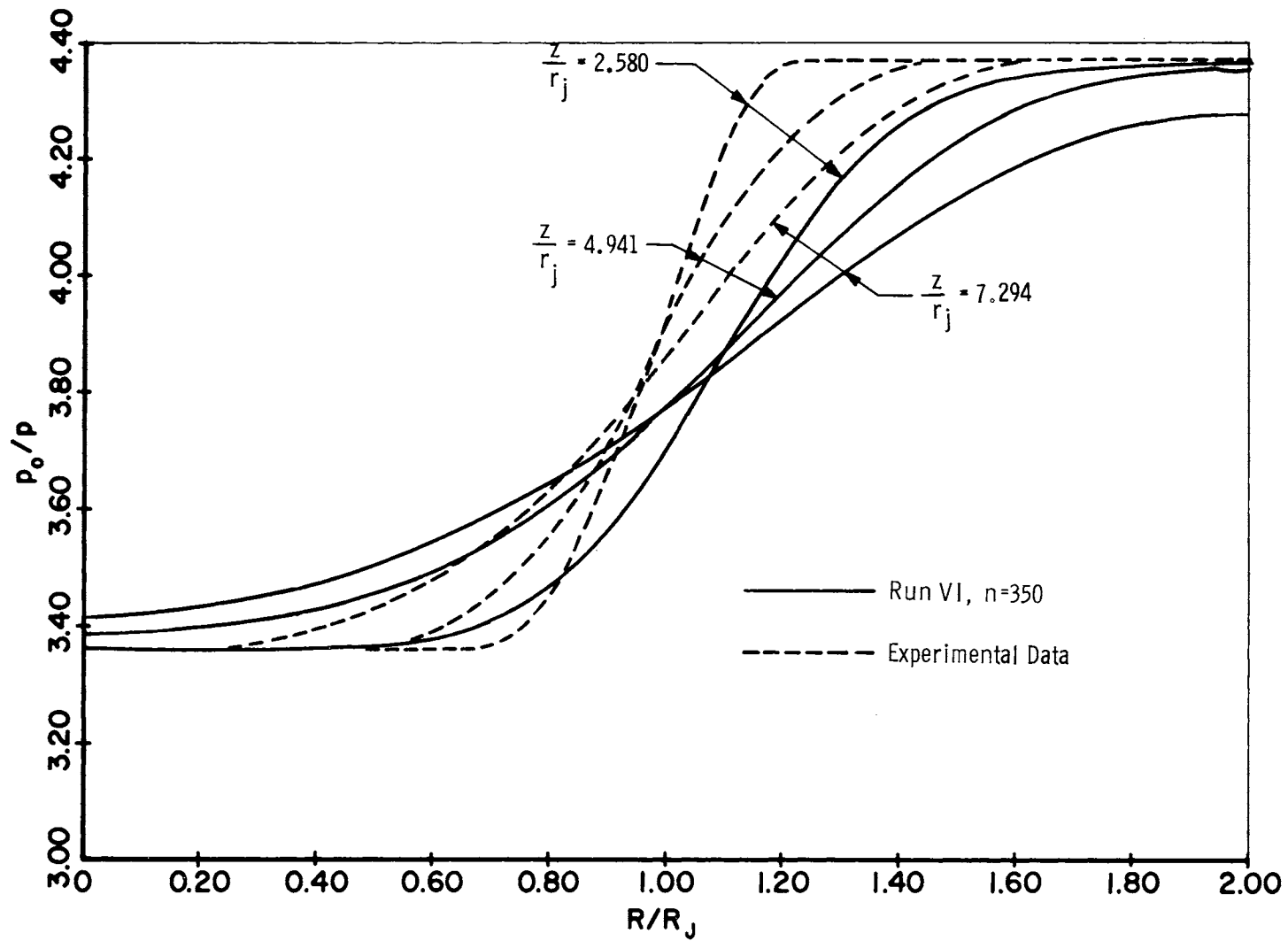


Figure 26. Stagnation Pressure Comparisons of Run VI (n = 350) with Experimental Data

Run V, that the form of the flow equations also effects the degree of the pressure instabilities.

The onset of a steady state condition is suggested by Figures 27 through 32. In these figures, dependent variables such as pressure, velocity, etc. are plotted versus time step number. The location of each dependent variable is indicated by the set of subscript numbers. The first subscript is the node number in the radial direction and the second subscript is the node number in the axial direction. When reviewing these plots the reader should bear in mind that there are thirty-two nodes in the radial direction and forty-one in the axial direction with point (1, 1) located on the centerline at the upstream boundary. The third number indicates that the n plus first time is being displayed. Furthermore, it should be noted that the scales differ from plot to plot. In fact, the largest variation indicated over the last one hundred time steps by these curves is less than one percent. It should be noted that the node points considered for these plots are scattered over the entire flow field and represent an attempt to select worst cases. In these figures, it was observed that, in the upstream region, a steady state condition is definitely indicated (Figures 27 and 28). In Figure 29, which displays information at the same axial location as that for Figure 28, the achievement of a steady state condition is not as strongly indicated. Nonetheless, the changes are in the fourth significant figure. Likewise, Figures 30, 31 and 32

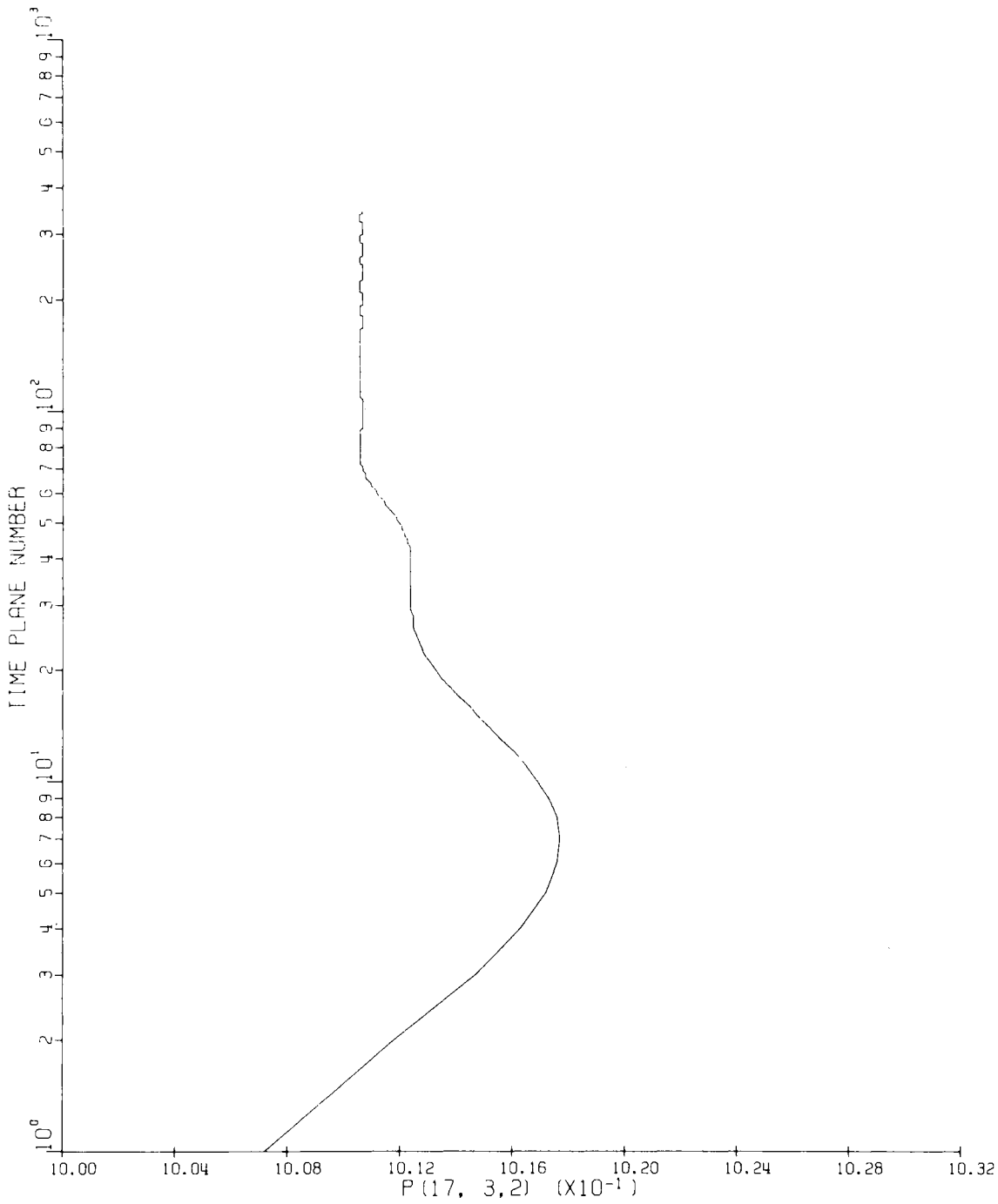


Figure 27. Time-History of the Pressure at Node m = 17,
 $l = 3$ for Run VI

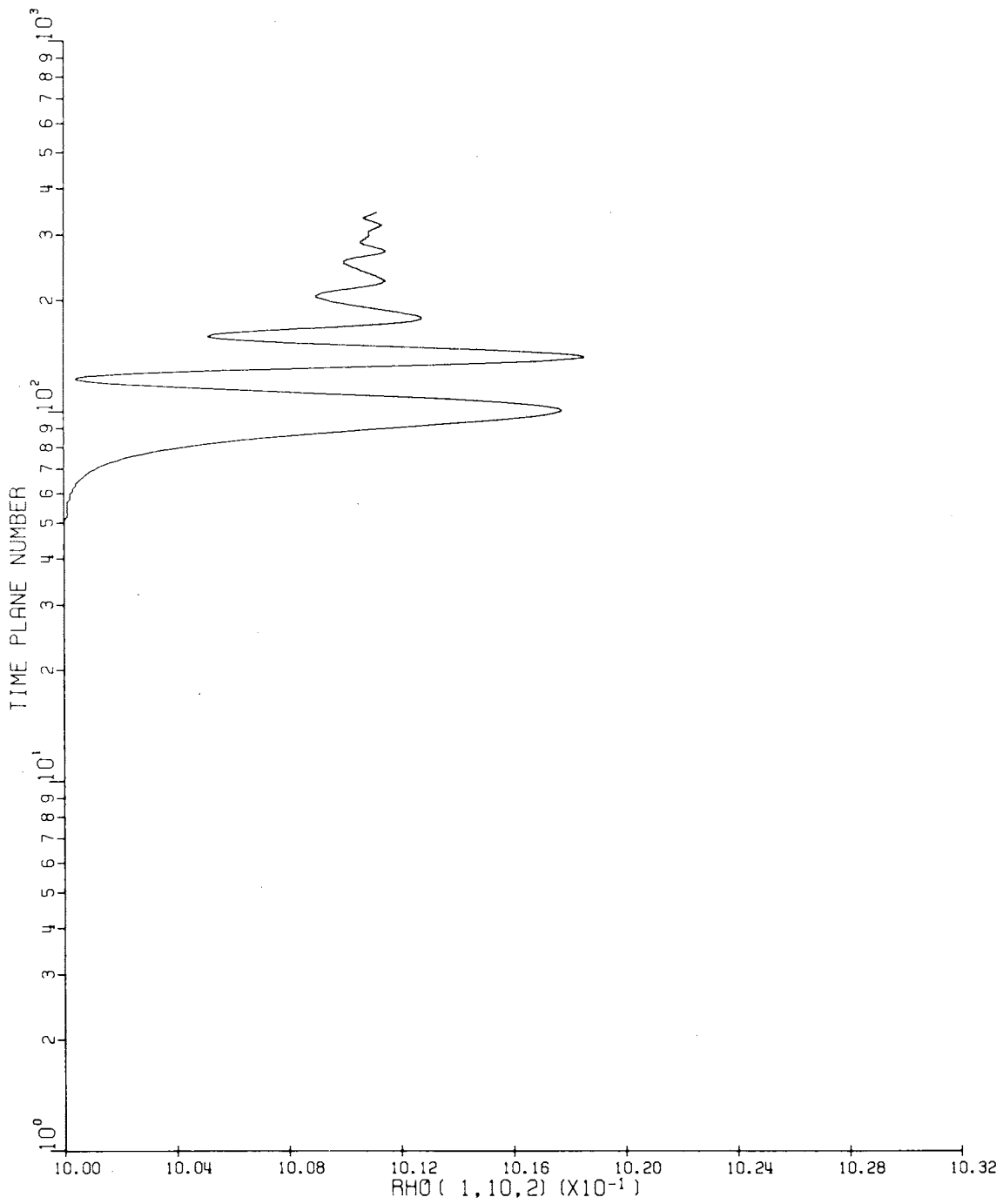


Figure 28. Time-History of the Density at Node $m = 1$,
 $l = 10$ for Run VI

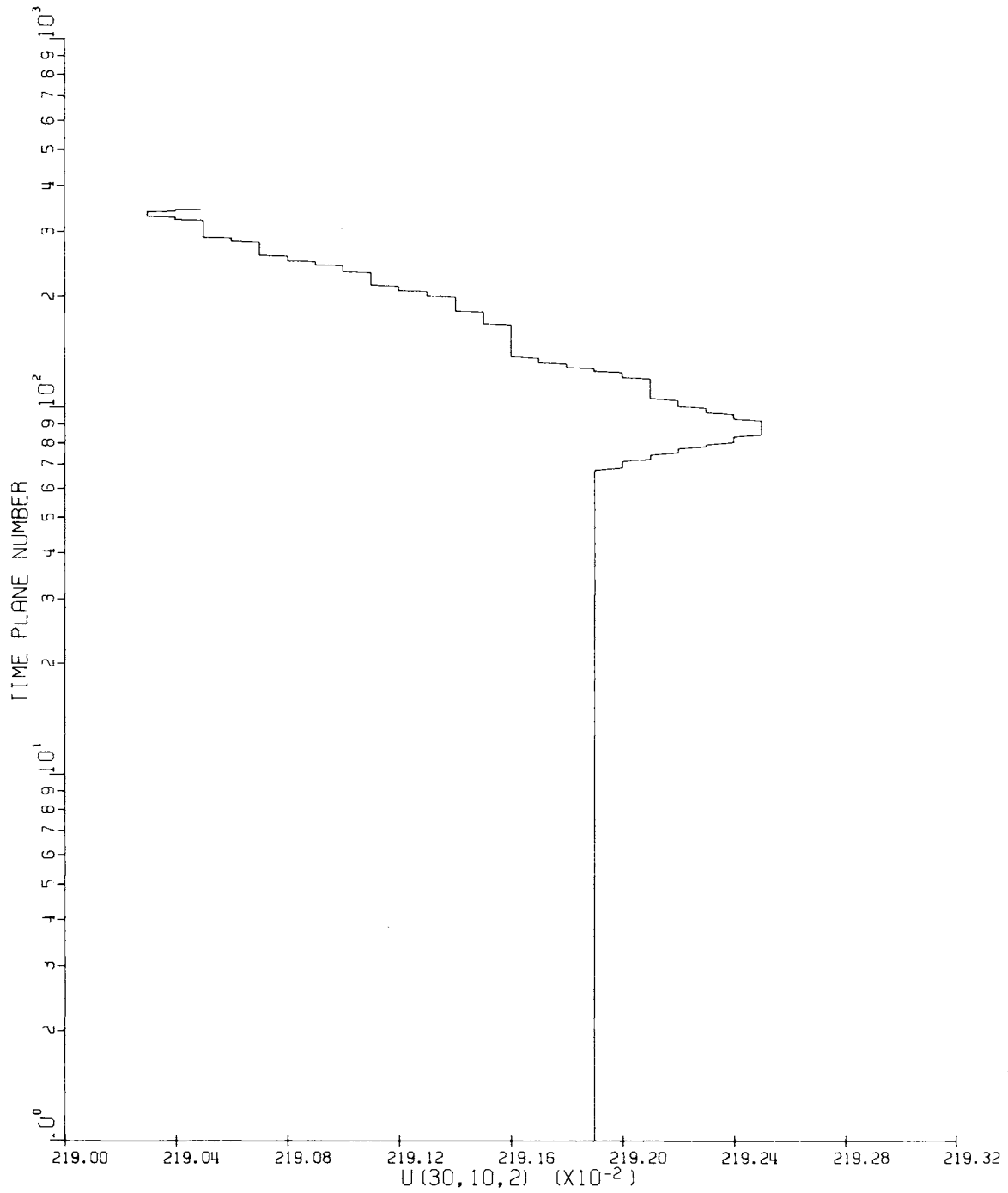


Figure 29. Time-History of the Axial Velocity at Node $m = 30$,
 $l = 10$ for Run VI

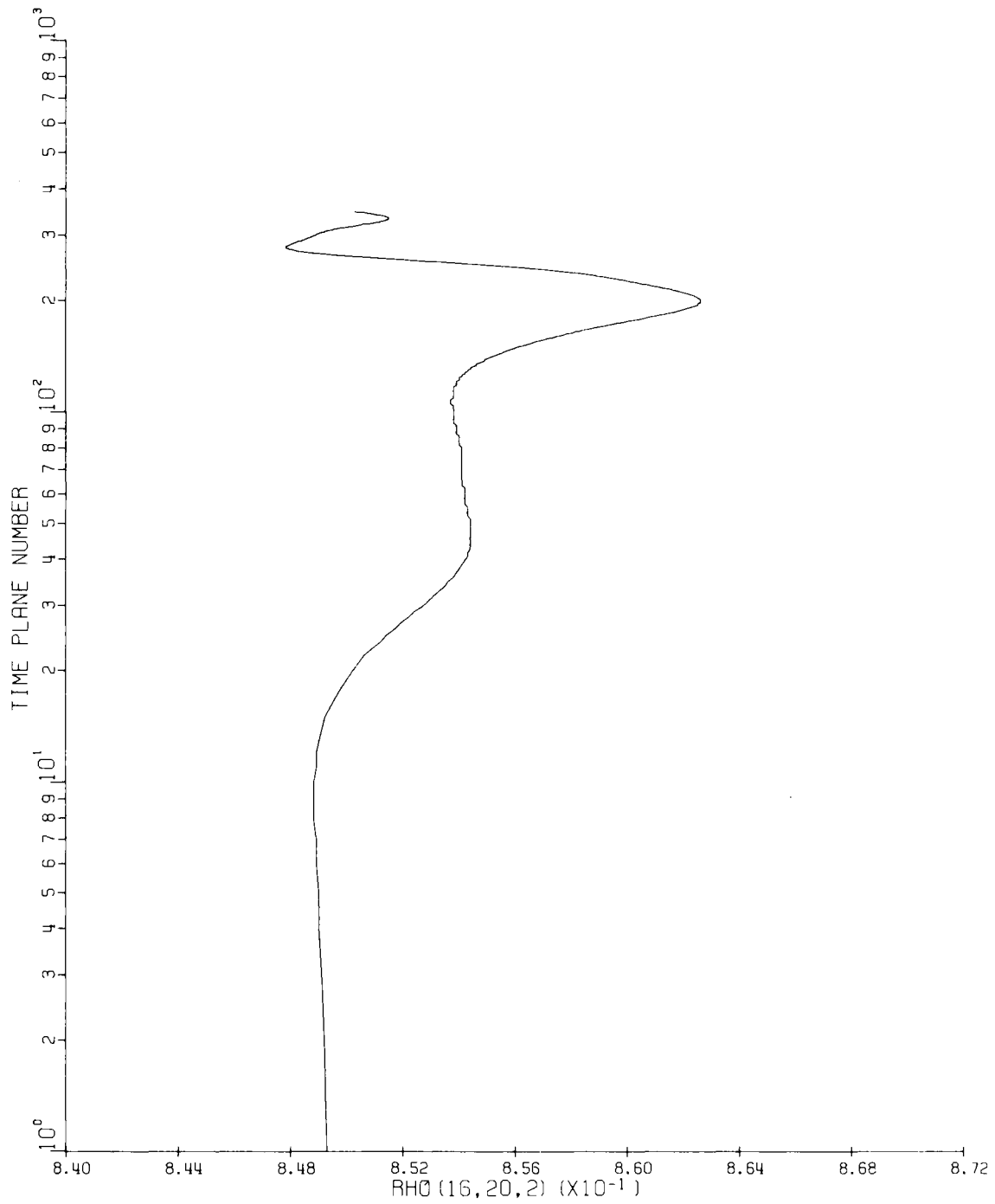


Figure 30. Time-History of the Density at Node $m = 16$,
 $l = 20$ for Run VI

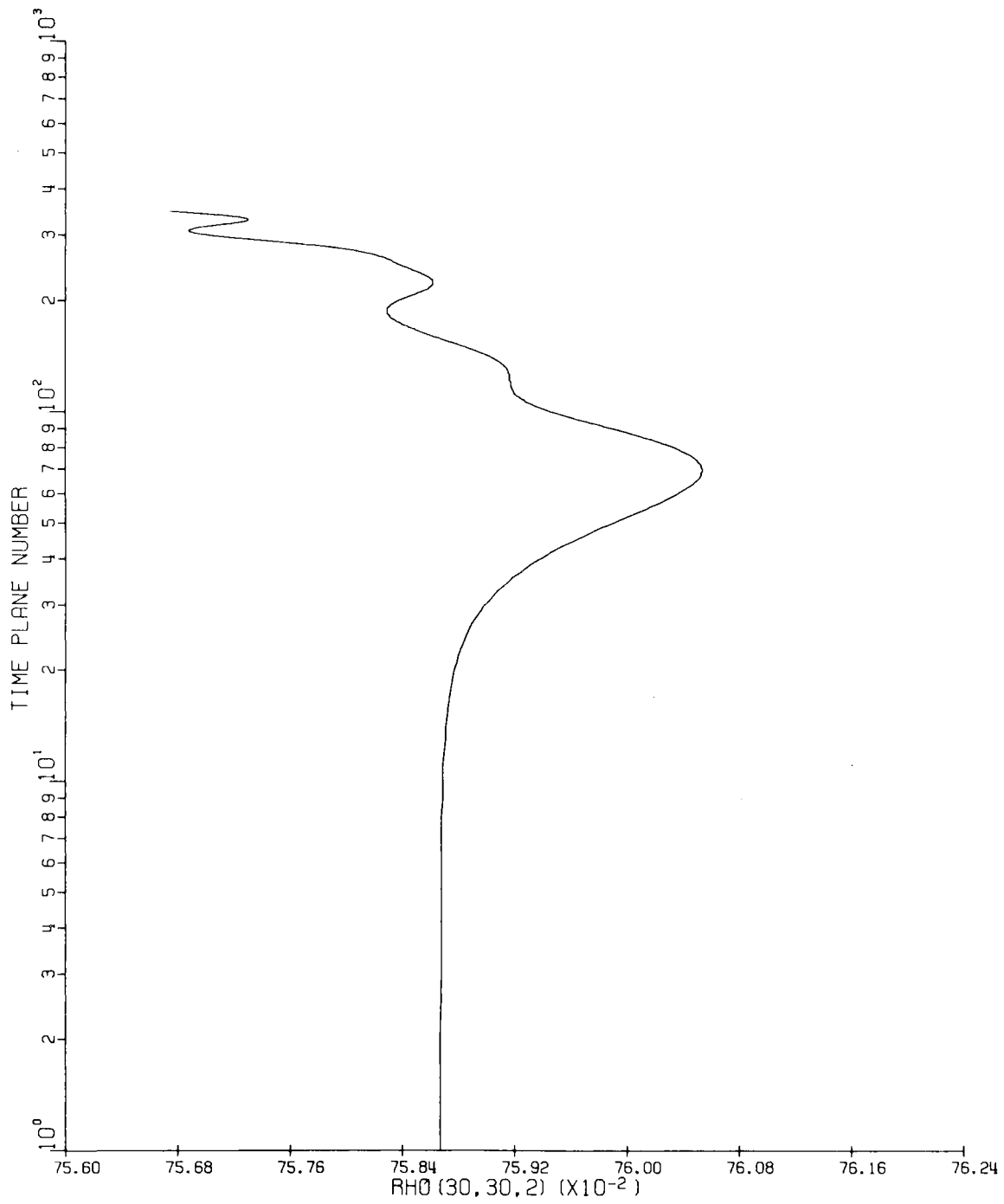


Figure 31. Time-History of the Density at Node $m = 30$,
 $\ell = 30$ for Run VI

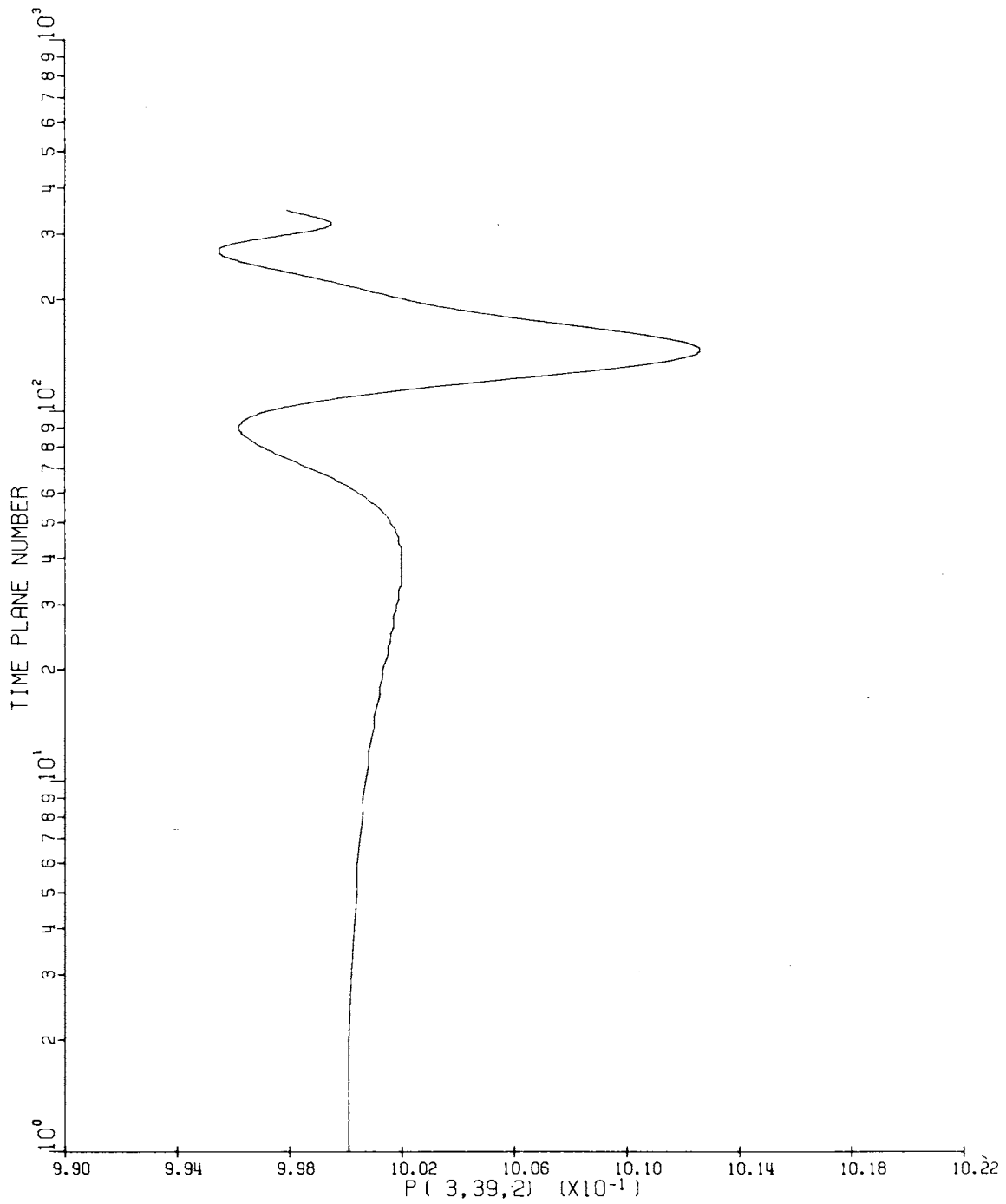


Figure 32. Time-History of the Pressure at Node $m = 3$,
 $l = 39$ for Run VI

are no assurance of a steady state condition; however, the change in the respective values is small for the last one-hundred time steps for each. Further, there appears to exist a tendency of each variable to oscillate, thus diminishing the rate at which the solution diverges (in comparison to a monotonic divergence) from the initial condition. Therefore, in view of the results displayed in Figures 27 and 28, it appears reasonable to suggest that, with additional calculation, the solution could readily approach a steady state condition.

Additional Points for Consideration

The insensitive nature of the carbon dioxide concentration radial profiles is exhibited in Figure 33. Because the profiles at a $z/r_j = 7.294$ displayed the greatest variation from case to case, they have been plotted in this figure. Data from all runs discussed above, with the exception of the results from Run V, where calculation did not proceed far enough for adequate comparison, are present in this figure.

In order to compare the concentration results with experimental data, the data from Run VI have been prepared in Figure 34 together with the experimental data. Because the agreement was only qualitative, a check was made to determine if the experimental data for carbon dioxide satisfied the conservation of mass. Application of this principle revealed that: at the $z/r_j = 2.588$ location there was a

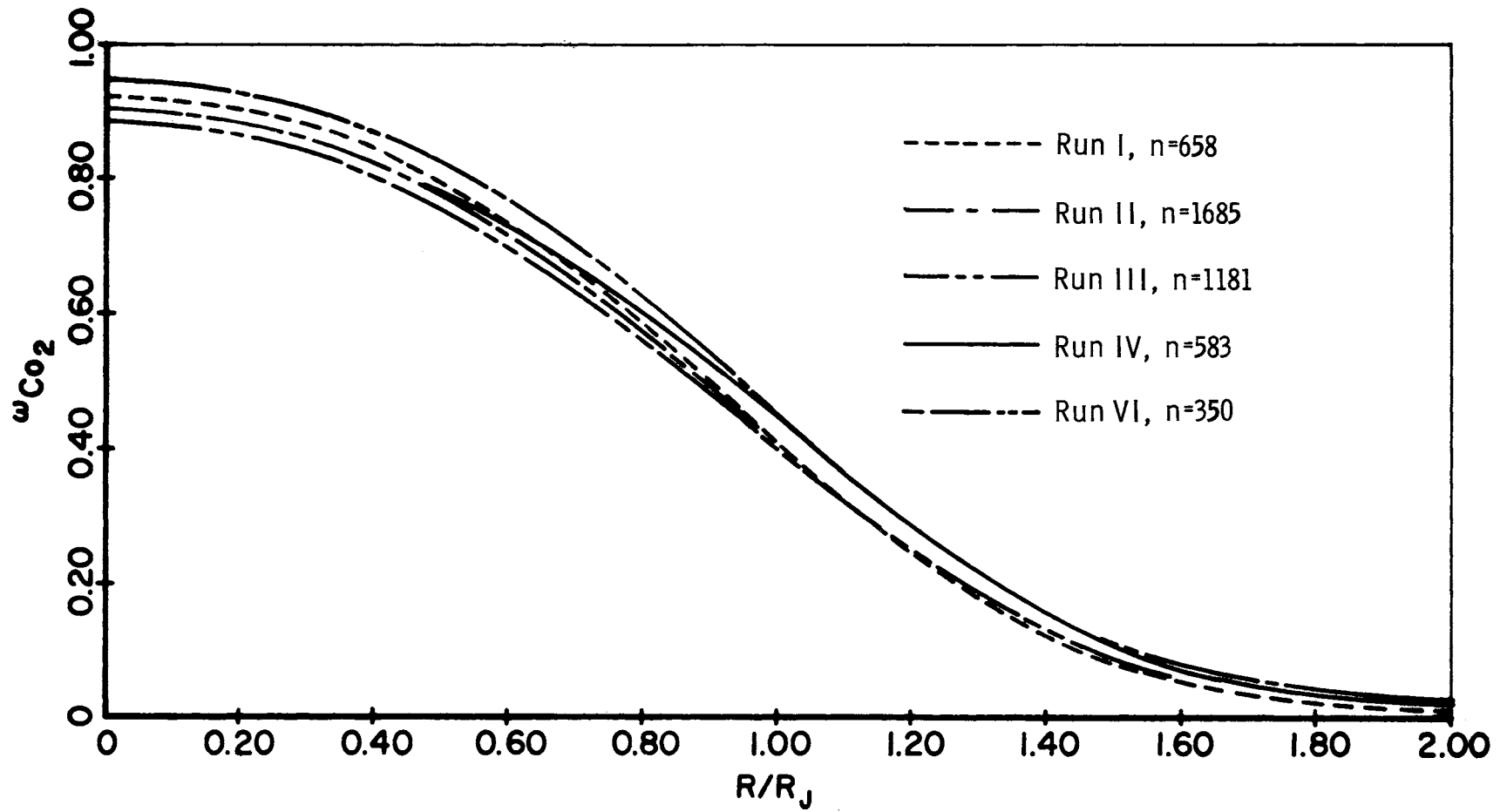


Figure 33. Carbon Dioxide Concentration Comparisons for Different Numerical Calculations

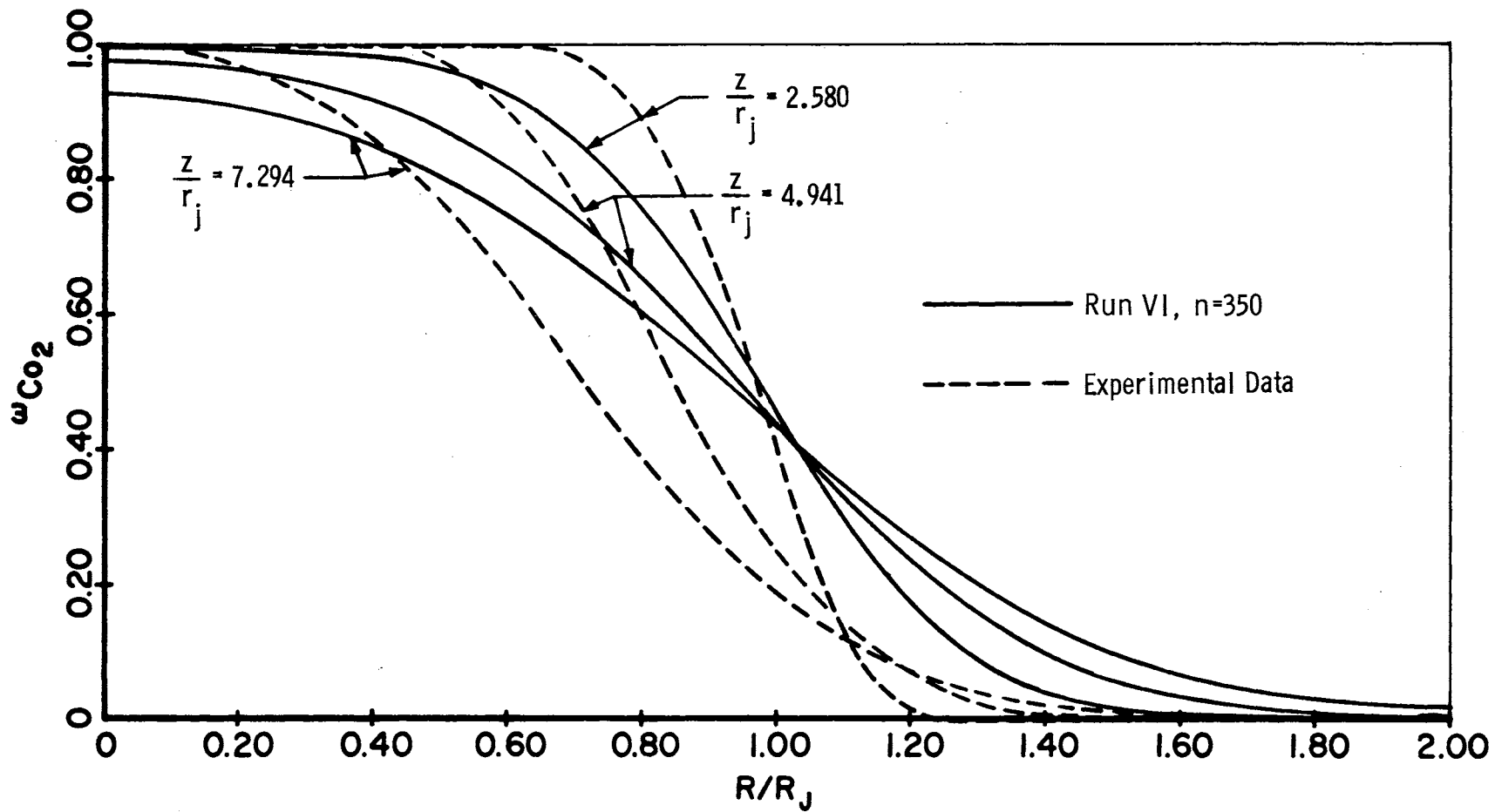


Figure 34. Carbon Dioxide Concentration Comparisons of Experimental Data and Run VI (n=350)

forty-six percent error, at the $z/r_j = 4.941$ location the error was fifty-five percent, and at the $z/r_j = 7.294$ location an error of sixty-three percent was indicated.

With respect to this error, several points are worthy of consideration. Recourse is first made to early discussions which concern the stagnation pressure ratio, p_o/p . The possibility of a pitot tube error is amplified when consideration is given to the comparisons which were made in Figure 26, for example. From inspection of this figure it appears that, if the experiment pressure curves were shifted in the direction of increasing radius (in accordance with the proposed nature of the pitot error) agreement between theory and experiment would be good (especially in light of the discussion concerning the effects of the types of turbulent shear stresses considered in this work). In fact, so far as the theory is concerned, it would be expected that the numerical method would "smear out" velocity gradients, but it would not be expected that the numerical method would result in a radial shift of the mixing region.

Next, the validity of the concentration measurements may be questioned. It is an experimental fact that small concentration levels are difficult to determine accurately. Furthermore, Alpinieri (56) pointed out that the probe tip design is crucial.

Finally, since integral conservation checks of all numerical runs indicated an error of less than one percent, and, in view of the

results obtained by use of, alternately, Case I and Case II turbulent shear stress representations, the possible utility of this scheme for analysis of multispecies turbulent mixing is suggested. Certainly, the results warrant further investigation. A differential, albeit approximate, and integral satisfaction of the fundamental principles may not be taken lightly.

It may be of interest to the reader that, in all runs, the concentrations of air and CO₂ were calculated separately and independently. The constraint that the concentrations must sum to unity everywhere was not employed in the computer programs. However, a check of this constraint for subsequent results indicated that, indeed, it was satisfied everywhere to at least five significant figures. This, of course, was not unexpected. In addition, a check was made on the constancy of the static pressure for all runs. This check indicated that, with the exception of the region in the vicinity of the point of separation, and in Run IV the static pressure was uniform within less than one percent. In Run IV, ten percent pressure changes occurred on the centerline where it would be expected that the expanding nature of the flow would decrease the static pressure.

As further demonstration of the reasonable nature of the results of calculation, velocity and density distributions are presented in Figures 35 and 36. The data for these curves were taken from the results of Run VI at time plane 350.

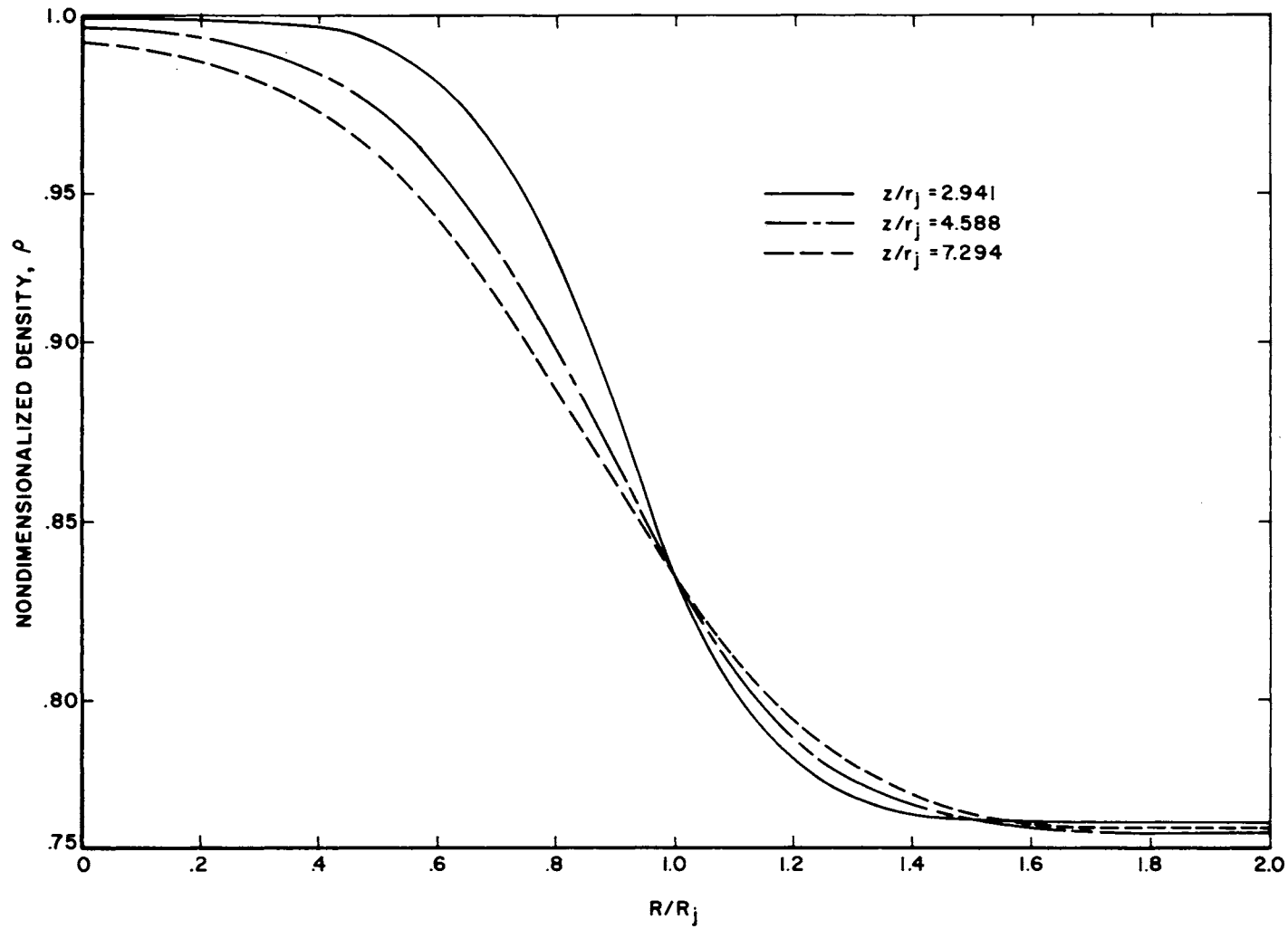


Figure 35. Density Radial Profiles for Run VI ($n = 350$)

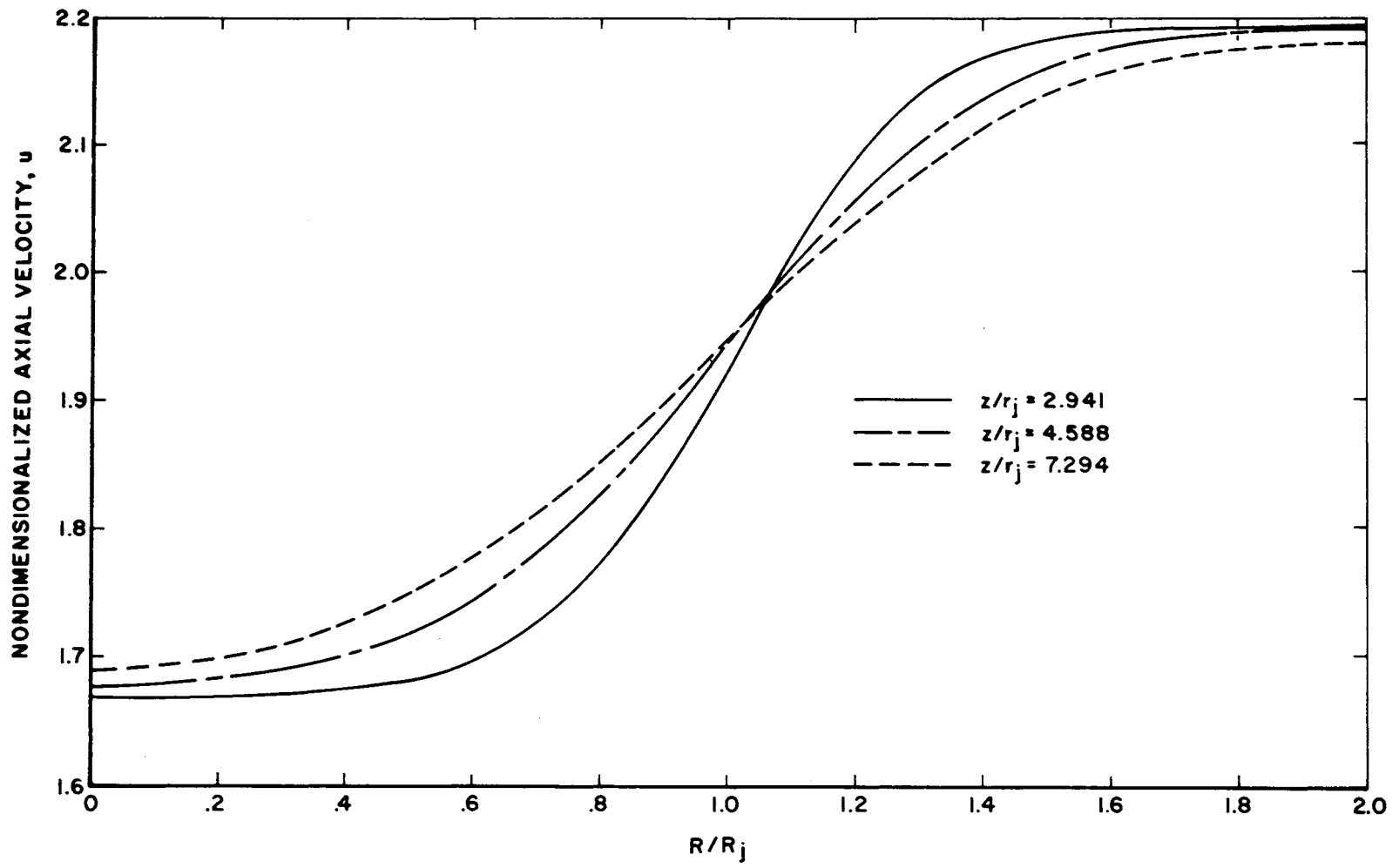


Figure 36. Axial Velocity Radial Profiles for Run VI ($n = 350$)

Conclusions

Below is presented an aperçu of the pertinent conclusions discussed above. Further conclusions will be drawn in Chapter V after comparison has been made with a currently available analytic solution.

1. Assumed boundary layer profiles at the upstream boundary had a pronounced effect on radial downstream distributions.

2. The use of a virtual origin, z_0 , for the purpose of mathematically increasing the level of turbulence at the initiation of free jet mixing was insufficient in the attempt to control localized instabilities.

3. It was found that an exponential decay of w from a value dictated by inviscid stability requirements to a value considerably below normally accepted values successfully established a stable solution in the region downstream of the point of separation.

4. A change in node spacing ratio, $\Delta z/\Delta r$, from a value of 4.5 to a value of 2.906 appeared to have had very little effect.

5. It was discovered that the form of the differential equations and the upstream boundary conditions also had an effect on the degree of instability in the region downstream of the point of initiation of jet mixing.

6. Both the divergent flow (Run IV) and the simulated turbulent boundary layer (Run VI) as upstream boundary conditions

appeared to produce reasonable results despite the number of arbitrary assumptions necessary for the development of the divergent flow boundary condition.

7. By themselves, Case I type turbulent shear stresses resulted in reasonable results whereas Case II type turbulent shear stresses did not. Moreover, it appeared that if these types of shear stresses were incorporated together in direct analogy with the form of the laminar shear stresses, better results than reported here are indicated.

8. Concentration profiles demonstrated insensitivity to the form of the upstream boundary conditions.

9. Comparison of numerical method results indicated fair agreement for the pressure ratio curves and only qualitative agreement for the concentration curves. However, it was also noted that the experimental data is inconsistent with the continuity equation -- the error being as large as sixty-three percent.

10. The dire need for accurate, comprehensive experimental data on a large scale was noted.

11. The length of computer run time necessary for the asymptotic approach to a steady state condition was found to be dependent upon the assumed initial conditions.

12. Integral conservation checks of the numerical results indicated errors of less than one percent.

CHAPTER V

APPROXIMATE ANALYTIC SOLUTION AND RESULTS

As noted in the previous chapter, the experimental data of Reference 24 was found to be inconsistent with the conservation of mass. Consequently, in order to better ascertain the degree of success achieved by the numerical method, a brief comparison was made with an approximate analytic solution that has been shown to be in agreement with experimental data (see Reference 19). In addition, in the description of the turbulent shear stresses in the numerical method, the spreading rate parameter, σ , was assigned the value of 15.3 since this was the value found by Forde (24) that best correlated the experimental data. The analytic solution was employed to determine if this value of σ was appropriate.

Analytic Solution for Constant Pressure Jet Mixing

To accomplish these goals, two different solutions were considered for application: (1) the solution reported by Korst and Chow in Reference 6, and (2) a solution developed by Kleinstein (9). While the solution of Korst and Chow assumes two-dimensional mixing

whereas Kleinstein's solution assumes axisymmetric flow, the former is much simpler to apply than the latter. Moreover, the former has been shown to be a good approximation for axisymmetric mixing (see Reference 19 for comparison with experimental data). Consequently, the Korst solution was used.

The mathematic details of the Korst solution for one-component two-stream mixing are thoroughly documented (6) (8) and only a brief summary will be presented here. The extension to two-specie jet mixing, which was original with this work, is also presented.

Because the Korst solution is described in terms of a coordinate system which is attached to the point of separation, the symbols (x, y) will be used instead of (r, z) ; see Figure 37.

For two-dimensional isobaric turbulent flow, the x-momentum equation,

$$u \frac{\partial u}{\partial x} + v \frac{\partial u}{\partial y} = \epsilon_m \frac{\partial^2 u}{\partial y^2}, \quad (5-1)$$

was adopted by analogy with Prandtl's laminar boundary layer equations. By small perturbation agreements (see References 6 and 8), equation (5-1) may be further linearized with the results:

$$\left(\frac{u_a + u_b}{2} \right) \frac{\partial u}{\partial x} = \epsilon_m \frac{\partial^2 u}{\partial y^2} \quad (5-2)$$

The eddy viscosity, ϵ_m , was assumed to have the form

$$\epsilon_m = \epsilon_{m\infty} f(x/\delta_a) \quad (5-3)$$

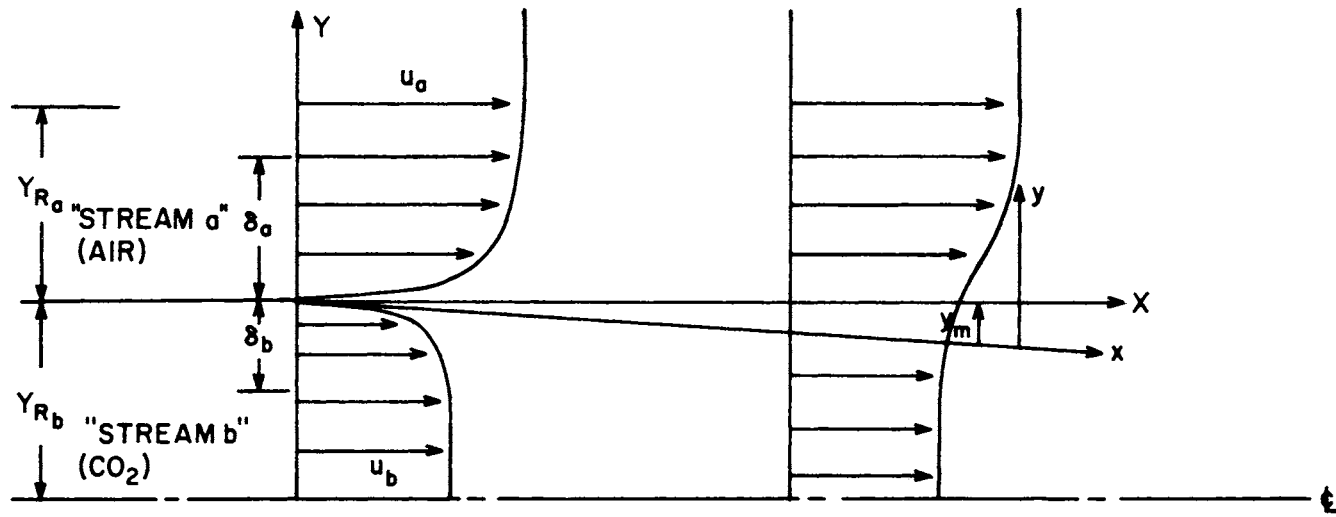


Figure 37. Nomenclature and Geometry for Analytic Solution

where

$$\epsilon_{m\infty} = \frac{x}{4\sigma^2} (u_a + u_b). \quad (5-4)$$

This development assumes that an appropriate average function for ϵ_m is used since it is well known (58) that ϵ_m varies in the lateral direction as well as in the streamwise direction. The function, $f(x/\delta_a)$, was conceptually employed to adjust the value calculated from equation (4-4) to account for the presence of initial boundary layers at the initiation of mixing. However, because of lack of knowledge of the exact nature of this function, it was assigned the value of unity, and was deleted from the development.

With the adoption of the definitions

$$\varphi = \frac{u}{u_a}, \quad \psi = \frac{x}{\delta_a}, \quad \zeta = \frac{y}{\delta_a} \quad (5-5)$$

equation (5-2) becomes:

$$\frac{\partial \varphi}{\partial \psi} = \frac{1}{2\sigma^2} \psi \frac{\partial^2 \varphi}{\partial \zeta^2} \quad (5-6)$$

with the deletion of $f(\psi)$. Further, the transformation:

$$\xi = \frac{1}{2\sigma^2} \int \psi d\psi \quad (5-7)$$

may be introduced which transforms equation (5-6) into the form:

$$\frac{\partial \varphi}{\partial \xi} = \frac{\partial^2 \varphi}{\partial \zeta^2} \quad (5-8)$$

For the case of initial boundary layers at the point of separation, the boundary conditions for integration are:

$$\begin{aligned}
 \varphi(0, \zeta) &= \varphi_b && \text{for } -\infty < \zeta \leq -\frac{\delta_b}{\delta_a} \\
 \varphi(0, \zeta) &= \varphi_{ib}(\zeta) && \text{for } -\frac{\delta_b}{\delta_a} \leq \zeta \leq 0 \\
 \varphi(0, \zeta) &= \varphi_{ia}(\zeta) && \text{for } 0 \leq \zeta \leq 1 \\
 \varphi(0, \zeta) &= 1 && \text{for } 1 \leq \zeta \leq \infty \\
 \varphi(\xi, \zeta) &\longrightarrow \varphi_b && \text{for } \zeta \longrightarrow -\infty \\
 \varphi(\xi, \zeta) &\longrightarrow 1 && \text{for } \zeta \longrightarrow \infty
 \end{aligned} \tag{5-9}$$

The solution of equation (5-8) with the boundary conditions (5-9) is:

$$\begin{aligned}
 \varphi &= \frac{1}{2} \left[(1 + \varphi_b) + \operatorname{erf}(\eta_u - \eta_p) - \varphi_b \operatorname{erf}\left(\eta_u + \frac{\delta_b}{\delta_a} \eta_p\right) \right] \\
 &+ \frac{1}{\pi} \left(\int_{\eta_u}^{\eta_u + \frac{\delta_b}{\delta_a} \eta_p} \varphi_{ib}\left(\frac{\eta_u - \beta}{\eta_p}\right) e^{-\beta^2} d\beta \right. \\
 &\left. + \int_{\eta_u - \eta_p}^{\eta_u} \varphi_{ia}\left(\frac{\eta_u - \beta}{\eta_p}\right) e^{-\beta^2} d\beta \right)
 \end{aligned} \tag{5-10}$$

where

$$\eta_p = \frac{1}{2\sqrt{\xi}}$$

$$\eta_u = \zeta\eta_p \quad (5-11)$$

$$\varphi_b = \frac{u_b}{u_a}$$

and

$$\operatorname{erf} \eta_u = \frac{2}{\sqrt{\pi}} \int_0^{\eta_u} e^{-\beta^2} d\beta \quad (5-12)$$

For the case of two initially uniform streams with no boundary layers, equation (4-10) simplifies to

$$\varphi = \frac{1}{2} [(1 + \varphi_b) + (1 - \varphi_b) \operatorname{erf}(\eta_u)] \quad (5-13)$$

This equation will prove useful by analogy later.

Since boundary layer approximations have been made, the boundary layer forms for the conservation of energy and specie were respectively expressed:

$$u \frac{\partial h_o}{\partial x} + v \frac{\partial h_o}{\partial y} = \frac{\epsilon_m}{Pr_t} \frac{\partial^2 h_o}{\partial y^2} \quad (5-14)$$

$$u \frac{\partial \omega_i}{\partial x} + v \frac{\partial \omega_i}{\partial y} = \frac{\epsilon_m}{Sc_{t,i}} \frac{\partial^2 \omega_i}{\partial y^2} \quad (5-15)$$

These equations were then further linearized in the same manner as the momentum equation.

As with the axial velocity, the stagnation enthalpy and concentration were nondimensionalized by the stream "a" free stream values.

Since the concentration of air in stream "a" was unity, and, since two-specie mixing was being considered, equation (5-15) was only solved for the concentration of air, ω_1 , and the concentration of carbon dioxide, ω_2 , was found by use of:

$$\omega_2 = 1 - \omega_1 \quad (5-16)$$

After linearization and substitution of the appropriate nondimensionalized variables, equations (5-14) and 5-15) respectively became:

$$\frac{\partial \Lambda}{\partial \psi} = \frac{\psi}{4\sigma^2 \text{Pr}_t} \frac{\partial^2 h_o}{\partial \zeta^2} \quad , \quad (5-17)$$

$$\frac{\partial \omega_1}{\partial \psi} = \frac{\psi}{4\sigma^2 \text{Sc}_{t,i}} \frac{\partial^2 \omega_1}{\partial \zeta^2} \quad , \quad (5-18)$$

where:

$$\Lambda = \frac{h_o}{h_{o_a}} \quad (5-19)$$

with ψ and ζ defined in Equation (5-5).

These equations were further transformed by implementing the definitions:

$$\xi_e = \frac{1}{2\sigma^2 \text{Pr}_t} \int \psi \, d\psi \quad , \quad (5-20)$$

$$\xi_s = \frac{1}{2\sigma^2 \text{Sc}_{t,i}} \int \psi \, d\psi \quad . \quad (5-21)$$

Equations (5-17) and (5-18) then became:

$$\frac{\partial \Lambda}{\partial \xi_e} = \frac{\partial^2 \Lambda}{\partial \zeta^2} \quad , \quad (5-22)$$

$$\frac{\partial \omega_1}{\partial \xi_s} = \frac{\partial^2 \omega_1}{\partial \zeta_s^2} . \quad (5-23)$$

Since the boundary conditions for these equations were different from those of the velocity where initial upstream boundary layers were assumed, Crocco's integral could not be used (previous investigators have used it). However, the boundary conditions for Λ and ω_1 are similar to the case of two uniform velocity profiles, without boundary layers, for which the solution was given by equation (5-13). Therefore, the solutions for equations (5-22) and (5-23) were expressed:

$$\Lambda = \frac{1}{2} [(1 + \Lambda_b) + (1 - \Lambda_b) \operatorname{erf}(\eta_u)] , \quad (5-24)$$

$$\omega_1 = \frac{1}{2} [1 + \operatorname{erf}(\eta_s)] \quad (5-25)$$

where:

$$\Lambda_b = \frac{h_{o_b}}{h_{o_a}} , \quad (5-26)$$

and

$$\eta_e = \sqrt{\operatorname{Pr}_t} \eta_u , \quad (5-27)$$

$$\eta_s = \sqrt{\operatorname{Sc}_{t,i}} \eta_u .$$

The expression for the density was derived by assuming constant pressure mixing of perfect gases. The result was:

$$\frac{\rho}{\rho_a} = \beta_1 \beta_2 \frac{1 - C_a^2}{\Lambda - \varphi^2 C_a^2} \quad (5-28)$$

where

$$\beta_1 = \frac{\bar{Y}}{Y_a}, \quad \beta_2 = \frac{Y_a - 1}{\bar{Y} - 1}, \quad (5-29)$$

and C_a is the Crocco number.

The solutions presented above are not, however, complete. These solutions are referenced to a coordinate system (x, y) whereas the flow field is referenced to a coordinate system (X, Y) . See Figure 37. Because the differential equations employed for integration incorporated the continuity equation, the relative location of the solutions, in terms of (x, y) , must be determined in terms of (X, Y) . To do this, the integral form of the conservation of mass must be satisfied. Application of this conservation principle produces a coordinate shift, determining y_m (see Figure 37). It was assumed that:

$$\begin{aligned} x &\cong X \\ y &= Y + y_m(x) \text{ with } y_m(0) = 0 \end{aligned} \quad (5-30)$$

The solution for y_m is presented in terms of $\eta_m = \zeta_m \eta_p$.

$$\begin{aligned} \eta_m = \eta_{R_a} - \frac{1}{1 - \varphi_b} &\left[(1 - C_a^2) \left(\int_{\eta_{R_a}}^{\eta_{R_a}} \frac{\varphi^2}{\Lambda - C_a^2 \varphi^2} d\eta - \varphi_b \int_{\eta_{R_a}}^{\eta_{R_a}} \frac{\varphi}{\Lambda - C_a^2 \varphi^2} d\eta \right) \right. \\ &\left. + \eta_p \left(\frac{\theta_b \rho_b}{\delta_a \rho_a} \varphi_b^2 + \frac{\theta_a}{\delta_a} + \frac{\delta_a^*(1 - \varphi_b)}{\delta_a} \right) \right] \end{aligned} \quad (5-31)$$

where θ_a , θ_b , and δ_a^* are the momentum thicknesses and the displacement thickness of the boundary layers of the respective streams. See

Reference 6 for details. The variables η_{R_a} and η_{R_b} are determined for sufficiently large values of Y_{R_a} and Y_{R_b} respectively, such that the mixing region is contained within these lateral dimensions. Furthermore, since this solution was for two two-dimensional semi-infinite streams whereas the problem under consideration was axisymmetric, calculation was not made for locations downstream of the point where the mixing region would reach the centerline. Fortunately, this point was downstream of the three locations for which the experimental data were available.

Comparisons of Numeric and Analytic Results

The variation of σ was first investigated. In Reference 6 an expression was derived, based on theoretical considerations, which indicated that the appropriate value for the spreading rate parameter, for the case under consideration here, should have been of the order of ninety. However, this was judged to be too large and a value of fifty was assumed for calculation. Stagnation pressure curves for this calculation are presented in Figure 38. In the calculation for these results, it was assumed that there existed no upstream boundary layers. However, the inclusion of boundary layers merely resulted in the downstream propagation of the stagnation pressure deficits associated with the boundary layers. From this investigation it was

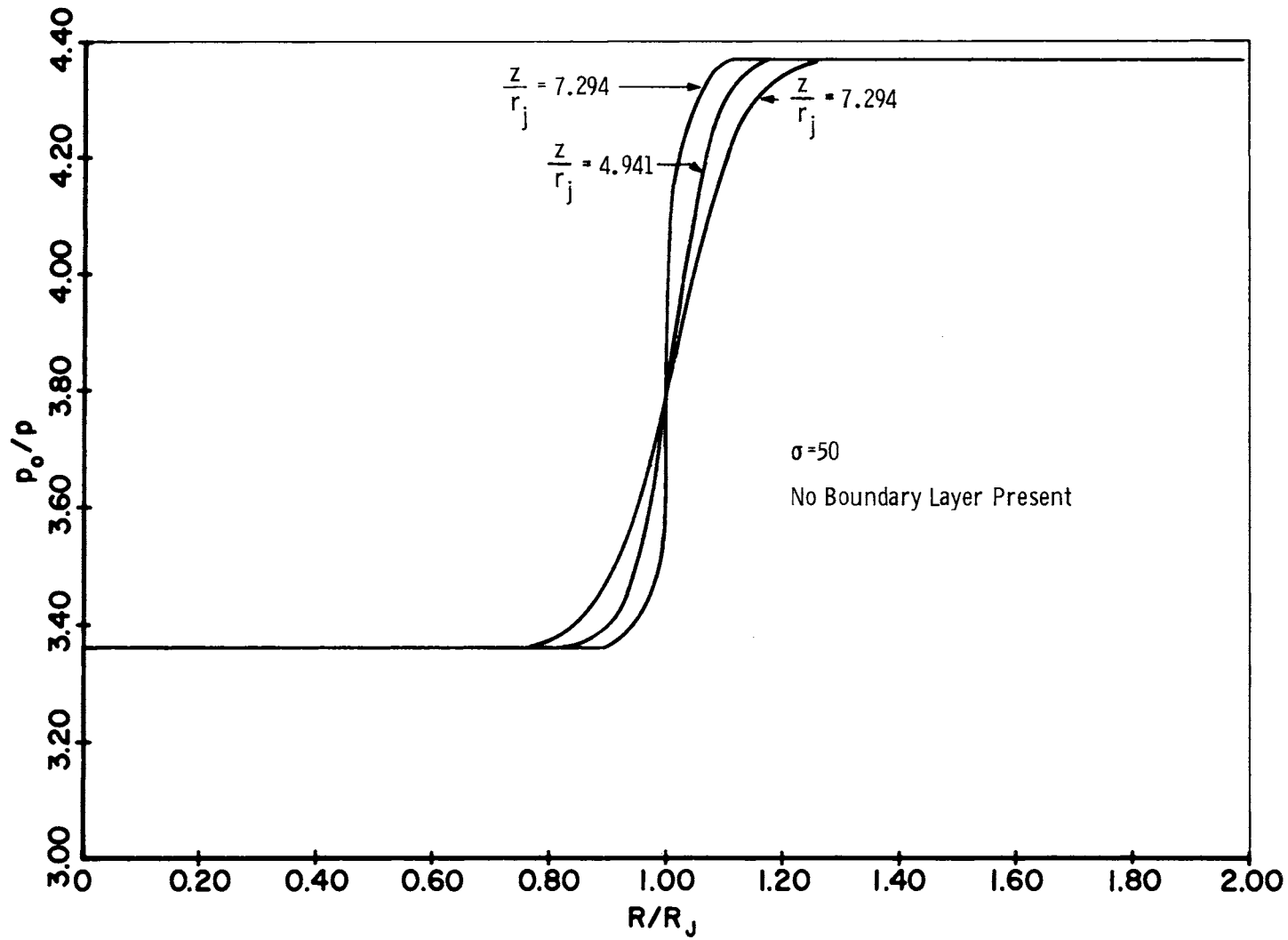


Figure 38. Analytic Solution Stagnation Pressure Profiles with $\sigma = 50$

observed that values of σ of the order suggested by Korst are unrealistic. Additional calculations, with decreasing values of σ , resulted in the conclusion that a value of 15.3 was, indeed, appropriate.

To achieve a comparison of the results of the numerical method and those from the analytic theory, the upstream boundary conditions for Run VI were applied to the analytic theory with $\sigma = 15.3$. For Run VI linear velocity boundary layer profiles were assumed such that the average velocity for such a profile was the same as that for a one-seventh power velocity profile which is typical of a turbulent boundary layer. From an analytic standpoint, such an assumption permitted a straightforward integration of the integrals in Equation (5-10) whereas the assumption of a typical turbulent velocity profile would have required a numeric integration.

The comparison of the stagnation pressure and carbon dioxide concentration results are presented in Figures 39 and 40, respectively. Whereas the Run VI stagnation pressure curves appeared shifted in the radial direction in comparison to experimental data (Figure 26), no such shift appears to exist in the comparison of analytic and numerical results. However, the analytical results show greater boundary layer effects than do the results of the numerical method. This might best be understood by realizing that $f(\psi)$ was taken to be unity for all calculations. Since the purpose of this function is to control the boundary layer decay, the above observation could be expected. At the same

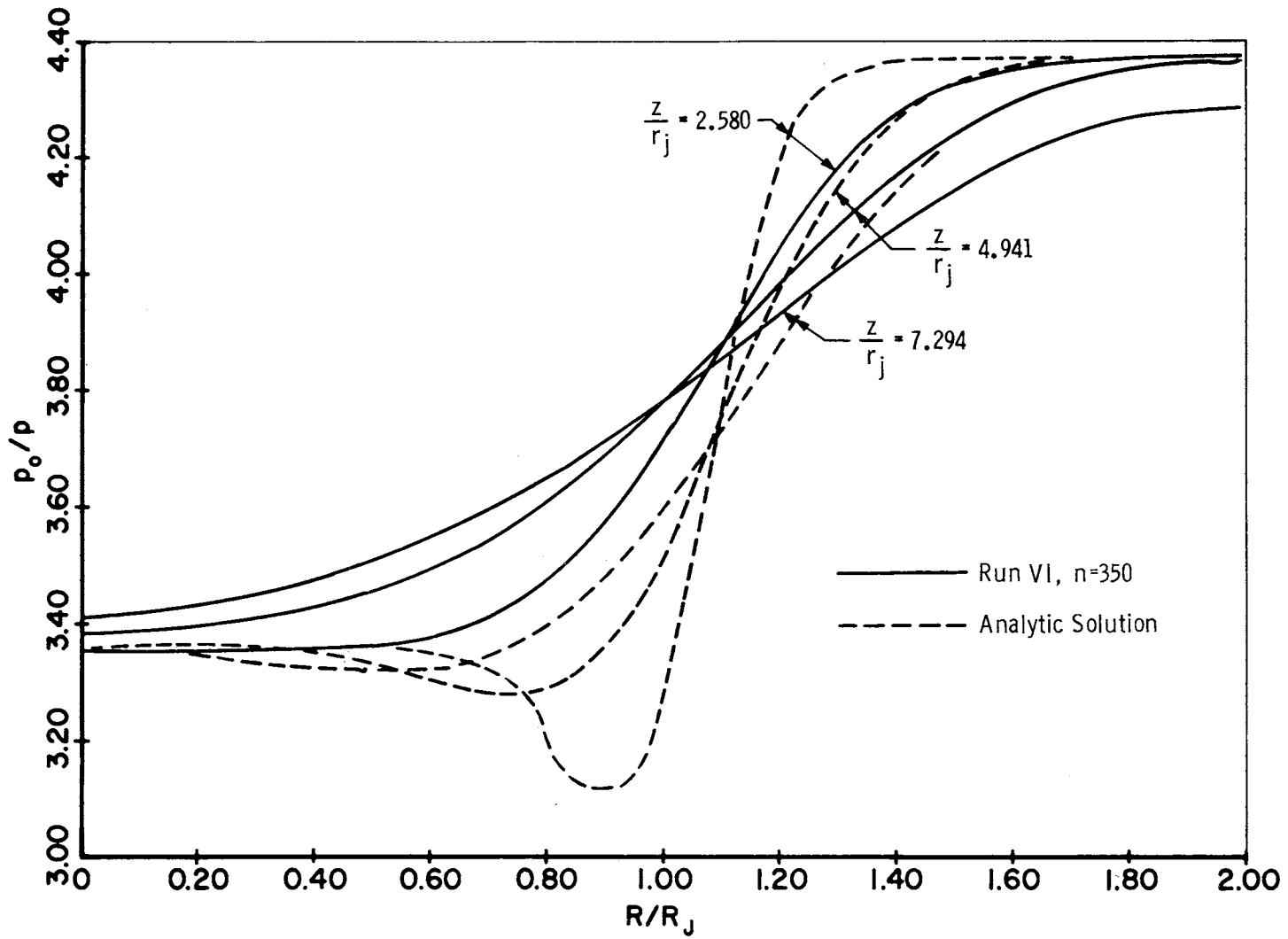


Figure 39. Stagnation Pressure Comparison for Run VI ($n = 350$) and the Analytic Solution

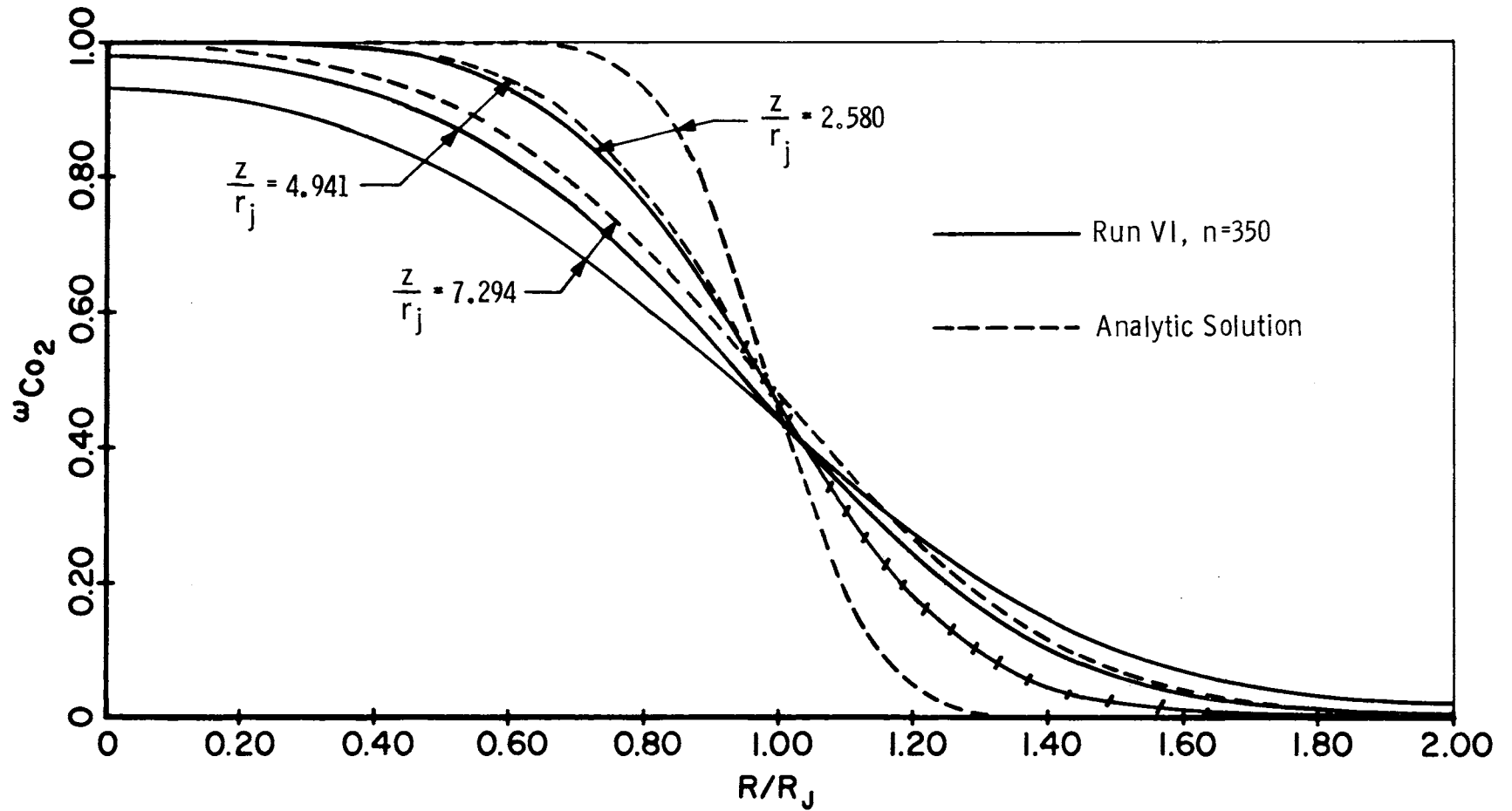


Figure 40. Comparisons of Carbon Dioxide Concentration Profiles for Run VI (n = 350) and the Analytic Solution

time, the comparisons in Figures 39 and 40 are further evidence that both Case I and Case II types of turbulent shear stress representations should be incorporated into the numerical method. This would result in a turbulent shear stress representation of the form:

$$\tau^{(t)} = \rho \epsilon_m \left(\frac{\partial u}{\partial r} + \frac{\partial v}{\partial z} \right). \quad (5-32)$$

The comparison of carbon dioxide profiles in Figure 40 shows much better agreement than was indicated in Figure 34 where the numerical method results were compared with experimental data. Therefore, in light of the discussions which concern the addition of the effects of the turbulent shear stress representations, it may be firmly concluded that the numerical method results compare very well with those of an experimentally verified analytic theory for turbulent jet mixing.

CHAPTER VI

CONCLUSIONS AND RECOMMENDATIONS

Conclusions

It was the purpose of this investigation to develop a method capable of describing steady state multispecie turbulent jet mixing. The accomplishment of this objective has been suggested. With the adoption of the phenomenological description of turbulence, the basic differential flow equations were developed. Because of the nebulous way in which the turbulent shear stress representations have been historically developed, two alternate schemes were considered. The differential equations were applied to the Rusanov numerical method and the results were compared with both an analytic solution and experimental data for constant pressure supersonic turbulent mixing of air and carbon dioxide. In addition, an investigation was conducted to determine the downstream effect of differing upstream boundary conditions.

In the application of the numerical method, with the exception of a small region in the vicinity of the point of separation, stable solutions were achieved with a value of the damping parameter, ω , that was

one-fifth the value required by inviscid stability considerations. The region of slight pressure instabilities was eliminated by employing a sharp exponential decay of the value of the damping parameter from the inviscid value to a value that was one-fifth that required by inviscid stability requirements. In addition, it was found that both the direction of the velocity and the shape of the velocity profile at the upstream boundary affected the degree of instability which was exhibited by the pressure.

Independent application of the two different turbulent shear stress representations resulted in the conclusion that one form produced reasonable radial profiles, whereas the other did not. However, closer inspection indicated that, if the shear stress representations were applied in complete analogy with the laminar shear stress expressions, improved results were suggested. Furthermore, this led to the important conclusion that, in the application of a numerical method where the conservation equations are applied at a point, simplifications of the shear stress expressions, in the spirit of the Prandtl simplification, are significantly harmful -- more so than has previously been expected. This point was demonstrated by the comparisons of the numerical method results with both the experimental data and the analytic solution.

The investigation of the sensitivity of the numerical method results to assumed upstream boundary conditions revealed that boundary layer effects significantly influenced the downstream radial

profiles. Comparison of numerical method results for different upstream conditions indicated that both the size and shape of the boundary layers are important parameters. Therefore, in the application of the method presented above, one must be careful to define the upstream boundary in accordance with the physical problem under investigation.

The achievement of a steady state solution was demonstrated by plotting various dependent variables versus time plane number. It was observed that, if the initial conditions were close approximations to the final solution, computer run time was significantly reduced.

Although the calculation scheme did not require that the pressure remain constant, the pressure did, in fact, achieve approximately a constant value. In addition, the concentrations for air and carbon dioxide were calculated independently in the numerical method and the sum of these concentrations always equaled unity.

The comparison of the numerical method results with experimental data indicated only qualitative agreement. However, the application of the conservation of mass principle to the experimental data indicated large discrepancies. Comparison with an experimentally verified analytic solution displayed good agreement.

In general, the results of this work indicate that the method presented in this thesis may be employed to solve a wide variety of multispecies turbulent mixing problems that have heretofore proven intractable. Furthermore, in view of the degree of success that the Rusanov numerical method has previously enjoyed, flow fields

containing such additional phenomena as shock waves should now be amenable to analysis.

Recommendations

Based upon the observations which have been made in the process of this investigation, the following recommendations are made:

1. Accurate, detailed, large-scale, multispecie, turbulent jet mixing experiments should be conducted. This information is very desperately needed, not only for the determination of more accurate transport expressions, but also for comparative studies, such as was performed above, of new methods of analysis.

2. To assert the generality of the method which has been presented above, variable pressure multispecie jet mixing experiments are needed. Specifically, experimental and numerical studies of flow fields which contain shock waves, as well as several different gases, are necessary to develop confidence for the analysis of flow fields as complex as that in a SCRAM jet.

3. Investigative numerical experiments should be conducted to determine if the use of the turbulent analogue of the laminar shear stress expressions is as advantageous as expected. Furthermore, the exact nature of the effects of any simplifications in the flow equations, as applied via a numerical method, needs investigation.

4. At this juncture in the development of the Rusanov numerical method, extension to chemically reacting gases is warranted if sufficient experimental data become available.

5. For electrofluiddynamic studies, the incorporation into the numerical method of the motion of electrically charged liquid drops is necessary. This investigation will also require experimental studies to determine rate expressions for the diffusion of the drops.

A SELECTED BIBLIOGRAPHY

1. Perini, L. L., Wilson, W. E., Walker, R. E., and Dugger, G. L. "Preliminary Study of Air Augmentation of Rocket Thrust." *Journal of Spacecraft and Rockets*, Vol. 1, No. 6 (November-December, 1964), 626-634.
2. Ferri, A. "Supersonic Combustion Progress." *Astronautics and Aeronautics*, Vol. 2, No. 8 (August, 1964), 32-37.
3. Ferri, A. "A Critical Review of Heterogeneous Mixing Problems." ARL 67-0187 (September, 1967).
4. Seddon, J., and Dyke, M. "Ejectors and Mixing Streams." Bibliography 6. Prepared for the Advisory Group for Aerospace Research and Development, North Atlantic Treaty Organization. Printed by Technical Editing and Reproduction, Ltd., London (November, 1964).
5. Schlichting, H. Boundary Layer Theory. New York: McGraw-Hill, 1960.
6. Korst, H. H., and Chow, W. L. "Non-isoenergetic Turbulent ($Pr_t = 1$) Jet Mixing Between Two Compressible Streams at Constant Pressure." NASA CR-419 (1966).
7. Zumwalt, G. W. "Analytical and Experimental Study of the Axially-Symmetric Supersonic Base Pressure Problem." Ph. D. Dissertation. University of Illinois (1959).
8. Tang, H. H., Gardinar, C. P., and Barnes, J. W. "Jet Mixing Theory, Extensions, and Applications in Separated Flow Problems." Douglas Missile and Space Systems Division Report DAC-59181 (February, 1967).
9. Kleinstein, G. "An Approximate Solution for the Axisymmetric Jet of a Laminar Compressible Fluid." Polytechnic Institute of Brooklyn PIBAL Report No. 648, ARL 51 (April, 1961). See also ARL 63-108 (June, 1963).

10. Libby, P.A. "Theoretical Analysis of Turbulent Mixing of Reactive Gases with Application to Supersonic Combustion of Hydrogen." *American Rocket Society Journal*, Vol. 32, No. 4 (March, 1962), 388-396.
11. Kleinstein, G. "Mixing in Turbulent Axially Symmetric Free Jets." *Journal of Spacecraft and Rockets*, Vol. 1, No. 4 (July-August, 1964), 403-408.
12. Victor, A. C., and Buecher, R. W. "An Analytical Approach to the Turbulent Mixing of Coaxial Jets." *Navweps Report 9057*, U.S. Naval Ordnance Test Station, China Lake, Calif. (October, 1966).
13. Donaldson, C., and Gray, K.E. "Theoretical and Experimental Investigation of the Compressible Free Mixing of Two Dissimilar Gases." *AIAA Aerothermochemistry of Turbulent Flows Conference*, Paper 65-822 (December, 1965). *AIAA Journal*, Vol. 4, No. 11 (November, 1966), 2017-2025.
14. Seubold, J. G. "Turbulent Mixing of a Two-Dimensional Free Jet." *AIAA Aerothermochemistry of Turbulent Flows Conference*, Paper 65-821 (December, 1965).
15. Casaccio, A. "Similar Solutions for the Turbulent Compressible Mixing of Two Streams with Streamwise Pressure Gradients." Republic Aviation Co. 822A. (March, 1963).
16. Abramovitch, G. N. The Theory of Turbulent Jets, Cambridge: M. I. T. Press, 1963.
17. Abramovich, G. N. "Mixing Turbulent Jets of Different Densities." Translation: Air Force Systems Command, Foreign Technology Division, FTD-TT-63-222.
18. Peters, C. E., Peters, T., and Billings, R. B. "Mixing and Burning of Bounded Coaxial Streams." *AECD*, TR-65-4, 1965.
19. Maydew, R. C., and Reed, J. F. "Turbulent Mixing of Compressible Free Jets." *AIAA Journal*, Vol. 1, No. 6 (June, 1963), 1443-1444.
20. Boynton, F. P. "Self-Preservation in Fully Expanded Round Turbulent Jets." *AIAA Journal*, Vol. 1, No. 9 (September, 1963), 2176-2178.

21. Channapragada, R. S. "Compressible Jet Spreading Parameter for Mixing." AIAA Journal, Vol. 1, No. 9 (September, 1963), 2188-2189.
22. Channapragada, R. S., and Woolley, J. P. "Turbulent Mixing of Parallel Compressible Free Jets." AIAA Propulsion Joint Specialist Conference, Paper 65-606 (June, 1965).
23. Peters, C. E. "A Model for Free Turbulent Eddy Viscosity." AEDC, TR-65-209, 1965.
24. Forde, J. M. "An Experimental Investigation of the Mixing of Supersonic Turbulent Streams of Non-Similar Fluids." McGill University Report 63-3, 1963.
25. Bauer, R. C. "An Analysis of Two-Dimensional Laminar and Turbulent Compressible Mixing." AEDC, TR-65-84, 1965.
26. Jacobs, P. F. "Turbulent Mixing of a Partially Ionized Gas." Guggenheim Labs, Princeton University, Aero. Eng. Report 625, 1962.
27. Chow, W. L., and Addy, A. L. "Interaction of Primary and Secondary Streams of Supersonic Ejector Systems and Their Performance Characteristics." AIAA Journal, Vol. 2, No. 4 (April, 1964), 686-694.
28. Chow, W. L., and Yeh, P. S. "Characteristics of Supersonic Ejector Systems with Non Constant Area Shroud." AIAA Journal, Vol. 3, No. 3 (March, 1965), 525-527.
29. Ladenburg, R., Van Voorhis, C. C., and Winckler, J. "Interferometric Studies of Faster than Sound Phenomena; Part II: Analysis of Supersonic Air Jets." Physical Review, Vol. 76, No. 5 (September, 1949), 625-677.
30. Savage, L. E., and Cate, E. G. "Air Augmented Rocket Power Plant Design Problem." Report No. AS-1927 (July, 1964).
31. Emmons, D. L. "Analysis of the Turbulent Mixing Between a Reactive Gas-Particle Rocket Exhaust and a Confined Airstream." AIAA Propulsion Joint Specialist Conference, Paper 65-609 (June, 1965).

32. Zakkay, V., Krause, E., and Woo, S.D.L. "Turbulent Transport Properties for Axisymmetric Heterogeneous Mixing." ARL 64-103 and PIRAL Report No. 813, 1964.
33. Fromm, J.E. "Lagrangian Difference Approximations for Fluid Mechanics." LA-2535, Los Alamos Scientific Laboratory of the University of California, Los Alamos, New Mexico (June, 1961).
34. von Neumann, J., and Richtmyer, R.D. "A Method for the Numerical Calculation of Hydrodynamic Shocks." J. Appl. Physics, Vol. 21, (1950), p. 232.
35. Fromm, J.E. "A Method for Computing Nonsteady, Incompressible, Viscous Fluid Flow." LA-2910, Los Alamos Scientific Laboratory of the University of California, Los Alamos, New Mexico (September, 1963).
36. Galowin, L.S. "A Finite Difference Method Solution of Non-Similar, Non-Equilibrium Air, Laminar and Turbulent Boundary Layer Flows, Part I: Analysis." General Applied Science Laboratories, Inc., Report No. 422 (March, 1964).
37. Lax, P. "Weak Solutions of Nonlinear Hyperbolic Equations and Their Numerical Computation." Comm. Pure and Applied Mathematics, Vol. 7 (1954), 159-193.
38. Lax, P., and Wendroff, B. "Systems of Conservation Laws." Comm. Pure and Applied Mathematics, Vol. 12 (1960), 217-237.
39. Richtmyer, R.D. "A Survey of Difference Methods for Non-Steady Fluid Dynamics." National Center for Atmospheric Research, NCAR TN-63-2, 1962.
40. Rusanov, V. "Calculation of Interaction of Non-Steady Shock Waves with Obstacles." National Research Council of Canada, Translation No. 1027, 1962.
41. Jackomis, W. N., "Transient Flow Field Analysis of a Blast Wave Intercepting a Stationary Cone at Zero Angle of Attack," Ph.D. Dissertation, Oklahoma State University, Stillwater, Oklahoma, May 1965; Published by Jackomis, W.N. and Zumwalt, G. W. as Sandia Report SC-DC-65-1916, August 1965.

42. Tyler, L. D., "Numerical Solutions of the Flow Field Produced by a Plane Shock Wave Emerging into a Cross-flow," Ph.D. Dissertation, Oklahoma State University, Stillwater, Oklahoma, August 1965; Published by Tyler, L. D., and Zumwalt, G. W. as Sandia Report SC-DC-66-1329, August 1965 and in Proc. Fl. Mech. and H. T. Inst., University of Santa Clara, June 1966.
43. Walker, W. F., "A Numerical Solution for the Interaction of a Moving Shock Wave with a Turbulent Mixing Region," Ph.D. Dissertation, Oklahoma State University, Stillwater, Oklahoma, May 1966; Published by Walker, W. F. and Zumwalt, G. W. as Sandia Report SC-DC-67-2531, May 1967 and in J. of Appl. Mech., June 1968.
44. Eaton, R. R., "A Numerical Solution for the Flow Field of a Supersonic Cone-Cylinder Entering and Leaving a Blast Sphere Diametrically," Ph.D. Dissertation, Oklahoma State University, Stillwater, Oklahoma, May 1967; Published by Eaton, R. R. and Zumwalt, G. W. as Sandia Report SC-DC-67-2532, May 1967.
45. Rao, B. M., "Analysis of Sonic Boom Waves Incident on Structures," Ph.D. Dissertation, Oklahoma State University, Stillwater, Oklahoma, May 1967.
46. Van Driest, E. R., "Turbulent Boundary Layer in Compressible Fluids," J. Aero. Sci., Vol. 18, No. 3, (1951) p. 145.
47. Frenkiel, F. N., "Comparison Between Molecular and Turbulent Diffusion Processes," Department of the Navy, David Taylor Model Basin, Report 1320, July 1959.
48. Donaldson, Coleman du P., "A Computer Study of an Analytical Model of Boundary Layer Transition," Paper 68-38, AIAA Sixth Aerospace Sciences Meeting, January 1968, New York.
49. Hinze, J. O., Turbulence, McGraw-Hill Book Co., New York, 1959.
50. Bradshaw, P., Ferris, D. H. and Atwell, N. P., "Calculation of Boundary Layer Development Using the Turbulent Energy Equation," J. of Fluid Mech., Vol. 28, part 3, 1967, pp. 593-616.

51. Taylor, G.I., "The Transport of Vorticity and Heat Through Fluids in Turbulent Motion," Proc. Roy. Sci. London, A135 (1932), p. 685.
52. Nikuradse, J., "Gesetzmässigkeit der Turbulent Strömung in Glatten Rohren," Forschung-Arb. Ing. -Wesen 356 (1932)
53. Tollmein, W., "Berechnung Turbulenter Ausbreitungsvorgänge," ZAMM6 (1926). Translated as NACA TM 1085, 1945.
54. Black, T. J., "A New Model of the Shear Stress Mechanism in Wall Turbulence," AIAA paper 68-42, presented at AIAA Sixth Aerospace Sciences Meeting, New York, January, 1968.
55. Forstall, W. Jr., and Shapiro, A.H., "Momentum and Mass Transfer in Coaxial Jets," J. Applied Mechanics, Vol. 7, No. 12 (1950), 399-408.
56. Alpinieri, L. J., "Turbulent Mixing of Coaxial Jets," AIAA J., Vol. 2, No. 9 (1964) 1560-1568.
57. Ferri, A., Libby, P.A., and Zakkay, V., "Theoretical and Experimental Investigation of Supersonic Combustion," Third Congress, International Council of the Aeronautical Sciences, Spartan Books, Baltimore, Md., 1964.
58. Boehman, L.I., "Mass and Momentum Transport Properties in Isoenergetic Coaxial Flows," Ph.D. Dissertation, Illinois Institute of Technology. Also see ARL 67-58, 1967.
59. Zakkay, V., Krause, E., and Woo, S.D.I., "Turbulent Transport Properties and Axisymmetric Heterogeneous Mixing," ARL 64-103 (1964).
60. Zakkay, V. and Krause, E., "The Radial Variation of the Eddy Viscosity in Compressible Turbulent Jet Flows," ARL 65-89 (1965).
61. Ting, L. and Libby, P.A., "Remarks on the Eddy Viscosity in Compressible Mixing," J. Aero. Sci., Vol. 27 (1960), 797-798.

62. Squire, H. B. and Trouncer, J., "Round Jets in a General Stream," Aeronautical Research Committee Technical Report R & M No. 1974 (1944).
63. Keagy, W.R. and Weller, A.E., "A Study of Freely Expanding Inhomogeneous Jets," Proc. and Fl. Mech. Inst., Am. Soc. Mech. Engr., New York, 1949, 89-98.
64. Morgenthaler, J.H., "Mixing in Supersonic Flow," GASL Technical Report No. 592 (September, 1966)
65. O'Brian, G.G., Hyman, M.A., and Kaplan, S., "A Study of the Numerical Solution of Partial Differential Equations," J. Math. and Phys., Vol. 29 (1951) 223-251.
66. Volluy, R.J., "Wind Tunnel Instrumentation and Operation," Handbook of Supersonic Aerodynamics, Sec. 20, NAVORD Report 1488, Vol. 6, Bureau of Naval Weapons (January 1961) p. 2. 2. 6.
67. Bird, R. B., Stewart, W.E., Lightfoot, E.N., Transport Phenomena, John Wiley and Sons, New York, 1960

APPENDIX A

DERIVATION OF INSTANTANEOUS TURBULENT PARTIAL DIFFERENTIAL FLOW EQUATIONS

The derivation of the transient laminar partial differential equations for multispecie fluid flow is well-documented in numerous textbooks (e. g. see Reference 66); these equations may be written in the form:

Conservation of mass:

$$\frac{\partial \rho}{\partial t} + \nabla \cdot (\rho \bar{V}) = 0 \quad (\text{A-1})$$

Conservation of momentum:

$$\frac{\partial \rho \bar{V}}{\partial t} + \nabla \cdot (\rho \bar{V} \bar{V}) + \nabla p = \nabla \cdot \hat{\tau} + \sum \rho_i \bar{g}_i \quad (\text{A-2})$$

Conservation of energy:

$$\begin{aligned} \frac{\partial}{\partial t} \left[\rho \left(e + \frac{1}{2} V^2 \right) \right] + \nabla \cdot \left[\rho \left(e + \frac{1}{2} V^2 \right) \bar{V} \right] + \nabla \cdot (p \bar{V}) = -\nabla \cdot \bar{q} + \nabla \cdot (\hat{\tau} \cdot \bar{V}) \\ + \sum \rho_i \bar{V}_i \cdot \bar{g}_i \end{aligned} \quad (\text{A-3})$$

Conservation of specie:

$$\frac{\partial \rho_i}{\partial t} + \nabla \cdot (\rho_i \bar{V}) = -\nabla \cdot \bar{j}_i + r_i \quad (\text{A-4})$$

In these equations, $\hat{\tau}$ is the conventional laminar shear stress tensor, \bar{g}_i is a generalized body force per unit of mass, \bar{q} is the

multicomponent energy flux, \bar{V}_i is the vector velocity of the i 'th specie, \bar{j}_i is the mass flux of the i 'th specie, $\bar{V} \bar{V}$ is a velocity dyadic and r_i is the rate of production of the i 'th specie. It is also important to note that V represents the magnitude of the velocity vector, $|\bar{V}|$, whereas \bar{V} is the velocity vector.

The multicomponent energy flux, \bar{q} , is usually expressed in terms of contributions which result from the conduction, interdiffusion and "diffusion-thermo" effects (the diffusion-thermo effect, Dufour effect, describes the energy flux due to gradients in concentration and pressure and the unequal action of external forces on various chemical species; usually the Dufour effect is negligible). The mass flux of specie i , \bar{j}_i , is represented by a summation of contributions which result from concentration, pressure, and temperature gradients and the unequal action of external forces on the various species. As should be evident, all the effects which contribute to the determination of \bar{q} and \bar{j}_i , as well as $\hat{\tau}$, are molecular effects. See Reference 66 for an analytic description of these effects.

However, in turbulent flow analysis, these effects were assumed to have negligible importance. Classically this assumption has been justified by nondimensionalizing the flow equations with the result that the molecular transport terms have a coefficient of the form $1/R_e$, where R_e is the Reynolds number. Since it is known that

turbulent flow usually has a large Reynolds number associated with it, terms which contain the Reynolds number in the denominator have been neglected (Reference 43 contains this analysis).

This analysis, however, is not conceptually sufficient for turbulent free jet mixing. In such flows, the free streams on either side of the turbulent mixing region may be laminar in nature (as for example was the case in Reference 58 where honeycomb was inserted in the adjacent streams upstream of the region of mixing). This makes the determination of an appropriate Reynolds number difficult if not meaningless as an indicating parameter for the nature of the flow (laminar or turbulent).

Consequently, turbulent jet mixing was considered in the spirit of Prandtl (see Reference 5). It was assumed that, in turbulent mixing, large agglomeration of fluid transport energy, momentum, species, etc. in a manner analogous to the molecular transport mechanism. Furthermore, it was assumed that these agglomerations form, move, and disperse sufficiently fast so that molecular interactions within and between these lumps are negligible. At the same time, since equations (A-1) through (A-5) were viewed as an instantaneous description of the conservation principles, this turbulent action is taken into account in the convective terms of the differential equations. Therefore, the molecular transport terms in the right-hand side of equations (A-1) through (A-4) have been neglected.

In addition, it was assumed that there were no significant external body forces ($\bar{g}_i = 0$) and the gases were nonreacting ($r_i = 0$). With these assumptions the differential equations (A-1) through (A-4) respectively became:

$$\frac{\partial \rho}{\partial t} + \nabla \cdot \rho \bar{V} = 0 \quad (\text{A-5})$$

$$\frac{\partial \rho \bar{V}}{\partial t} + \nabla \cdot (\rho \bar{V} \bar{V}) + \nabla p = 0 \quad (\text{A-6})$$

$$\frac{\partial}{\partial t} \left[\rho \left(e + \frac{1}{2} V^2 \right) \right] + \nabla \cdot \left[\rho \left(e + \frac{1}{2} V^2 \right) \bar{V} \right] + \nabla \cdot p \bar{V} = 0 \quad (\text{A-7})$$

$$\frac{\partial \rho_i}{\partial t} + \nabla \cdot (\rho_i \bar{V}) = 0 \quad (\text{A-8})$$

These equations were rearranged for convenient application to the Rusanov numerical method. Since

$$e = h - p/\rho, \quad (\text{A-9})$$

$$\rho_i = \rho \omega_i \quad (\text{A-10})$$

the energy and specie equations were rewritten respectively as:

$$\frac{\partial}{\partial t} \left[\rho \left(h + \frac{1}{2} V^2 \right) - p \right] + \nabla \cdot \left[\rho \left(h + \frac{1}{2} V^2 \right) \bar{V} \right] = 0 \quad (\text{A-11})$$

$$\frac{\partial}{\partial t} (\rho \omega_i) + \nabla \cdot (\rho \omega_i \bar{V}) = 0 \quad (\text{A-12})$$

Finally, because interest was centered on axisymmetric flow, the flow equations were rewritten in the form:

Conservation of mass:

$$\frac{\partial \rho}{\partial t} + \frac{1}{r} \frac{\partial}{\partial r} (r \rho v) + \frac{\partial}{\partial z} (\rho u) = 0 \quad (\text{A-13})$$

Conservation of radial momentum:

$$\frac{\partial}{\partial t}(\rho v) + \frac{1}{r} \frac{\partial}{\partial r} (r \rho v^2 + p) + \frac{\partial}{\partial z} (\rho u v) = 0 \quad (\text{A-14})$$

Conservation of axial momentum:

$$\frac{\partial(\rho u)}{\partial t} + \frac{1}{r} \frac{\partial(r \rho u v)}{\partial r} + \frac{\partial(\rho u^2 + p)}{\partial z} = 0 \quad (\text{A-15})$$

Conservation of energy:

(A-16)

$$\frac{\partial}{\partial t} \left[\rho \left(h + \frac{1}{2} V^2 \right) - p \right] + \frac{1}{r} \frac{\partial}{\partial r} \left[r \rho \left(h + \frac{1}{2} V^2 \right) v \right] + \frac{\partial}{\partial z} \left[\rho \left(h + \frac{1}{2} V^2 \right) u \right] = 0$$

Conservation of specie:

$$\frac{\partial}{\partial t} (\rho \omega_i) + \frac{1}{r} \frac{\partial}{\partial r} (r \rho \omega_i v) + \frac{\partial}{\partial z} (\rho \omega_i u) = 0 \quad (\text{A-17})$$

In these equations it is important to note that the dependent variables describe the instantaneous state of a flow field. See Appendix B for the time-averaging scheme.

APPENDIX B

PERTURBATION AND TIME-AVERAGING SCHEME

To render equations (2-1) through (2-5) useful for application, the instantaneous dependent variables were decomposed, in the spirit of Van Driest (46), into time dependent mean and fluctuation values. After decomposition, a time-averaging process was performed. Because of the complexity of this procedure, each differential equation will be considered separately in turn. Further, two schemes were found to be possible and both will be presented below.

Essential to this development are the rules of time averaging. If f and g are two dependent variables whose mean values are to be formed and if s denotes any one of the independent variables r , z , t then, according to Schlichting (4), the rules for time averaging are

$$\begin{aligned}\overline{\overline{f}} &= \overline{f} & \overline{\overline{f + g}} &= \overline{f} + \overline{g} \\ \overline{\overline{f \cdot g}} &= \overline{f \cdot g} & & \quad (B-1)\end{aligned}$$

$$\overline{\frac{\partial f}{\partial s}} = \frac{\partial \overline{f}}{\partial s} \qquad \overline{\int f ds} = \int \overline{f} ds$$

where the bar indicates an average. In the discussion below, a bar

($\bar{\quad}$) will indicate an average value and a prime ($'$) will indicate a fluctuation quantity.

Continuity Equation

The instantaneous form of the continuity equation is:

$$\frac{\partial \rho}{\partial t} + \frac{1}{r} \frac{\partial (r \rho v)}{\partial r} + \frac{\partial (\rho u)}{\partial z} = 0. \quad (\text{B-2})$$

For decomposition it was assumed that:

$$\begin{aligned} \rho &= \bar{\rho} + \rho' \\ \rho u &= \bar{\rho u} + (\rho u)' \\ \rho v &= \bar{\rho v} + (\rho v)' \end{aligned} \quad (\text{B-3})$$

With the substitution of equations (B-3) into equation (B-) and subsequent time-averaging in accordance with the rules (B-1), the time-averaged differential equation for the conservation of mass became:

$$\begin{aligned} \frac{\partial}{\partial t} [\bar{\rho} + \overline{\rho'}] + \frac{\partial}{\partial r} [\bar{\rho v} + \overline{(\rho v)'}] + \frac{\partial}{\partial z} [\bar{\rho u} + \overline{(\rho u)'}] \\ + \frac{\overline{\rho v} + \overline{(\rho v)'}}{r} = 0 \end{aligned} \quad (\text{B-4})$$

Because of the definition of the fluctuation variables, their time-average is zero:

$$\begin{aligned} \overline{\rho'} &= 0 \\ \overline{(\rho u)'} &= 0 \\ \overline{(\rho v)'} &= 0 \end{aligned} \quad (\text{B-5})$$

Consequently, the continuity equation became:

$$\frac{\partial \bar{\rho}}{\partial t} + \frac{1}{r} \frac{\partial}{\partial r} (r \bar{\rho v}) + \frac{\partial (\bar{\rho u})}{\partial z} = 0 \quad (\text{B-6})$$

It is important to note that, although the time-average of a fluctuation variable is zero, the time-average of the mean variable is not zero since the time interval for averaging is small in comparison to the time scale of the problem of interest.

Radial Momentum Equation

In the decomposition of the variables in the radial momentum equation it was initially assumed that the radial momentum per unit volume, ρv , should be perturbed as a unit. This resulted in the scheme:

$$\begin{aligned} \rho v &= \bar{\rho v} + (\rho v)' \\ u &= \bar{u} + u' \\ v &= \bar{v} + v' \\ p &= \bar{p} + p' \end{aligned} \quad (\text{B-7})$$

The radial momentum equation became, after substitution of assumptions (B-7):

$$\begin{aligned} \frac{\partial}{\partial t} [\bar{\rho v} + (\rho v)'] + \frac{1}{r} \frac{\partial}{\partial r} [r(\bar{\rho v} + (\rho v)'(\bar{v} + v'))] + \frac{\partial}{\partial z} [\bar{p} + p'] \\ + \frac{\partial}{\partial z} [(\bar{\rho v} + (\rho v)'(\bar{u} + u'))] = 0 \end{aligned} \quad (\text{B-8})$$

After time-averaging and deletion of terms of the form $\overline{(\rho v)v'}$ which are zero, equation (B-8) became:

$$\begin{aligned} \frac{\partial \overline{\rho v}}{\partial t} + \frac{\partial}{\partial r} [r(\overline{\rho v} \bar{v} + (\overline{\rho v})'v')] + \frac{\partial}{\partial r} [\bar{p} + p'] \\ + \frac{\partial}{\partial z} [\overline{\rho v} \bar{u} + (\overline{\rho v})'u'] + \frac{\overline{\rho v} \bar{v} + (\overline{\rho v})'v'}{r} = 0 \end{aligned} \quad (\text{B-9})$$

However, there is no hard fast rule that requires the perturbation to proceed as just described. In fact, with the substitution of $\rho u = \bar{\rho u} + (\rho u)'$, instead of $u = \bar{u} + u'$, into the instantaneous radial momentum equation instead of equation (B-8), the result was

$$\begin{aligned} \frac{\partial}{\partial t} [\overline{\rho v} + (\rho v)'] + \frac{1}{r} \frac{\partial}{\partial r} [r(\overline{\rho v} + (\rho v)'(\bar{v} + u'))] + [\bar{p} + p'] \\ + \frac{\partial}{\partial z} [(\bar{\rho u} + (\rho u)')(\bar{v} + v')] = 0 \end{aligned} \quad (\text{B-10})$$

After time-averaging, equation (B-10) became

$$\begin{aligned} \frac{\partial \overline{\rho v}}{\partial t} + \frac{1}{r} \frac{\partial}{\partial r} [r(\overline{\rho v} \bar{v} + (\overline{\rho v})'v')] + [\bar{p} + p'] \\ + \frac{\partial}{\partial z} [\bar{\rho u} \bar{v} + (\overline{\rho u})'v'] = 0 \end{aligned} \quad (\text{B-11})$$

Equation (B-11) differs from equation (B-9) in the expression in axial derivative.

Axial Momentum Equation

The axial momentum equation was perturbed in a manner analogous to that employed for the radial momentum equation. By first perturbing, as a unit, the axial momentum per unit volume, ρu , just as the radial momentum per unit volume, ρv , was perturbed above, a subsequent time-averaging resulted in:

$$\frac{\partial \overline{\rho u}}{\partial t} + \frac{1}{r} \frac{\partial}{\partial r} [r(\overline{\rho u v} + \overline{(\rho u)'v'})] + \frac{\partial}{\partial z} [\overline{\rho u u} + \overline{(\rho u)'u'} + \overline{p}] = 0 \quad (\text{B-12})$$

On the other hand, with the perturbation of the respective mass fluxes per unit area, the result after time-averaging was:

$$\frac{\partial \overline{\rho u}}{\partial t} + \frac{1}{r} \frac{\partial}{\partial r} [r(\overline{\rho v u} + \overline{(\rho v)'u'})] + \frac{\partial}{\partial z} [\overline{\rho u u} + \overline{(\rho u)'u'} + \overline{p}] = 0 \quad (\text{B-13})$$

A comparison of equations (B-13) and (B-14) indicated that they differed in both the second and third terms.

Energy Equation

To perturb the transient term in the instantaneous energy equation (2-4), it was assumed that:

$$\begin{aligned} \rho h &= \overline{\rho h} + (\rho h)' \\ p &= \overline{p} + p' \\ \rho &= \overline{\rho} + \rho' \\ u &= \overline{u} + u' \\ v &= \overline{v} + v' \end{aligned} \quad (\text{B-14})$$

Substitution into the transient term produced

$$\begin{aligned} \frac{\partial}{\partial t} (\rho h + \frac{1}{2} \rho V^2 - p) &= \frac{\partial}{\partial t} [\rho h + \frac{1}{2} \rho (u^2 + v^2) - p] \\ &= \frac{\partial}{\partial t} \{ \overline{\rho h} + (\rho h)' - \overline{p} - p' + \frac{1}{2} [(\overline{\rho} + \rho')((\overline{u} + u')^2 + (\overline{v} + v')^2)] \} \end{aligned} \quad (B-15)$$

After time-averaging and the adoption of the assumptions:

$$\begin{aligned} 1. \quad \overline{(u')^2} &\ll \overline{u^2} \quad \text{and} \quad \overline{(v')^2} \ll \overline{v^2} \\ 2. \quad \overline{u \rho' u'} &\ll \frac{1}{2} \overline{\rho} \overline{u^2} \quad \text{and} \quad \overline{v \rho' v'} \ll \frac{1}{2} \overline{\rho} \overline{v^2} \end{aligned} \quad (B-16)$$

there resulted for the transient term:

$$\overline{\frac{\partial}{\partial t} (\rho h + \frac{1}{2} \rho V^2 - p)} \cong \frac{\partial}{\partial t} (\overline{\rho h} + \frac{1}{2} \overline{\rho} \overline{V^2} - \overline{p}) \quad (B-17)$$

where

$$\overline{V^2} = \overline{u^2} + \overline{v^2} \quad (B-18)$$

For the remaining terms in the energy equation, equation

(2-4), the following perturbations were assumed:

$$\begin{aligned} \rho u &= \overline{\rho u} + (\rho u)' \\ \rho v &= \overline{\rho v} + (\rho v)' \\ h &= \overline{h} + h' \\ u &= \overline{u} + u' \\ v &= \overline{v} + v' \end{aligned} \quad (B-19)$$

These were substituted in the following manner:

$$\begin{aligned} \frac{1}{r} \frac{\partial}{\partial r} [r \rho v (h + \frac{1}{2} V^2)] &= \frac{1}{r} \frac{\partial}{\partial r} \{ r (\overline{\rho v} + (\rho v)') [\overline{h} + h' + \frac{1}{2} ((\overline{u} + u')^2 \\ &\quad + (\overline{v} + v')^2)] \} \end{aligned}$$

$$\frac{\partial}{\partial z} [\rho u (h + \frac{1}{2} V^2)] = \frac{\partial}{\partial z} \{ (\overline{\rho u} + (\rho u)') [\overline{h} + h' + \frac{1}{2} (\overline{u} + u')^2 + (\overline{v} + v')^2] \} \quad (\text{B-20})$$

After time-averaging equations (B-21) and with the use of assumptions in (B-17), together with the result (B-18), the time-mean energy equation became:

$$\begin{aligned} \frac{\partial}{\partial t} [\overline{\rho h} + \frac{1}{2} \overline{\rho V^2} - \overline{p}] + \frac{1}{r} \frac{\partial}{\partial r} [r (\overline{\rho v h} + \overline{(\rho v)' h'} + \frac{1}{2} \overline{\rho v V^2} + \overline{u (\rho v)' u'} + \overline{v (\rho v)' v'})] \\ + \frac{\partial}{\partial z} [\overline{\rho u h} + \overline{(\rho u)' h'} + \frac{1}{2} \overline{\rho u V^2} + \overline{u (\rho u)' u'} + \overline{v (\rho v)' v'}] = 0 \end{aligned} \quad (\text{B-21})$$

The scheme presented above appeared to be straightforward without other logical physical alternatives. However, other schemes were attempted and these invariably resulted in the appearance of terms for which no reasonable assumptions could be made and for which no mean value expressions could be found.

Specie Equation

For the perturbation of the specie equation, it was assumed that:

$$\begin{aligned} \rho \omega_i &= \overline{\rho \omega_i} + (\rho \omega_i)' \\ \omega_i &= \overline{\omega_i} + (\omega_i)' \\ \rho u &= \overline{\rho u} + (\rho u)' \\ \rho v &= \overline{\rho v} + (\rho v)' \end{aligned} \quad (\text{B-22})$$

These assumptions were substituted into the instantaneous conservation of specie equation in the following manner:

$$\begin{aligned} \frac{\partial}{\partial t} [\overline{\rho\omega_i} + (\rho\omega_i)'] + \frac{1}{r} \frac{\partial}{\partial r} [r(\overline{\rho v} + (\rho v)')(\overline{\omega_i} + \omega_i')] \\ + \frac{\partial}{\partial z} [(\overline{\rho u} + (\rho u)')(\overline{\omega_i} + \omega_i')] = 0 \end{aligned} \quad (\text{B-23})$$

and after time-averaging:

$$\frac{\partial}{\partial t} \overline{\rho\omega_i} + \frac{1}{r} \frac{\partial}{\partial r} [r(\overline{\rho v} \overline{\omega_i} + (\overline{\rho v})' \overline{\omega_i}')] + \frac{\partial}{\partial z} [\overline{\rho u} \overline{\omega_i} + (\overline{\rho u})' \overline{\omega_i}'] = 0 \quad (\text{B-24})$$

In the above discussion, whereas one form of the continuity, energy and specie conservation equations was developed, two forms for both the radial and axial momentum equations were developed. For application, it was assumed that it was more appropriate to use the momentum equations that resulted from perturbation of the respective momentum per unit volume. Consequently, equations (B-6), (B-9), (B-13), (B-22) and (B-25) were used for analysis in this work.

APPENDIX C

NUMERICAL EXPANSION OF CENTERLINE TRANSPORT EXPRESSIONS

In the centerline numerical equations for the satisfaction of the conservation principles there are contained variables which account for turbulent transport phenomena. These variables, themselves, were expressed in terms of spacial derivatives of the flow variables. The expansions of these derivatives are presented below.

For node points that were at least two mesh spacings away from either the upstream or downstream boundaries, ($3 \leq l \leq l_{\max} - 2$) the following numerical expansions were used:

$$\tau_{zz_{1, l \pm 1}} \cong \pm (\rho \epsilon_m)_{1, l \pm 1} [(u_{1, l \pm 2} - u_{1, l}) / 2\Delta z] \quad (C-1)$$

$$\tau_{zr_{2, l}} \cong (\rho \epsilon_m)_{2, l} [(u_{3, l} - u_{1, l}) / 2\Delta r] \quad (C-2)$$

$$\tau_{rz_{2, l \pm 1}} \cong \pm (\rho \epsilon_m)_{2, l \pm 1} [(v_{2, l \pm 2} - v_{2, l}) / 2\Delta z] \quad (C-3)$$

$$\tau_{rz_{2, l}} \cong (\rho \epsilon_m)_{2, l} [(v_{3, l} - v_{1, l}) / 2\Delta r] \quad (C-4)$$

$$q''_{z_{1, l \pm 1}} \cong \pm \frac{(\rho \epsilon_m)_{1, l \pm 1}}{\text{Pr}_t} [(h_{1, l \pm 2} - h_{1, l}) / 2\Delta z] \quad (C-5)$$

$$q''_{r_{2,l}} \cong \frac{(\rho \epsilon_m)_{2,l}}{\text{Pr}_t} [(h_{3,l} - h_{1,l})/2\Delta r] \quad (\text{C-6})$$

$$D_{z_{1,l \pm 1}} \cong \pm \frac{(\rho \epsilon_m)_{1,l \pm 1}}{\text{Sc}_{t,i}} [((w_i)_{1,l \pm 2} - (w_i)_{1,l})/2\Delta z] \quad (\text{C-7})$$

$$D_{r_{2,l}} \cong \frac{(\rho \epsilon_m)_{2,l}}{\text{Sc}_{t,i}} [((w_i)_{2,l} - (w_i)_{1,l})/2\Delta r] \quad (\text{C-8})$$

In the above approximations, centered differences have been used. For both the node point $l = 2$ and $l = l_{\text{max}} - 1$, the centered difference approach would require information at imaginary node points which would be outside of the nodal grid. Consequently, at the node point $l = 2$, when axial derivatives were required at $l = 1$ a forward difference was used. For example, $\tau_{zz_{1,1}}$ was approximated

by:

$$\tau_{zz_{1,1}} \cong (\rho \epsilon_m)_{1,1/2} [(u_{1,2} - u_{1,1})/\Delta r] \quad (\text{C-9})$$

Notice that the transport coefficients were evaluated at the midpoint between the two appropriate nodes.

Similarly, at the node $l = l_{\text{max}} - 1$, for axial derivatives at the node $l = l_{\text{max}}$ a backward difference was employed. Hence,

$$\tau_{zz_{1,l_{\text{max}}}} \cong (\rho \epsilon_m)_{1,l_{\text{max}}-1/2} [(u_{1,l_{\text{max}}} - u_{1,l_{\text{max}}-1})/\Delta z] \quad (\text{C-10})$$

Derivatives in the radial direction were always evaluated by the scheme shown in equations (C-2), (C-4), (C-6), and (C-8).

APPENDIX D

DIVERGENT FLOW UPSTREAM BOUNDARY CONDITION

The divergent flow condition at the exits of the concentric nozzles was defined by assuming that the flow from the center nozzle emanated from a point and the flow from the outer concentric nozzle emanated from a ring (see Figure 41). In the following discussion the subscripts e and s refer to the central and external streams respectively.

The calculation procedure for the central nozzle was as follows. Since the exit radius and Mach number were known, the throat radius was determined from the "area ratio" expression:

$$\left(\frac{r_e}{r_j}\right)^2 = \frac{A_e}{A_j^*} = \frac{1}{M_e} \left[\left(\frac{2}{\gamma+1}\right) \left(1 + \frac{\gamma-j}{2} M_e^2\right) \right]^{\frac{\gamma+1}{2(\gamma-1)}} \quad (D-1)$$

It was assumed that the nozzle wall was straight between the exit and the throat. This, most likely, was not the actual case, but, since a pure guess would eventually be required anyway, such an assumption appeared justified. With this assumption, the distance between the exit and the throat is related to the wall divergence angle by:

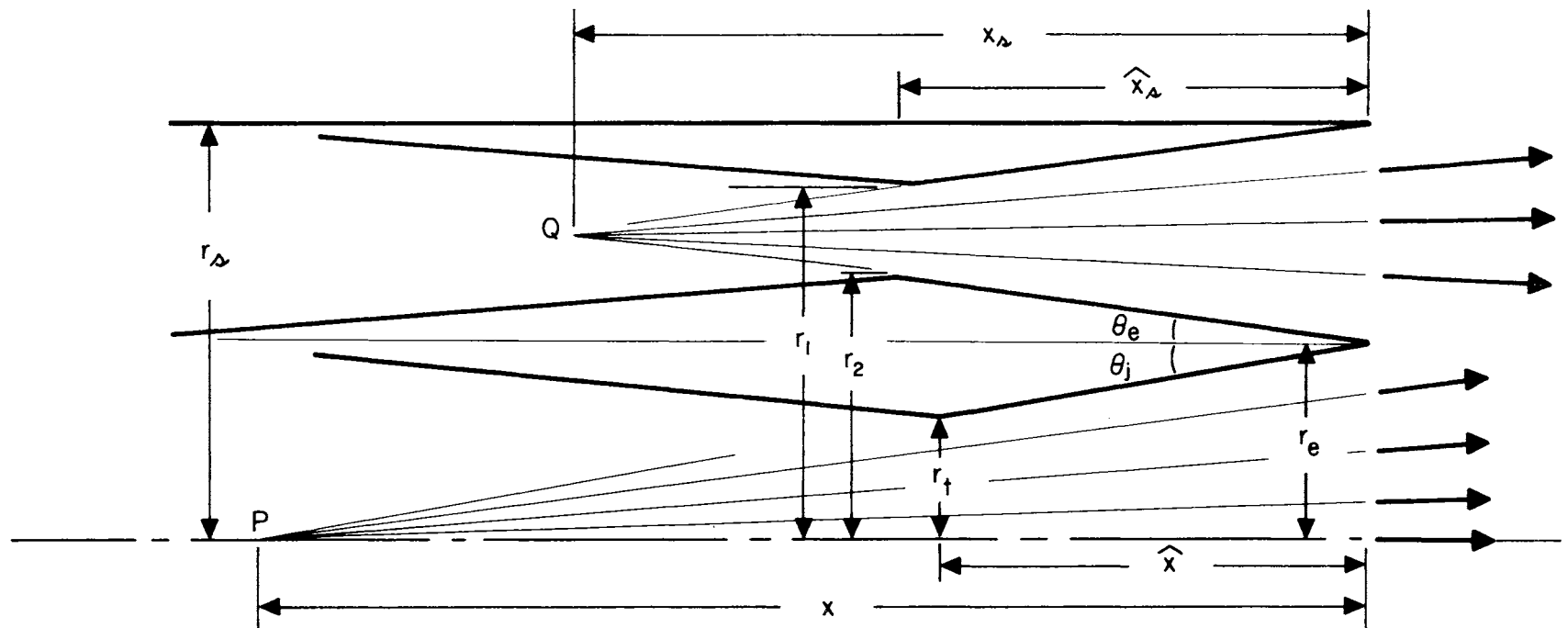


Figure 41. Divergent Flow Field Nomenclature

$$\tan \theta_e = \frac{r_e - r_t}{\hat{x}} \quad (D-2)$$

Once \hat{x} was picked, the angle θ_e was determined. Next, the distance, x , between the exit and the assumed source point, P, was calculated by:

$$x = r_e / \tan \theta_e \quad (D-3)$$

The velocities at each node point were then calculated by:

$$\begin{aligned} v &= V_e \sin \varphi_e \\ u &= V_e \cos \varphi_e \end{aligned} \quad (D-4)$$

where φ_e was determined for each node by:

$$\varphi_e = \tan^{-1} \left[\frac{(m-1)\Delta r}{x} \right] \quad (D-5)$$

where V_e was assumed constant and determined by:

$$V_e = M_e T_{oe} \sqrt{\gamma_e R_e} \left[1 + \frac{\gamma_e - 1}{2} M_e^2 \right]^{1/2} \quad (D-6)$$

There was one exception to the above procedure. At the node adjacent to the nozzle wall, the magnitude of the velocity was assumed to be one-half of the free stream value in order to simulate a boundary layer. Further, the u and v velocity components were not calculated by the above procedure but were determined in a manner described in the "Boundary Layer Corrections" section of this appendix.

The outer stream exit conditions were determined in a manner similar to that used for the center flow. However, corrections were made to account for the fact that the external nozzle was in the shape of

ring. Therefore, the area ratio (which was determined by the Mach number in the manner of equation (D-1)) for the external stream was set equal to

$$\frac{A_s}{A_s^*} = \frac{r_s^2 - r_e^2}{r_1^2 - r_2^2} \quad (D-7)$$

where the nomenclature is defined in Figure 41. The value for r_s was assumed to be 0.5 inch.

The distance, d , was determined by:

$$d = \frac{1}{2} \left[r_s - r_e - \frac{r_s^2 - r_e^2}{A_s/A_s^*} \right] \quad (D-8)$$

Once d was determined, the angle θ_s was calculated with:

$$\theta_s = \tan^{-1} \left(\frac{\theta}{x_s} \right), \quad (D-9)$$

and x_s was determined by:

$$x_s = \left(\frac{r_s - r_e}{2} \right) / \tan \theta_s \quad (D-10)$$

The angle, φ_s , for any node, was determined by

$$\varphi_s = \tan^{-1} \left[\frac{\frac{r_s - r_e}{2} - (m-1)\Delta r - r_e}{x_s} \right] \quad (D-11)$$

$$v = -V_s \sin \varphi_s \quad (D-12)$$

$$u = V_s \cos \varphi_s$$

where V_s was determined by:

$$V_s = M_s T_{os} \sqrt{\gamma_s R_s \left[1 + \frac{\gamma_s - 1}{2} M_s^2 \right]^{1/2}} \quad (D-13)$$

Again, for the node next to the wall, the magnitude of the velocity was assumed to have a value that was one-half of the free-stream value, and the velocity components were determined as described below.

Several different values of \hat{x}_e and \hat{x}_s were considered. The values that were finally employed were those that resulted in a θ_e and θ_s equal to approximately 5.5 and 2.9 degrees respectively.

Boundary Layer Corrections

To correct for the slight divergence associated with a boundary layer, a very simplified analysis was performed. In both streams, this analysis was only applied to the velocities at the nodes next to the wall.

Basically, along the wall in both streams, it was assumed that the linear velocity profile at the exit started as a uniform profile. Because of the change in shape of the profile, the distance between the wall and the first node next to the wall is greater, for the same mass flow rate, than that upstream where the velocity profile was uniform. It was further assumed that the "growth" occurred at a rate dictated by the approximate rate at which a turbulent boundary layer grows:

$$\frac{\delta}{x} = \frac{.376}{\text{Re}_x^{1/5}} \quad (\text{D-14})$$

where δ is the turbulent boundary layer thickness, and Re_x is the free stream Reynolds number based on x , measured from the location where the velocity profile is uniform. This equation permitted the determination of the distance, x .

It then was assumed that there was some thickness of the uniform velocity profile such that the mass flow rate between the wall and this thickness was the same as the mass flow rate for the linear velocity profile for the region between the wall and the node point next to the wall.

With the description of a linear velocity profile by:

$$u = s y + t \quad (\text{D-15})$$

and with y measured perpendicular from the wall, the thickness of the uniform velocity profile that will contain a mass flow rate equal to that for the linear velocity profile between the wall and the distance y was determined to be:

$$b_y = \frac{\gamma_p}{(\gamma-1) s \rho_\infty u_\infty} \left\{ \sqrt{1 + 2 \left(\frac{\gamma-1}{\gamma_p} \right) B (s y + t)^2} + 1 \ln \left[\frac{\sqrt{2 \left(\frac{\gamma-1}{\gamma_p} \right) B}}{\sqrt{1 + 2 \left(\frac{\gamma-1}{\gamma_p} \right) B (s y + t)^2} + 1} \right] \right\} \quad (\text{D-16})$$

where

$$B = \rho_{\infty} \left(1 + \frac{\gamma - 1}{2} \frac{u_{\infty}^2}{\gamma p} \rho_{\infty} \right) \quad (D-17)$$

These equations were applied separately to both streams with the appropriate free stream values (designated in the above equations by the infinity symbol).

The angle with which the flow diverged from the wall was then determined by:

$$\Omega = \tan^{-1} \left(\frac{y - b}{x} \right) \quad (D-18)$$

By considering that the walls themselves diverged and by including the corrections made by this analysis, the velocity components at the nodes next to the wall were calculated by:

central stream:

$$\begin{aligned} u &= \frac{V_e}{2} \cos \Omega_e \cos \varphi_e + \frac{V_e}{2} \sin \Omega_e \sin \varphi_e \\ v &= \frac{V_e}{2} \cos \Omega_e \sin \varphi_e - \frac{V_e}{2} \sin \Omega_e \cos \varphi_e \end{aligned} \quad (D-19)$$

external stream:

$$\begin{aligned} u &= \frac{V_s}{2} \cos \Omega_s \cos \varphi_s + \frac{V_s}{2} \sin \Omega_s \sin \varphi_s \\ v &= -\frac{V_s}{2} \cos \Omega_s \sin \varphi_s + \frac{V_s}{2} \sin \Omega_s \cos \varphi_s \end{aligned} \quad (D-20)$$

APPENDIX E

COMPUTER LOGIC DIAGRAM

In the numerical analysis, several versions of the "main" computer program were employed. In addition, the input and output programs also had a variety of forms. In this section, the logic for the fastest "main" program will be presented. Since the input and output programs are of little importance, they will not be discussed further.

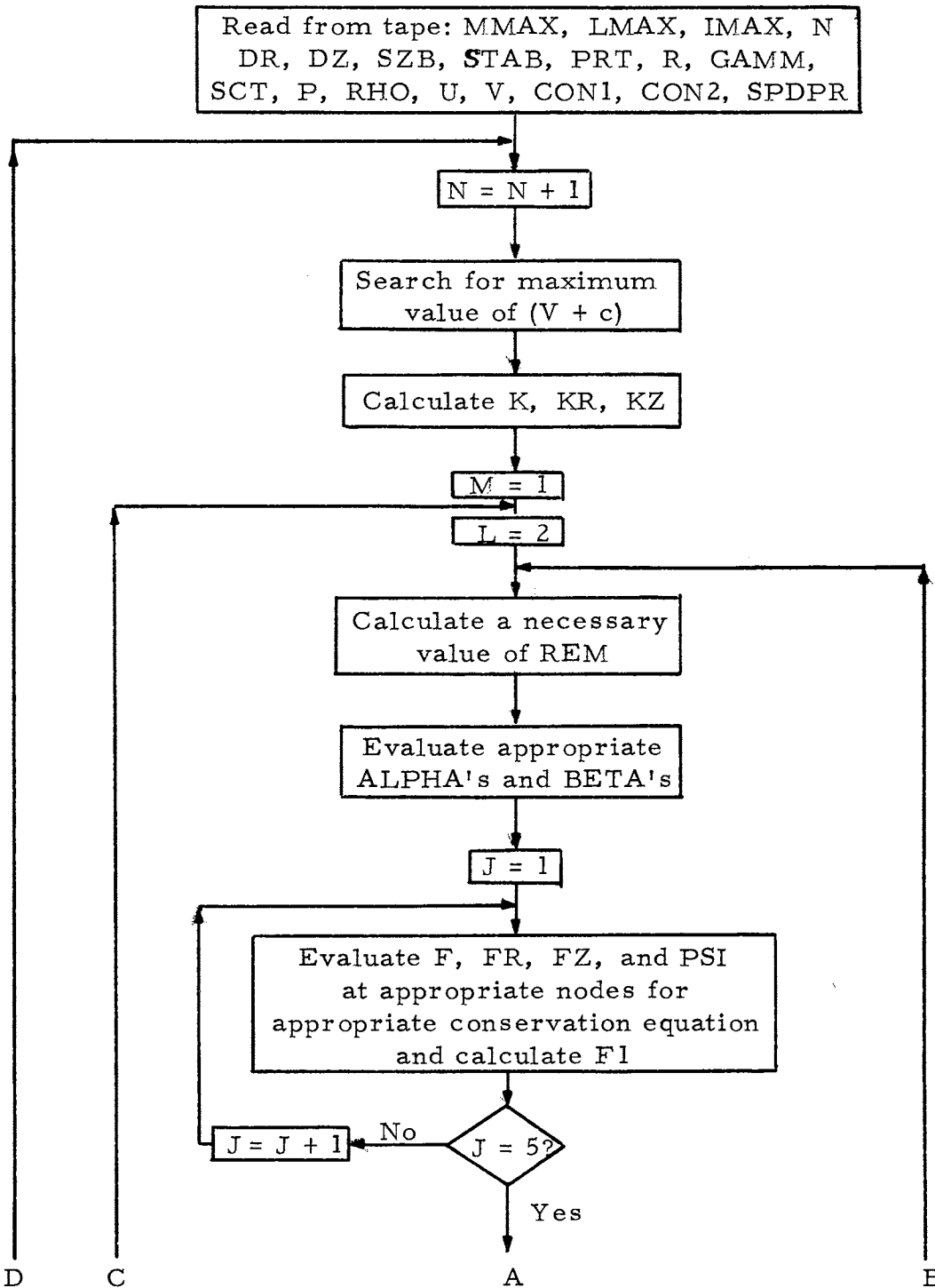
Of principal significance in the logic, presented below, of the "main" program is the recognition that appropriate values of $\rho_{e_m}^n$, $\alpha_{m,l}^n$ and $\beta_{m,l}^n$ need only be evaluated once for each node since they are independent of the particular definite differenced flow equations in which they are used. They need not be evaluated over and over again for each conservation equation at each node. Implementation of this fact very significantly reduced run times.

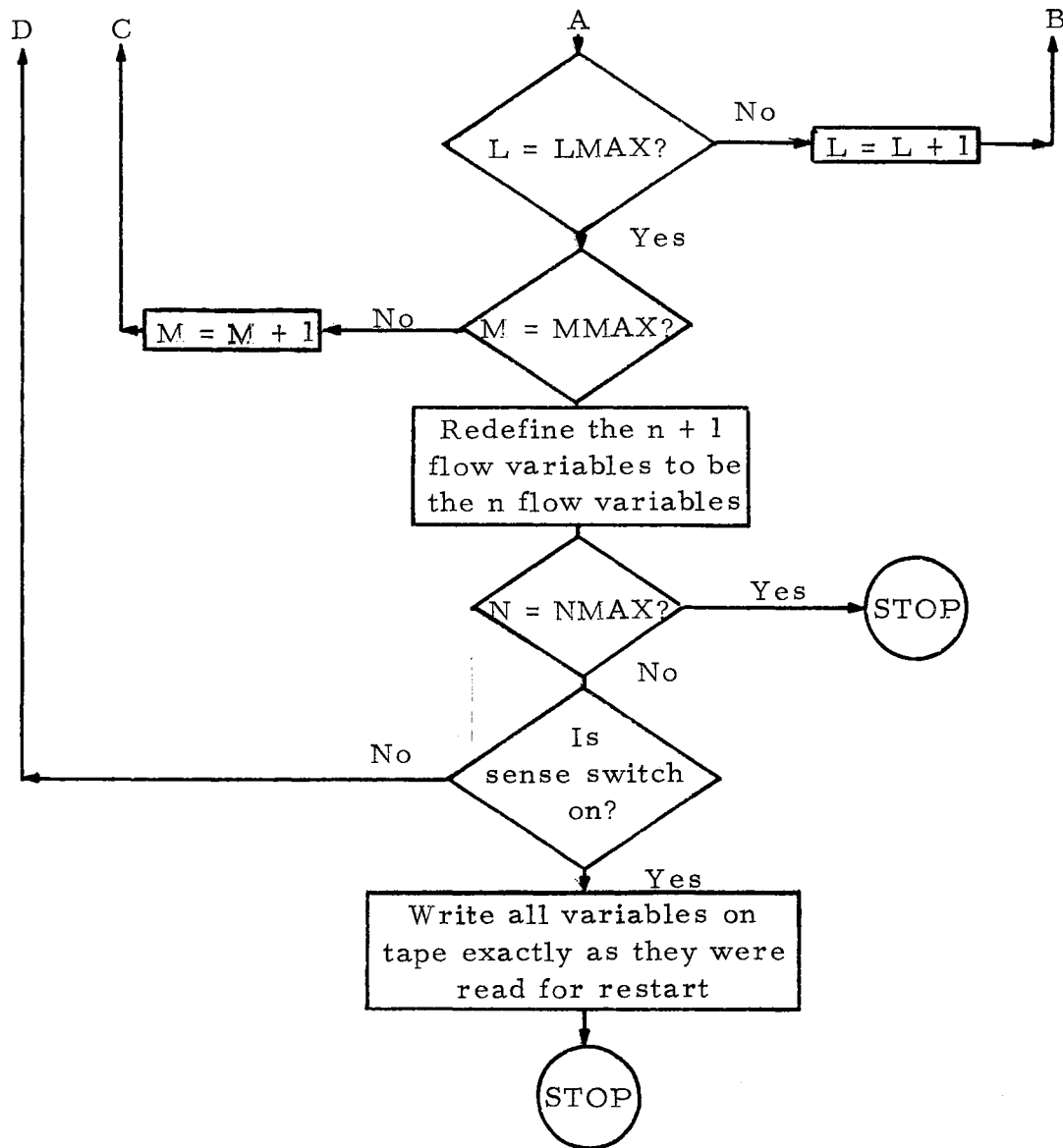
In the logic diagram below, the following definitions are used:

P	pressure array
U	axial velocity array
V	radial velocity array
RHO	density array

CON1	concentration of CO ₂ array
CON2	concentration of air array
MMAX	maximum value of m
LMAX	maximum value of l
IMAX	maximum number of gases to be considered
N	time plane number
ALPHA	$\alpha_{m, l}^n$
BETA	$\beta_{m, l}^n$
DR	Δr
DZ	Δz
SZB	$\bar{\sigma}_o$
STAB	ω
PRT	Pr_t
SCT	array of $Sc_{t, i}$
R	array of gas constants
GAMM	array of specific heat ratios
SPDPR	σ
KR	K_r
KZ	K_z
M	m
L	l

REM	$\rho \epsilon_m$
F	f^n
FR	F^r
FZ	F^z
PSI	ψ
F1	f^{n+1}
J	an indexing parameter that indicates which conservation equation is being applied to the finite difference equations





VITA

Paul Thomas Bauer

Candidate for the Degree of

Doctor of Philosophy

Thesis: AN EULERIAN NUMERICAL METHOD FOR MULTISPECIE,
TURBULENT, SUPERSONIC JET MIXING

Major Field: Mechanical and Aerospace Engineering

Biographical:

Personal Data: Born in Pittsburgh, Pennsylvania, June 24,
1942, the son of Jerome L. and Anna Mae Bauer.

Education: Attended grade school in Pittsburgh and Wexford,
Pennsylvania; graduated from North Catholic High School,
Pittsburgh, Pennsylvania in 1960; received a Bachelor of
Science degree in Aeronautical Engineering from Parks
College of Aeronautical Technology of St. Louis Univer-
sity, East St. Louis, Illinois in July 1963; received a
Master of Science degree in Mechanical Engineering from
Oklahoma State University, Stillwater, Oklahoma, in
May 1965; completed the requirements for the Doctor of
Philosophy degree in Mechanical and Aerospace Engineer-
ing at Oklahoma State University, Stillwater, Oklahoma,
in July 1968.

Professional Experience: Wind Tunnel Instructor and Super-
visor at Parks College of St. Louis University, East
St. Louis, Illinois from September 1962 to July 1963;
Teaching Assistant at Oklahoma State University, Still-
water, Oklahoma from September 1966 to May 1967;
Instructor in the Mechanical Engineering Department and
Research Engineer at the University of Dayton, Dayton,
Ohio from July 1967 to May 1968; National Aeronautics
and Space Administration Summer Faculty Fellow at
Lewis Research Center, Cleveland, Ohio from June 1968
to August 1968.

Organizations and Awards: The author is a member of the following: American Institute of Aeronautics and Astronautics, Pi Mu Epsilon, Sigma Pi Sigma, and Pi Tau Sigma. He was the recipient of a National Aeronautics and Space Administration three year predoctoral fellowship, and an American Society of Engineering Educators-National Aeronautics and Space Administration Summer Faculty Fellowship.